2013

Late summer Iowa rainfall events in weakly forced environments

Michael Edward Greve
Iowa State University

Late summer Iowa rainfall events in weakly forced environments

by

Michael E. Greve Jr.

A thesis submitted to the graduate faculty

in partial fulfillment of the requirements for the degree of

MASTER OF SCIENCE

Major: Meteorology

Program of Study Committee:
Tsing-Chang Chen, Major Professor
Xiaoqing Wu
Eugene S. Takle

Iowa State University
Ames, Iowa
2013

TABLE OF CONTENTS

ABSTRACT

This study analyzes convective events that propagate through Iowa, but do not initiate near a major frontal boundary. Storm reports taken from the National Climatic Data Center (NCDC) for the state of Iowa and surface analysis maps from the Weather Prediction Center (WPC) are used to determine if the convective event occurred near a major front. Fifteen cases characterized by the vertical phase reversal of the monsoon circulation were selected for analysis. A synoptic and mesoscale diagnostic analysis is done to gain an understanding of the mechanisms responsible for convection. An analysis of the North American Mesoscale Model's (NAM) forecasting capability for these non-frontal convective rainfall events was also pursued.

A detailed study for one of the 15 cases was conducted to illustrate the characteristics of this type of summer rain-producing disturbance. The rainfall propagates through Iowa in the warm sector southeast of the low-pressure system and south of a warm front. Low-level warm and moist air advection along with convergence at the terminus of the Great Plains low-level jet (LLJ) develop an unstable environment for convection. The Great Plains LLJ is defined as a wind magnitude maximum in the lower troposphere. Systematic and vertical shear below 700 hPa is conducive to create the instability needed for convection. The anticyclone prohibits the perturbation from growing at initiation because of heavy, dry air just above 700 hPa. Strong positive vortex stretching generates convective vorticity to initiate the convection. The semidiurnal wave also proves to create a perturbation in an unstable environment, helping to strengthen the convection or even initiate it. A composite analysis of all 15 cases shows similar results.

The NAM 12 hour forecast is analyzed for its capability to simulate the non-frontal convection accurately. The divergent circulation associated with convection is not forecasted correctly, suppressing (enhancing) the rainfall where it should be stronger (weaker). Analysis of the precipitable water error in the forecast shows that the

forecasted moisture in the atmosphere is not correct either. It is either too strong when the rainfall is over-predicted or not strong enough when the rainfall is under-predicted.

CHAPTER 1. GENERAL INTRODUCTION

1. Background

The late summer months in Iowa, mainly July and August, tend to be the warmest and driest of the warm months. The late summer monsoon anticyclone dominates the circulation and prevents synoptic-scale waves from entering the United States (Higgins et al. 1997 and Wang et al. 2009). Eighty percent of the rainfall that occurs in late summer is associated with mesoscale convective systems (MCSs) (Wallace 1975, Stensrud and Fritch 1993, and Heideman and Fritch 1988). Most of these MCSs are associated with some type of frontal boundary, but there are convective events that occur away from these boundaries. Events that do not occur near a frontal boundary have not been paid attention to in the past literature. Fifteen cases showing rainfall not occurring near a frontal boundary and the dominant monsoon anticyclone at mid- to upper levels are examined to determine the causes of initiation and then the mechanism to sustain the storms as they move through Iowa. The research task also tests the capability of the North American Mesoscale Model's (NAM) forecast in predicting the non-frontal convective rainfall events.

The North American Monsoon dominates the circulation in much of the U.S. resulting in northwesterly flow over the Central Plains and Iowa. The anticyclonic circulation dominates the mid- and upper levels creating a dynamically weak environment not conducive for deep spring and early summer like troughs. Given these conditions, the low-level conditions become very important to late summer time convection. The monsoon trough (west) and Bermuda High (east) help to fuel warm and moist air advection into the Central Plains (Wang et al. 2009). These conditions along with small short waves that develop in the lower levels help to create a favorable environment for convection to initiate. These shortwaves act to enhance the low-level convergence in the Central plains and can initiate and sustain rainfall (Heideman and Fritch 1988) often without the presence of a front.

Along with the conditions mentioned above, the Great Plains low-level jet (LLJ) helps to create an area of convergence at its northern terminus (Wang et al. 2009). This and the conditions mentioned above create large conditional instability, which can create an environment favorable for convection in a large-scale environment not favorable for synoptic scale waves

(Johns 1984). Directional shear resulting from the turning of the wind from southerly to northwesterly aloft can also enhance the instability.

Any type of perturbation in an environment that is unstable will initiate the convection or increase the intensity. The semidiurnal pressure wave can create a perturbation in the surface pressure, creating convergence at the surface, initiating just enough of a perturbation to create favorable conditions for convection. Mesoscale boundaries or waves at the surface can also create the perturbation needed to initiate convection in a conditionally unstable environment.

The forecast of these events can prove to be difficult, especially because these events are not associated with any type of boundary or synoptic cyclone. Heideman and Fritch (1988) discovered that the worst threat scores occurred during the summer months. Predicting the MCS's in northwesterly flow also proved to be difficult for the NAM to handle. In a study done by Wang et al. (2009), they found that the NAM lagged the observed rainfall and the observed small short wave perturbation. The NAM was not able to handle the vortex stretching associated with convective vorticity generation, nor accurately reproduce the positive vorticity tendency associated with the convection and mid-tropospheric perturbation.

The goal of this study is to analyze the initiation and propagation of the convection occurring away from the front. The synoptic environment is depicted using the vorticity, wind, temperature, divergence, and moisture fields. A diagnostic analysis using cross-sections near where the convection is and a vorticity budget analysis help to detail the origin of convection, and the reason for sustaining the convection as it travels through Iowa. A detailed analysis of the NAM forecast for these events evaluates the forecast capability for non-frontal, weak synoptically forced events. This study also details the error of the NAM forecast in trying to predict the circulation especially the monsoon anticyclone.

2. Thesis Organization

This thesis follows the journal paper format. Chapter 1 includes the general introduction to the thesis. Chapter 2 contains the literature review detailing past research on late summer thunderstorms and the forecasting capability of numerical models. Chapter 3 includes the paper itself that will be submitted to *Journal of Applied Meteorology*. Chapter 4 contains additional results and chapter 5 is the general conclusion. Acknowledgments and references follow chapter 5.

CHAPTER 2. LITERATURE REVIEW

Rainfall in the Central Plains in late summer shows a decrease in amount compared to late spring and early summer. This reduction is mainly due to a quasi-stationary North American anticyclone, which hinders synoptic waves from entering the U.S. (Higgins et al. 1997 and Wang et al. 2009). Nearly 80% of the rainfall in late summer is often associated with mesoscale convective systems (MCS) (Wallace 1975, Stensrud and Fritch 1993, and Heideman and Fritch 1988). These convective systems can be difficult to predict because they are not usually associated with well-organized extra-tropical cyclones. Late summer rainfall is usually associated with a predominant ridge in the upper levels creating northwest flow over the Central Plains (Wang et al. 2009). This is much different from the late spring and early summer rainfall that is commonly associated with extratropical cyclones and large scale troughs throughout the depth of the troposphere.

The predominant ridge in the late summer is a result of the North America Monsoon. The classic accepted mechanism for the maintenance of the summer monsoon are; 1) land-ocean differential heating; 2) a monsoon high (oceanic trough) at upper levels and thermal low (anticyclone) over the continent (ocean) at lower levels; and 3) coincidence of a monsoon high (thermal low) with a divergent (convergent) center (Chen 2002). This monsoon acts to reduce the precipitation in the Central Plains by transporting in drier air at mid to upper levels. The North American monsoon consists of the monsoon anticyclone and thermal low centered over northwest Mexico driven by the land-sea thermal contrast between the warm land and the cooler ocean. The east-west differential heating between the Pacific and Atlantic oceans is the maintenance mechanism for the divergent circulation of the North American Monsoon. Cooling occurs over the eastern tropical Pacific and heating over the western tropical Atlantic (Chen 2002).

While much of the Central Plains experiences the northwest flow associated with the monsoon anticyclone at mid to upper levels, small shortwaves develop in the lower troposphere under this regime. These shortwaves act to enhance the low-level convergence in the Central plains and can initiate and sustain rainfall (Heideman and Fritch 1988). MCS's in late summer often occur under this northwest flow regime accompanied by a sub-synoptic, cyclonic

perturbation in the mid-troposphere (Wang et al. 2009). These mid-level perturbations can provide the forcing mechanism for MCSs to initiate and propagate through the Central Plains.

The vertical extent of these perturbations is limited in comparison to the late spring and early summer extratropical cyclones. The monsoon anticyclone confines the perturbations to the lower levels, so therefore the low-level conditions become much more important. Forcings such as warm air advection and thermal instability along a quasi-stationary front help to initiate convection (Wang et al. 2009). The monsoon trough at lower levels over much of the western half of the U.S. helps to transport warm air poleward towards the plains area from the southwest. The strong meridional thermal gradients and large vertical shear help to add to the instability seen in the Central Plains. The mid-troposphere over the Rocky Mountains becomes dynamically unstable and conducive to the small-scale shortwaves responsible for MCSs in the Central Plains (Wang et al. 2009). The high values of conditional instability created by these conditions can compensate for the weak dynamics induced by the predominant ridge (Johns 1984). According to Maddox and Doswell (1982), significant severe weather can occur under a weak regime, as seen in late summer MCSs that propagate through the Central Plains.

Johns (1984) researched severe weather outbreaks that occurred in northwest flow at the mid- and upper-levels. His research found that over 2/3 of northwest flow severe weather outbreaks are associated with 500 hPa jets occurring south of the jet. His research also led him to find that 850 hPa warm air advection was very pronounced in the genesis area of the outbreaks. The surface dewpoints, temperatures, and sea level pressure values were all higher than those associated with general severe weather. The surface patterns associated with these outbreaks typically showed either a NW-SE pressure trough or a quasi-stationary front oriented in a WNW-ESE direction emanating from a low-pressure system to the NW and a high to the SE. The research also found that most of the severe weather outbreaks occurred in the right front quadrant of the 500 hPa jet. The major result of his research led him to conclude that the low-level warm air advection and other low-level conditions, such as mass discontinuities induced by convective activity, are very important for providing vertical motion necessary for convection.

Maintaining the severe local system consists of continuous, strong low-level relative inflow of conditionally unstable air (Newton 1950, Marwitz 1972b, and Browning 1977). The strong low-level inflow is typically a result of the low-level jet (LLJ) in the Central Plains area. The LLJ is a result of the boundary layer interaction with the ground layer creating a stable layer

just above the surface. This stable layer helps to accelerate the winds and the LLJ develops just above it (Stull 1988). The synoptic environment associated with the development of the LLJ creates a strong pressure gradient across the Central Plains, which helps to accelerate the winds near 925 hPa (Bonner 1968). The LLJ has its core in the lowest 1 km of the troposphere as indicated by the stable layer near the ground. The LLJ follows a diurnal cycle of strong low-level warm air advection and is a response to the boundary layer. In late summer, the combination of the Bermuda high in the southeastern part of the U.S. and the monsoon trough in the western half help to provide the synoptic environment necessary for the development of the LLJ. This combination also helps to bring in moisture and warm air to the Central Plains from the Gulf of Mexico. The LLJ also helps to form strong convergence at its northern terminus and can enhance the convergence of water vapor flux over the Central Plains area. The low-level convergence at the terminus of the LLJ provides positive vortex stretching, which helps to amplify the perturbations responsible for the MCS (Wang et al. 2009). The LLJ acts favorably to enhance convection in an environment where large-scale dynamics are weak.

In a detailed study of the convection that occurs in the Central Plains under the North American anticyclone, Wang et al. (2009) found that mid-level perturbations could provide the forcing mechanism for MCS's in the late summer. They found that moisture pooling along low-level convergence boundaries at the northern terminus of the LLJ created large values of CAPE in the Central Plains. MCS's that are long lived are able to initiate in areas of enhanced CAPE and in northwesterly shear (Trier et al. 2006). Wang et al. (2009) performed a diagnostic analysis on the mid-tropospheric perturbations that formed the MCS's. The vorticity budget analysis shows that vortex stretching was dominant at initiation, but vorticity advection grows substantially from the beginning. The positive values of vortex stretching on the leading edge of the perturbation maintain the upward motion and cyclonic vorticity. The dipole of positive and negative vortex stretching confines the perturbations to the lower and mid-levels.

These mid-tropospheric perturbations and the MCS's themselves have proved to be difficult for the numerical weather models to handle. Heideman and Fritch (1988) discovered that the worst threat scores occurred during the summer months. Their research led them to distinguish that the best threat scores were in the cool season and the cause of these better scores is twofold; 1) cool-season precipitation is frequently of a stable regime that covers large areas; and 2) most of the precipitation is associated with better-forecasted mid-latitude cyclones. The

warm season forecast of convective precipitation is not only sensitive to the forecast of the environment but to the convective parameterization schemes. Contrasting this argument, Clark et al. (2007) found that finer grid spacing in the model without any convective parameterization schemes worked better to simulate MCS's.

In an evaluation of the North American Mesoscale Model's ability in accurately forecasting MCSs and the associated mid-tropospheric perturbations (MPs), Wang et al. (2009) found that forecasted MPS constantly lagged the observed MPs. The forecast of the MP improves when the model is initialized at the genesis time of the MP, but the perturbation is still too weak and its life cycle too short. The diagnostic analysis performed on the forecast led them to find that the vorticity tendency is constantly under-simulated, which leads to the lag of the MP in the forecast. Wang et al. (2009) also examined the simulation of the mid- to late-summer anticyclone and found that the anticyclone in the NAM forecast was much stronger. The forecasted LLJ in the Central Plains was constantly weaker than the observed. Their research led them to discover that the removal of the MP position error improves the precipitation forecast, which is often under-simulated. Improving the forecasts will start with a better simulation of the strong baroclinicity of the environmental flow, whether that is in the form of vorticity advection or surface frontogenesis (Jankov and Gallus 2004). The improvement of the operational models may come from using much finer grid spacing or finding ways to improve the convective parameterization schemes.

CHAPTER 3. LATE SUMMER IOWA RAINFALL EVENTS IN WEAKLY FORCED ENVIRONMENTS

A paper to be submitted to *Journal of Applied Meteorology*

Michael E. Greve, Jr. and Tsing-Chang Chen

3.1 Abstract

This study analyzes late summer convective events in Iowa that do not initiate near a major frontal boundary. Storm reports taken from the National Climatic Data Center (NCDC) for the state of Iowa and surface analysis maps from the Weather Prediction Center (WPC) are used to select convective events occurring with some distance away from major fronts. Fifteen cases characterized by the vertical phase reversal of the monsoon circulation were selected for analysis. A synoptic and mesoscale diagnostic analysis was done to gain an understanding of the mechanisms responsible for convection. An analysis of the North American Mesoscale Model's (NAM) forecasting capability for these non-frontal convective rainfall events was also pursued.

A detailed study for one of the 15 cases was conducted to illustrate the characteristics of this type of summer rain-producing disturbance. Low-level warm and moist air advection along with the LLJ develop an unstable environment for convection. The anticyclone prohibits the perturbation from growing at initiation because of heavy, dry air just above 700 hPa. Strong positive vortex stretching in the lower troposphere generates convective vorticity to initiate the convection. The semidiurnal wave proves to create a perturbation in an unstable environment, helping to strengthen the convection or even initiate it. A composite analysis of all 15 cases showed similar results.

The NAM 12 hour forecast allows for the spin up of microphysical variables and is analyzed for the case study. The divergent circulation and precipitable water were not forecasted correctly suppressing rainfall in the case study.

3.2 Introduction

The late summer months in Iowa, mainly July and August, tend to be the warmest and driest. The late summer monsoon anticyclone dominates the circulation and prevents synoptic-scale waves from entering the United States (Higgins et al. 1997 and Wang et al. 2009). Eighty percent of the rainfall that occurs in late summer is associated with mesoscale convective systems (MCSs) (Wallace 1975, Stensrud and Fritch 1993, and Heideman and Fritch 1988). Most of these MCSs are associated with some type of frontal boundary such as in fig. 1 (Rauber et al. 2002), but there are convective events that occur away from these boundaries. These events have not had much attention in the past, but can be very important to farmers and others relying on rainfall especially when rainfall is sparse. Fifteen cases, spanning the years of 2004 to 2011, showing rainfall irrelevant to a frontal boundary are examined to determine the similar causes of initiation and then what helps to sustain the storms as they move through Iowa. The capability of the North American Mesoscale Model's (NAM) forecast in predicting the non-frontal convective rainfall events is tested as well.

The North American Monsoon dominates the circulation in much of the U.S. resulting in northwesterly flow over the Central Plains and Iowa (Chen 2002). The anticyclonic circulation dominates the mid- and upper levels creating a dynamically weak environment not suitable for deep spring and early summer like troughs. Given these conditions, the low-level conditions become very important to late summer time convection. The combination of the monsoon trough to the west and the Bermuda High to the east create a favorable environment for the Great Plains low-level jet (LLJ) to develop and transport warm, moist air into Iowa. These conditions along with small short waves that develop in the lower levels help to create a favorable environment for shallow convection to initiate. These shortwaves act to enhance the low-level convergence in the Central Plains and can initiate and sustain rainfall (Heideman and Fritch 1988).

Along with the conditions mentioned above, the LLJ helps to create an area of convergence at its northern terminus (Newton 1950, Chen and Kpaeyeh 1993). This and the conditions mentioned above create large conditional instability, which can create an environment favorable for convection in a large-scale environment not favorable for synoptic scale waves (Johns 1984) or lacking a major convergent boundary (front). The LLJ coupled with the mid- to

upper level northwesterly flow creates large values of directional shear, adding to the instability of the environment.

Any type of perturbation in an environment that is unstable will initiate convection or increase the intensity. The semidiurnal pressure wave can create a negative perturbation in surface pressure, initiating convergence at the surface, providing the forcing mechanism for convection to initiate or deepen. Mesoscale boundaries or waves at the surface can create perturbations needed to initiate convection in a conditionally unstable environment underneath an inversion layer. The convergence caused by these phenomena can be enough to overcome an environment that lacks a strong convergent frontal boundary.

The forecast of these events can prove to be difficult, especially because these events are not associated with any type of boundary or synoptic cyclone. Heideman and Fritch (1988) discovered that the worst threat scores occurred during the summer months. Predicting the MCS's in northwesterly flow also proved to be difficult for the NAM to handle. In a study done by Wang et al. (2009), they found that the NAM lagged the observed rainfall and the observed small short wave perturbation. The NAM was not able to handle the vortex stretching associated with convective vorticity generation, nor accurately reproduce the positive vorticity tendency associated with the convection and mid-tropospheric perturbation.

It is hypothesized that the shallow convection initiating in a weakly forced environment develops in a very unstable environment characterized by strong warm and moist air advection underneath the monsoon anticyclone. The LLJ, warm air advection, low-level short waves, mesoscale boundaries, and the semidiurnal pressure wave provide sources of lift in the absence of fronts underneath and inversion layer. A case study demonstrates the characteristics of these non-frontal convective rainfall events. Section 3 examines the data sources and the case selection criteria. Section 4 examines the case and its synoptic environment including a diagnostic analysis using the vorticity budget. Section 5 shows the composite analysis of all 15 cases to show the similarities of the cases to each other. Section 6 entails the NAM forecasting capability of these events and section 7 includes the conclusion and future work.

3.3 Data and Case Selection Criteria

3.3.1 Data Sources

The study presented here utilizes the North American Regional Reanalysis (NARR) for observational atmospheric data. The NARR was developed by the National Center for Environmental Prediction (NCEP) using data assimilation techniques from the Eta model (Black 1994). The resolution of the NARR is 32 km, 45 vertical layers on pressure levels, and three hourly outputs. Mesinger et al. (2006) has proved the validity of the NARR compared to rain gauge, rawinsondes, and surface station observations. The NARR data were obtained from the National Climate Data Center's (NCDC) National Operational Model Archive and Distribution System (available at nomads.ncdc.noaa.gov/data.php?name=access#narr_datasets).

Rainfall measurements are taken from the Tropical Rainfall Measuring Mission (TRMM) satellite. TRMM, a joint mission between NASA and JAXA, the Japanese Space Agency, was launched in 1997. According to the TRMM Senior Review Proposal (2007), the use of both active and passive microwave instruments, and the low inclination orbit have made TRMM the world's foremost satellite for studying precipitation. Kumerow et al. (2000) showed that the TRMM precipitation radar (PR) compared very well with ground based radar estimates at NASA's Florida ground validation site. They also state operational agencies are considering using the TRMM PR as a calibration constant for ground based radars calibrated independently. The dataset used in this study utilizes the 3B42 version 7 of the TRMM satellite. The 3B42 algorithm uses merged-IR precipitation and root-mean-square precipitation-error estimates. The resolution of the TRMM dataset is 0.25 degree by 0.25 degree at a temporal resolution of three hours. The variable provided in the 3B42 dataset is the rainfall rate so it is multiplied by three to obtain the three-hour rainfall amount. The dataset can be accessed by way of ftp at ftp://disc2.nascom.nasa.gov.

To supplement the NARR data at the surface and to provide a more detailed mesoanalysis, the Iowa Environmental Mesonet (IEM) station data is used. The IEM uses a combination of AWOS, ASOS, RWIS, SchoolNet, and other COOP stations to archive a record of the surface observations in Iowa. This study utilizes data for the years of 2003 to 2011 from ASOS, AWOS, RWIS, and SchoolNet data. These stations proved to be the most reliable for the needed wind and pressure fields. The station data was then converted into gridded data at a resolution of 12 km and a temporal resolution of three hours to match the NARR and TRMM

data. The data can be found in the archive section of the IEM website (www.mesonet.agron.iastate.edu/archive/data).

This study uses the North American Mesoscale Model (NAM) for examining the forecasting capability of these non-frontal rain events. The NAM has 12 km grid spacing with 45 vertical layers. The NAM initializes four times daily with three hourly outputs. Because of the temporal extent of this study, three different versions of the NAM were used, the Meso-Eta, the NAM 2005, and the Nonhydrostatic Mesoscale Model of the Weather Research and Forecasting Model (WRF-NAM, Bernadet et al. 2005). Wang et al. (2009) found that the NAM and WRF-NMM were similar in their treatment of MCSs and did not make a distinction between the two. The same implementation is utilized in this study for all three versions. In order to compare to the NARR and the TRMM, the grid spacing is reduced to 32 km and 0.25 degrees respectively using bilinear interpolation. The NAM outputs are provided by the NCDC (http://nomads.ncdc.noaa.gov/).

3.3.2 Case Selection Criteria

Late summer convective rainfall events were chosen from gathering storm reports from the NCDC record of storm reports for the state of Iowa for 15 June-31 August, determined to be the late summer and when the North American Monsoon has become its strongest. From these reports, each storm is analyzed using surface analysis charts from the Weather Prediction Center or the National Weather Service weather map archived at Colorado State University. Using these sources, cases were selected based on whether or not their initiation was influenced by a front. The analysis of these cases revealed two different types of cases. One case showed an early summer, late spring type dominant trough over or near Iowa. The other type exhibited the monsoon anticyclone from 700 hPa vertically extending to the top of the troposphere. This type also showed a thermal low, most often in the northwest region of the Northern Plains and another in the Southwest. These thermal lows remain shallow throughout the entirety of the cases, because the anticyclonic air prohibits the cyclonic vorticity from gaining vertical extent. From these cases, the focus narrowed to those cases that demonstrated the dominant monsoon anticyclone and northwest flow over Iowa. These events lasted anywhere from 14 to 24 hours and typically had their heaviest rainfall during the nighttime hours, when the LLJ has developed and become its most intense, as would be expected in the Central Plains.

3.4 Case study 02 August 2004

To demonstrate the typical characteristics of these non-frontal rain events, one case is chosen to represent the other cases. The other cases were analyzed to find resemblance to this case, and it was determined that the cases were very similar to this one particular case.

3.4.1 Synoptic Life Cycle

Examining the synoptic charts in fig. 2, a quasi-stationary front in South Dakota with a low-pressure system in western North Dakota exists over the area of initiation. One can also clearly see the high-pressure system in the Ohio area, also seen later in the composite surface analysis chart. The rainfall initiates just south of the low-pressure system and will propagate southeastward across South Dakota into Iowa in the warm sector evidenced by the warm front seen in fig. 2 at 1200 UTC. The warm front remains north of Iowa while the low pressure system propagates southeastward finally ending up in southeast South Dakota. The rainfall intensifies two different times in the warm sector away from any type of front and in front of the marked trough on the synoptic analysis chart. In most of the other cases, this trough appears as a cold front that reaches central Nebraska by the time the rainfall has diminished (1800 UTC).

At the time of initiation, the monsoon anticyclone (fig. 3a) is present over much of the central part of the country extending from 200 to 700 hPa showing northwest flow over the Central Plains. A small shortwave trough reveals itself (fig 5a) at 700 hPa where the rainfall initiates and where the low-pressure system is situated. There is a small shortwave trough developing at 850 and 925 hPa over southern South Dakota and northern Nebraska (figs. 4b and c). As the rainfall becomes the most intense at 1200 UTC (figs. 5a, b, and c), the LLJ at 925 hPa is its strongest as well creating convergence in the streamlines over the area of strongest convection along with a small shortwave trough at 850 and 700 hPa. The 200 hPa (fig. 3b) flow at 1200 UTC remains northwesterly, as does the 700 hPa flow over much of the Central Plains and Iowa. The jet stream has moved farther east and now the rainfall is located in the right entrance region of the jet. The 700 hPa chart shows a developing jet over Iowa centered in the shortwave trough also located there. Once the rainfall has diminished, the jets at 925 and 850 hPa diminish as well (figs. 6a and b). The 700 hPa jet becomes stronger over Iowa where the rainfall had been its heaviest. The monsoon anticyclone still dominates the middle to upper

levels and remains nearly stationary throughout. Another important feature that shows in these figures is that the rainfall north of Iowa, which is north of the warm front, is behind a lower-level trough but in front of a trough at the upper levels. The rainfall in Iowa is only low-level forced because the perturbation does not extend past the 700 hPa level, while the perturbation causing the rainfall to the north is more upper level driven.

An analysis of the relative vorticity field (figs. 7a and b) at the initiation of convection shows the cyclonic perturbations at 925 and 850 as indicated in the streamlines. Looking at 1200 UTC (figs. 7c and d), the time of heaviest rainfall in Iowa, it can be clearly seen that the LLJ at 925 hPa is transporting positive vorticity into the area of heavy rainfall. The cyclonic perturbations at 850 and 925 hPa near the area of heavy rainfall help to sustain the convective rainfall over Iowa. By the time the rainfall has diminished, the perturbations at 925 and 850 hPa have lost intensity (figs. 7e and f). The cyclonic vorticity perturbations at 925 and 850 hPa appear to be important in the maintenance of the heavy rainfall and in perturbing the unstable lower troposphere.

The divergence field at the time of initiation of rainfall for this case shows strong convergence near the low-pressure system (fig. 8) in North Dakota. There are also some areas of convergence associated with small shortwave troughs at the lower levels in northern Nebraska. At 1200 UTC, (fig. 9) the heavy rainfall is associated with strong convergence at the lower levels as would be expected. The LLJ is strongest at this time and the zone of convergence at its northern terminus is evident in fig. 9b and c. One can also clearly see the response of the atmosphere to convection with strong divergence (fig. 9a) centered exactly over the area of heavy rainfall. Similar to the diminishing cyclonic vorticity, the convergence also becomes weaker when the rainfall has dissipated (not shown). Strong convergence from the lower levels is necessary for the initiation and sustaining of convection. In this and other cases, the convergence arises out of small-scale cyclonic vorticity perturbations at lower levels and from the LLJ. The rainfall north of the warm front is much different than the

When the large-scale dynamics are weak and provide little or no forcing, the low-level conditions become much more important especially warm and moist air advection. Figures 10a, b, 11a, and b show strong warm and moist air advection present in the area of initiation at 925 and 850 hPa. These two ingredients are necessary for convection to initiate and these two components continue to follow the rainfall as it becomes more intense. The LLJ is its strongest

at 1200 UTC and continues to transport warm and moist air into the area of convection in figs. 10c, d, 11c, and d. The warm and moist air advection helps to erode any CIN that was present in the area before and the warm air advection can of course provide another source of lift. The diminishing jets at 925 and 850 in the dissipating (1800 UTC) rainfall stage (figs. 10e, f, 11e, and f) signal the end of warm and moist air advection.

The stability of the environment is determined from an analysis of CAPE and CIN. At the time of initiation, it is evident that the environment is unstable with values approaching 5000 J/kg in northwest Iowa, and values near 1000 J/kg in the area of initialization (fig 12c) indicating that the area is primed for convection. Both in Iowa and in the areas of initiation, there is no significant amount of CIN (fig 12d), because the warm and moist air advection has eroded the CIN that was present earlier in the day (fig. 12a and b). At 1200 UTC, the rainfall has passed through the CAPE maximum and is now located in an area of <1000 J/kg (fig. 12e). The CIN remains insignificant and does not have an effect on the convection (fig. 12d). At the time of dissipation, the CAPE has again increased, but this is due mainly to daytime heating since the time of dissipation is 1800 UTC.

3.4.2 Mesoanalysis

The IEM data provides the mesoanalysis data for an analysis of any type of boundary or wave not seen in the surface analysis map. At the time of initiation (fig. 13), the surface wind in Iowa is mainly out of the south. In examining the wind field over Iowa, there is nothing significant to point out, besides a very small trough in north-central Iowa. This trough is also present in the pressure and vorticity fields. Near the time when the rainfall is on the northwest corner of Iowa, a boundary appears in central Iowa. This boundary persists into the time of heaviest rainfall demonstrated well by the solid black line in the divergence field in Central Iowa (fig. 14b). An east-west oriented wave indicated by the different color solid lines in figs. 13 and 14 develops in the initiation stage. The wave persists into the time of heaviest rainfall in all three fields, and indicates instability in the warm sector and can be the means by which air can lift and initiate deep convection.

3.4.3 Diagnostic Analysis

Vertical cross-sections of the wind field, divergence, and the soundings near the rainfall help to demonstrate the vertical extent of the disturbance. Analysis of the vorticity budget shows details of the cyclonic short wave perturbation that helped to initiate and sustain the rainfall. The effect of the semidiurnal surface pressure wave is also analyzed as well.

Figure 15 shows the meridional wind along with the vertical velocity and the divergence field for three time steps. The area of rainfall is highlighted in the black lines, with the heaviest rainfall highlighted in the green lines. Figures 15a and b show the cross-section at the time of the convective initiation. The wind profile (fig. 15a) shows a change in wind direction near the 700 hPa level indicating strong shear and the presence of the anticyclone. Figure 15b also shows convergence near the initiating convection as well, but the convergence is very shallow (below 700 hPa) at initiation. Figures 15c, d, e, and f show the two times the rainfall becomes intense. The vertical velocity is very strong and nearly upright indicative of strong convection, but the heaviest rainfall is located directly in the area of the strongest vertical motion. The co-location of the strongest vertical motion and heaviest rainfall is the reason that the rainfall will soon dissipate after this stage, because the updraft is cut off by strong downdrafts as a result of the the heavy rainfall. This is different from the typical squall line case shown in fig. 1, because the updraft does not tilt with height as in the squall line case. This case and other cases are classified as air-mass thunderstorms because of the vertically straight updraft. The LLJ increases in strength from initialization helping to create the strong convergence (figs. 15c and e) for convection at its northern terminus. The convection is very strong (figs. 15d and f) in the lower troposphere with a strong divergent response in the upper troposphere. The LLJ as shown is very important to initiate strong upward motion in the absence of a front. When the convection initiates, it does not penetrate the upper levels and therefore does not shear out as seen in fig. 1. The convergence remains below the mid-levels at initiation because of anticyclonic air above 700 hPa, which is heavy and dry. The cyclonic perturbations in the lower levels and the LLJ help to create convergence in the lower troposphere underneath the monsoon anticyclone in the absence of a front.

Figure 16 shows soundings at three different locations, Bismarck, ND (BIS), Aberdeen, SD (ABR), and Omaha, NE (OMA). The top two soundings are from BIS at 1200 UTC 01 August 2004 and 0000 UTC 02 August 2004. The 1200 UTC sounding shows an inversion layer

below 850 hPa. OMA and ABR show a dry layer near or just above 850 hPa. This dry, inversion layer is a result of the monsoon anticyclone bringing in dry air from the desert southwest into the Central Plains. The LLJ and cyclonic perturbations in the lower troposphere provide the forcing mechanism for the air parcels to push past the inversion layer and initiate deep convection. It also helps to transport warm and moist air into the area to erode the inversion layer and allow the atmosphere to utilize the CAPE present in the area. The presence of the strong LLJ eliminates the need for a front to lift the air that is unstable past the inversion layer. The additional mesoscale boundary at the surface also helps to lift the air parcels as well.

In order to determine the cause for the lower troposphere perturbation that initiated the convection and then what sustains the propagating convection, a vorticity budget analysis was performed. The vorticity budget equation can be written in the following way with conventional symbols (Holton 2004),

$$\zeta_t \left(= \frac{\partial \zeta}{\partial t}\right) \approx -\vec{\boldsymbol{V}} \cdot \nabla\zeta - v\beta - f\nabla \cdot \vec{\boldsymbol{V}} - \boldsymbol{\zeta\nabla} \cdot \vec{\boldsymbol{V}} \ . \quad (1)$$

A variance test is performed to determine the more dominant terms at three different levels. Terms that account for more than 15% of the total variance of ζ_t are considered dominant and are kept in the equation. The same result was found at all levels and thus the ζ_t equation can be written as

$$\zeta_t \approx -\vec{\boldsymbol{V}} \cdot \nabla\zeta - f\nabla \cdot \vec{\boldsymbol{V}} \ . \quad (2)$$

The first term on the right side of equation (2) is the horizontal advection of vorticity (ζ_A) and the second term is the vortex stretching term (ζ_x).

These terms along with relative vorticity and vorticity tendency are shown in fig. 17 at 0000 UTC. Strong ζ_x (fig. 17d) in the lower troposphere is responsible for the positive ζ_t and for initiating the convection. There is also a clear dipole of ζ_x near 700 hPa keeping the perturbation confined to the lower levels at initiation. Looking at figs. 18 and 19, the two times of heavy rainfall; it becomes evident that the ζ_A (figs. 17b, 18b, and 19b) grows from initiation to become its strongest at 1200 UTC. At 0600 UTC, the ζ_x (fig. 18d) remains dominant shown by the resemblance of ζ_t to ζ_x. The negative ζ_x above 500 hPa cancels out most of the positive ζ_A and prohibits the cyclonic perturbation from gaining vertical extent. At 1200 UTC, ζ_x (fig. 19d) still

dominates the lower troposphere, but ζ_A has become much stronger, because the convection has now deepened and is affected by the upper level winds. The ζ_t cross-section (fig. 19c) resembles more of a combination of ζ_A and ζ_x. ζ_x reaches it maximum just below 900 hPa, and just below the positive/negative dipole in ζ_t and ζ_A. Clearly, ζ_x initiates the convection and supplies convective vorticity generation to the rainfall, but remains shallow below the monsoon anticyclone. ζ_A contributes more positive ζ_t as the convection deepens and propagates downstream. ζ_A also provides more positive ζ_t at the upper levels but, because of strong negative ζ_x at the beginning of the event, positive ζ_t cancels out and the perturbation remains in the lower troposphere.

3.4.4 Semidiurnal Pressure Wave

As seen before, the environment in Iowa is very unstable with high values of CAPE so that any perturbation can cause the convection to become stronger or can cause initiation of convection as seen in fig. 20. After using a high-pass band filter on the area averaged, surface pressure data over Iowa to eliminate the passage of synoptic-scale systems, the semidiurnal component has a clear effect on the rainfall seen in the filtered and observed pressure lines. The convergence created by the negative surface pressure tendency is enough to cause the rainfall, which went from intense at 0600 UTC to nearly dissipated at 0900 UTC, and then much more intense at 1200 UTC. All of the other cases showed similar results (not shown here) where the perturbation in surface pressure either strengthened or initiated convection.

3.5 Composite Analysis

A composite analysis was done for all 15 cases exhibiting rainfall not occurring near a front. The composite analysis was broken up into six time steps to represent three stages of the convection. Table 1 shows the time and date of each case, the maximum 200 hPa height and location, the maximum 925 hPa wind speed and location, and the maximum 850 hPa wind speed and location. Outliers are highlighted in yellow. Although there are outliers, each case appeared to have very similar structure as will be discussed further later especially a dry layer, just above a very warm, moist layer.

3.5.1 Synoptic Life Cycle

Many of these events had their initiation in the western part of the Central Plains in Central Nebraska or central South Dakota. The composite, hand drawn synoptic analysis map for all stages is shown in fig. 21 with the area of rainfall in the box. The synoptic analysis chart for the initiation stage (fig. 21a) shows a low pressure system in western South Dakota and in Western Kansas. The synoptic chart also shows a stationary front in the Southern Plains area along with another quasi-stationary front in the northern part of North Dakota and Minnesota.

The mature stage (fig. 21b) shows the low-pressure system has now moved farther southeast into central South Dakota and the system in Kansas has moved slightly east. There is a warm front draped east to west across southern Minnesota and the stationary front in southern Missouri has not moved at all. The cold front can also be seen advancing from the west but is still located just to the west of Nebraska. Clearly, this stage demonstrates that the rainfall occurs in the warm sector far in advance of the cold front.

Figure 21c, the dissipation stage, shows a cold front to the west of Iowa, a warm front to the north, and a stationary front in Southern Missouri. The low-pressure system has moved into southeastern South Dakota and the low to the south has moved into north-central Kansas. By this stage, the rainfall has since moved out of Iowa and is dissipating or has completely dissipated.

Figure 22 shows the lower levels of the troposphere for all three stages. As in the case study, the increasing LLJ at both 925 and 850 in the mature stage leads to more intense rainfall. The convergence created by the LLJ is enough to perturb the already unstable low-level conditions and cause intensification in the rainfall or be the cause for initiation as seen in the initiation stage. A small shortwave trough develops at 700 hPa (not shown) along with a jet, which also happened in the case study signaling the dissipating rainfall. The diminishing jets at 850 and 925 hPa agree well with the case study, signaling the dissipation of the rainfall.

Figure 23 shows the temperature fields at 925 and 850 hPa at all three stages. The monsoon trough in the lower levels provides the necessary circulation to transport the warm air to the regions of convection evidenced by the low-pressure system and the initiating convection. Strong warm air advection is present all three levels over the Central Plains helping to provide an unstable environment for rainfall to initiate in. As the rainfall intensifies, the stronger LLJ is able to transport warm air into the areas of intense convection, helping to increase upward

motion. Once the rainfall dissipates, the winds at 925 and 850 hPa are still transporting warm air, but the 700 hPa flow is now bringing cooler air into Iowa (not shown).

The combination of the Bermuda High to the east and the monsoon trough to the west help to transport moisture from the Gulf of Mexico into the Central Plains at the lower levels of the troposphere. Figure 24 depicts this process and shows strong moisture advection directly into the areas of initiation and into the areas of heaviest rainfall. Maxima of specific humidity show at 850 and 925 hPa in the area of intense rainfall during the mature stage. As would be expected, the diminishing jets at 925 and 850 are not able to transport as much moisture to the area of convection so the rainfall diminishes. The specific humidity also decreases at 850 and 700 hPa (not shown), because of the presence of the anticyclone above these layers starting to mix down. The anticyclone keeps the moisture confined to the lower troposphere as will be seen when looking at an array of soundings for these cases.

The combination of the warm and moist air and the developing LLJ helps to create significant amounts of conditional instability in the Central Plains and Iowa. The instability of the environment can be examined using the convective available potential energy (CAPE). Figures 25a and b show the surface based CAPE values over the Central Plains at the time of initiation. Maxima show in central Nebraska and central South Dakota with very little if any significant convective inhibition (CIN) (figs. 25c and d) at the time of initiation. The latter stages are not shown because convective contamination eliminates the CAPE during the mature stage, while daytime heating at the dissipation stage increases the CAPE values for the next round of convection if it occurs.

3.5.2 Mesoanalysis

Using the gridded mesonet data from the IEM, an analysis of the wind, vorticity, divergence, and surface pressure field was done to discover if any common feature existed. The initiation stage is shown in fig. 26. The composite surface wind is mainly out of south over much of the state. The vorticity and divergence fields do show a wave like structure in western Iowa where the heaviest rainfall will occur. A clear alternation of positive and negative values of vorticity and divergence exists as shown in figs. 26b and c. The pressure field also indicates this wave in western Iowa as seen in fig. 26d. Another wave oriented SW-NE across Iowa can be identified in the vorticity, divergence, and pressure fields. This wave could be the

perturbation responsible for strengthening or initiating convection that propagates with an eastward component.

The mature stage mesoanalysis plots (fig. 27) show very similar results to the initial stage. The wave in western Iowa appears to be stronger in both the vorticity and divergence fields. This wave is still evident in the pressure field in western Iowa. It becomes clear that this wave in western Iowa has as significant effect on the composite rainfall. The environment is clearly unstable as evidenced in the CAPE plot and so any type of perturbation will initiate or intensify convection. The SW-NE oriented wave still exists, possibly having an effect on any rainfall travelling across Iowa.

The dissipation stage (not shown) shows distinctly southern flow over most of the state. The wave in western Iowa is still present, but slightly diminished, in the divergence and vorticity fields, but since the convection has already moved through the area, does not have a significant impact anymore. A trough in the pressure field is located in Central and western Iowa and has been nearly stationary in all three stages. This trough in the pressure field may also play a role in helping to back the winds at the surface creating a source of inflow for the convection that occurs in western Iowa and any other rainfall that may propagate across the state.

3.5.3 Diagnostic Analysis

In addition to examining the synoptic environment for these non-frontal convective events, vertical cross-sections at the location of the rainfall are plotted. These cross-sections along with the soundings enable one to examine the shear, and the vertical extent of the perturbations causing the convection. A vorticity budget analysis was also performed for the composite to reaffirm results from the case study.

Shown in fig. 28 is an array of the soundings launched at the closest time to the initialization of convection. Analysis of these soundings shows that there is definitely an indication of instability evidenced from the CAPE profiles in most of the soundings. Many of these soundings show a dry, inversion layer in the lower troposphere, which can inhibit the vertical extent of the convection at initiation, but once sustained and strong vertical motion is established, the convection can deepen. This dry layer is a result of the monsoon anticyclone at middle and upper levels over much of the Central Plains. The anticyclonic circulation mainly above 700 hPa transports in dry air from the desert southwest and weighs down the air below it.

The dry air layer can also have an effect on the severe weather as well. Heideman and Fritch (1988) demonstrated that mid-level dry air in a sheared environment can enhance production of moist downdrafts, and these downdrafts can enhance convection. The intrusion of dry air in many of these cases, which do have large values of directional shear (south wind at the surface and northwest flow at 700 hPa) provides the ingredients for severe weather. Below the inversion layer in many of these cases is moist and warm air, which act to build the instability, and then once the LLJ becomes strong enough, convection is able to explode and become intense as what happens in the case study because of strong convergence in the lower troposphere. This is different from a typical case where a front initiates the convection below the dry inversion layer. The front acts as the convergence to lift the air as seen in fig. 1 from Rauber et al. (2002). The LLJ or other perturbations in the lower troposphere are able to lift the air above the inversion layer by strong vertical motion because of strong convergence.

Cross-sections were produced as was done for the case study. Looking at the initiation stage first, fig. 29a shows that there is strong shear near 700 hPa located in the area of convection. The strong shear helps to provide instability to the atmosphere and the 700 hPa flow prohibits the convection from gaining vertical extent at initiation. Strong convergence (fig. 29b) is evident near the surface where the rainfall is initiating and divergence just above it remaining below 700 hPa. Upward motion is not significant in this stage, but the convection is not nearly strong enough yet to see strong vertical motion.

At the mature stage, the first noticeable change is seen in the vertical motion. Very strong vertical motion exists over the areas of heavy rainfall (fig. 29c), which is indicative of strong convection. The LLJ increases as well which also acts to increase the shear near or just below 700 hPa where the anticyclone is beginning to dominate. Strong convergence shows at the northern terminus of the LLJ and over the area of deep convection (fig. 29d). Strong divergence at the upper levels is the result of the atmospheric response to convection.

The dissipation stage shown in fig. 29e reveals diminishing upward motion as expected with diminishing convection. It also appears that the northerly component of the wind is beginning to mix down into the lower troposphere decreasing the shear that was present at the initiation and mature stage. The LLJ also as was mentioned in the synoptic analysis diminishes as well. With the diminishing LLJ, the strong convergence (fig. 29f) at the lower levels diminishes as well signaling the dissipating convection.

Vortex stretching is very strong (fig. 30d) at the initiation stage accounting for most of the positive ζ_t. ζ_x remains positive at the lower levels throughout the three stages (figs. 30d, 31d, and 32d). While ζ_A remains small at first, it grows substantially as the convection intensifies. During the mature stage, ζ_A (fig. 31b) is much more significant and accounts for most of the total variance of ζ_t. Less friction in the upper atmosphere allows for stronger winds and thus ζ_A dominates at these levels.

The constant positive ζ_x near the convection agrees well with theory in that positive ζ_x supplies cyclonic vorticity and indicates convective vorticity generation (Zhang 1992). The positive ζ_x also produces upward motion at the leading edge of convection and helps to intensify or sustain the convection. As seen in figs. 31d, 31d, and 32d, there is a positive/negative dipole of ζ_x in the middle troposphere confining the convective vorticity generation to the lower troposphere at the initial stages. As the convection becomes stronger, the ζ_t more closely resembles the ζ_A. The convection deepens and becomes more intense and is now steered by the upper level flow from the northwest. The positive ζ_A helps to sustain the cyclonic ζ_t and the heavy rainfall. As the rainfall diminishes (fig. 32), the positive ζ_x becomes weaker, yet the positive ζ_A remains strong and accounts for most of the ζ_t. Clearly, the ζ_x at the lower levels is very important in maintaining the intense convection.

3.6 Evaluation of NAM Forecast for the Case Study

For brevity, the case study used in this research will also serve as the case study for the evaluation of the NAM forecast on these non-frontal rain events. The results of the other cases were very similar to this case and will be discussed as needed in this section but not shown.

3.6.1 Geopotential Height, Precipitable Water, and Precipitation Error

The forecast initialized 12 hours before the time of convection is used in this analysis. The 12 hour forecast is used because previous research shows that forecast hour 12 is generally when the mesoscale portion of the kinetic energy spectrum reaches a fully developed state (Skamarock 2004) and the model has accomplished the spin up of its microphysical variables (Clark et al. 2007). Figure 33a shows the geopotential height error at 200 hPa at 0600 UTC and the error in precipitation. This error in height is a result of the forecasted height being much lower than the observed height. The same error exists at 1200 UTC when the rainfall has once

again become intense (fig. 33b). The geopotential height error is a response to the intense convection not forecasted well in the NAM forecast. It is clear from these two figures that the convergence near the surface would not be predicted well either. The error in the divergence field at 925, 850, 700, and 200 hPa along with the precipitation error is shown in fig. 34 and 35 for 0600 and 1200 UTC, respectively. The convergence in the lower levels is not forecasted correctly showing divergence in the area of the observed rainfall and therefore suppresses the forecasted rainfall. Generally, if the model over-predicted the rainfall, the error response at 200 hPa would be higher forecasted heights and the reverse would be true for under-forecasted rainfall.

Figures 33c and d show the error in the forecasted precipitable water, which is the measure of the amount of water in the column. Shown in the figure are the times when the rainfall was its heaviest at 0600 and 1200 UTC. From examining these figures, another deficiency is revealed in the forecast. The model clearly does not predict the observed moisture well, which primarily accounts for the under-forecasted amounts in the model for this case. If the measure of the total water in the column is wrong, the forecasted moisture transport and convergence will also be wrong and therefore will not be able to produce the amount or location of the observed rainfall. Again, this error shows in all of the 15 cases and follows the same principle of the geopotential height error. If the rainfall is under-predicted, the forecasted precipitable water is much less and the reverse applies for over-predicted rainfall.

3.6.2 Wind/Circulation Errors

Not only is the area of the perturbation examined for the error in the forecast, but the circulation over the entire U.S. is examined as well. Looking at the 200 hPa error (fig. 36), it is clear that the monsoon anticyclone is not simulated correctly. It appears to be under-simulated showing the wrong flow in the streamline error and weaker winds near the center of the anticyclone. Over the area of initiation highlighted in fig. 37, convergence in the streamlines at 200 hPa coincides with divergence at 925 hPa showing that the divergent circulation is not produced correctly in the forecast. The divergence at 925 hPa inhibits the strength of the cyclonic perturbation that generates the observed rainfall. Although the divergence error at 0000 UTC is not strong, fig. 37 clearly indicates that the shallow convergence is not accurately forecasted. This is again seen in fig. 38 at 1200 UTC when the rainfall is its heaviest. There is a

clear cyclone in the streamline error at 200 hPa over eastern Iowa, and divergence in the streamlines at 925 hPa. This is of course the opposite of the observed streamlines.

The model actually predicts a stronger LLJ than the observed data and the heavy rainfall occurs in the section of the error plot where the over-predicted wind magnitudes meet the under-predicted wind magnitudes. The LLJ is simulated differently in each case showing no clear-cut under- or over-prediction. As pointed out before, the heavy rainfall occurring in between the positive/negative errors in the wind magnitude is a result of the divergent circulation forecasted incorrectly.

The case shown here shows an underestimated anticyclone in the forecast at 200 hPa. Not all cases showed similar results with some showing a better ability to predict the anticyclone wind directions correctly but others show similar results to the case studied in this paper. The one thing that does show in every case is the stratification of the magnitude error at 200 hPa. This is further evidence of the model's inability to produce the large-scale divergent circulation. If the larger continent scale circulation cannot be produced correctly, the mesoscale divergent circulation will not be predicted well either.

3.6.3 Vorticity Budget Error

The vorticity budget was used before to discover the cause of the convection and the associated lower troposphere perturbation. A vorticity budget analysis was also performed on the forecast and then compared to the observed. At the time of initiation (not shown), the error around the convection is not large at 925 or 850 hPa, but does show anticyclonic bias at 700 hPa. As the perturbation and convection become stronger, the error becomes much more defined. At 0600 UTC (figs. 39, 40, and 41), anticyclonic errors exist at 925, 850, and 700 hPa for ζ_t and ζ_x. ζ_A shows an anticyclonic error at 850 and 700 hPa, but shows a cyclonic error at 925 hPa. The errors at 1200 UTC (figs. 42, 43, and 44) also show anticyclonic bias at 925 and 700 hPa. A cyclonic bias in the error due to convergence in the streamline error of the wind shows at 850 hPa at 1200 UTC. The anticyclonic bias seen when the convection becomes intense is the cause for the model to predict the location and amount of rainfall incorrectly.

3.7 Conclusions and Discussion

Convection initiating away from major frontal boundaries can be very important to the Central Plains especially in the late summer where the North American Monsoon dominates the mid- to upper level circulation and reduces the rainfall in Iowa. The monsoon anticyclone prevents large-scale waves from developing and signifies weaker large-scale dynamics for deep troughs. In this weak dynamic regime, the low-level conditions become very important, especially because of the inversion layer seen in many soundings for these convective events. Low-level warm and moist air advection below the inversion layer aided by the LLJ helps to initiate convection away from major fronts and helps to create a conditionally unstable environment. Large values of surface based CAPE and strong shear create an environment that any type of small-scale perturbation can initiate convection.

The monsoon anticyclone suppresses the convection at initiation and prohibits it from gaining vertical extent. Vertical cross-sections of the vorticity budget show that intense vortex stretching at the lower levels coupled with the LLJ and some type of perturbation either at the surface or in the lower troposphere are able to produce rainfall without the presence of a major front. The divergent circulation in the forecast seems to be the reason for inaccurate forecasts showing anticyclonic bias or divergence (convergence) when there is convergence (divergence) expected where the observed rain is falling. Also common was the inability of the forecast to produce the precipitable water correctly. Smaller (larger) values of precipitable water in the forecast are associated with under-forecasted (over-forecasted) rainfall amounts.

From what has been shown in this paper, it is evident that the forecast needs to be improved. The late summer brings many problems because many convective rainfall events are not associated with extratropical cyclones. As shown, some events are not even associated with fronts and the model cannot reproduce the observed results. Accounting for the error in the divergent circulation is an improvement that clearly needs to be done when updating the Weather Research and Forecasting (WRF) model. Understanding the shallow convection at initiation, and how it is not steered by the upper level flow, will immensely help the improvement of the NAM and other models. This may occur in the form of improving the parameterization schemes or using much finer grid spacing in the models, which may account for a better simulation of the divergent circulation. Those relying on rainfall will especially benefit from further research on these events because of the importance of rainfall in late summer when it is fairly sparse.

3.8 Acknowledgements

Partial funding was given to support this work by the Cheney Research Fund. The authors would like to thank Jenq-Dar (Paul) Tsay for help with learning GrADS and FORTRAN and Daryl Herzmann for his assistance with the Iowa Environmental Mesonet data. The authors would also like to thank Dr. Jordan Alpert at NCEP for some assistance in gaining access to the NAM forecast data.

3.9 References

Bernardet, L. R., L. B. Nance, H.-Y. Chuang, A. Loughe, M. Demirtas, S. Koch, and R. Gall, 2005: The Developmental Testbed Center Winter Forecasting Experiment (DWFE). Preprints, *21st Conf. on Weather Analysis and Forecasting/17th Conf. on Numerical Weather Prediction*, Washington, DC, Amer. Meteor. Soc., 7.1. [Available online at http://ams.confex. com/ams/pdfpapers/94730.pdf.]

Bonner, W. D., 1968: Climatology of the low level jet. *Mon Weather Rev*, **96**, 833–850.

Browning, K. A., 1977: The structure and mechanisms of hailstorms. *Meteor. Monogr.*, **38**, 1-46.

Black, T. L., 1994: The new NMC mesoscale Eta model: description and forecast examples. *Wea. Forecasting*, **9**, 265–278.

Chen, T. C., 2003: Maintenance of summer monsoon circulations: a planetary-scale perspective. *J. Climate*, **16**, 2022–2037.

_____ , and J. A. Kpaeyeh, 1993: The synoptic-scale environment associated with the low-level jet of the great plains. *Mon. Wea. Rev.*, **121**, 416–420.

Clark, A. J., W. A. Gallus Jr., and T. C. Chen, 2007: Comparison of the diurnal precipitation cycle in convective-resolving and non-convection-resolving mesoscale models. *Mon. Wea. Rev*., **135**, 3456–3473.

Heideman, K. F., J. M. Fritsch, 1988: Forcing mechanisms and other characteristics of significant summertime precipitation. *Wea. Forecasting*, **3**, 115–130.

Higgins W. R., Y. Yao, X.L. Wang, 1997: Influence of the North American Monsoon System on the United States summer precipitation regime. *J. Clim*., **10**, 2600–2622.

Holton, J. R., 2004: *An Introduction to Dynamic Meteorology*. 4th ed. Academic Press, 535 pp.

Jankov, I., and W. A. Gallus, 2004: MCS rainfall forecast accuracy as a function of large-scale forcing. *Wea. Forecasting*, **19**, 428–439.

Johns, R. H., 1984: A synoptic climatology of northwest-flow severe weather outbreaks. Part II: Meteorological parameters and synoptic patterns. *Mon. Wea. Rev.*, **112**, 449–464.

Kummerow, C., and Coauthors, 2000: The status of the Tropical Rainfall Measuring Mission (TRMM) after two years in orbit. *J. Appl. Meteor.,* **39,** 1965–1982.

Maddox, R. A., C. A. Doswell, 1982: An examination of jet stream configurations, 500 mb vorticity advection and low-level thermal advection patterns during extended periods of intense convection. *Mon. Wea. Rev.*, **110**, 184–197.

Marwitz, J. D., 1972: The structure and motion of severe hailstorms. Part II: Multi-cell storms. *J. Appl. Meteor.*, **11**, 180–188.

Mesinger, F., and Coauthors, 2006: North American Regional Reanalysis. *Bull. Amer. Meteor. Soc*., **87**, 343–360.

Newton, C. W., 1950: Structure and mechanism of the pre-frontal squall line. *J. Meteor.*, **7,** 210-222.

Rauber, R. M., J. E. Walsh, and D. J. Charlevoix, 2002: *Severe and Hazardous Weather.* Kendall/Hunt, 616 pp.

Stensrud, D. J. and J. M. Fritsch, 1994: Mesoscale convective systems in weakly forced large-scale environments. Part II: Generation of a mesoscale initial condition. *Mon. Wea. Rev*., **122**, 2068–2083.

Stull, R. B., 1988: *An Introduction to Boundary Layer Meteorology*. Kluwer, 666 pp.

Trier, S. B., C. A. Davis, D. A. Ahijevych, M. L. Weisman, and G. H. Bryan, 2006: Mechanisms supporting long-lived episodes of propagating nocturnal convection within a 7-Day WRF model simulation. *J. Atmos. Sci*., **63**, 2437–2461.

TRMM Senior Review Proposal, 2007. [Available online at http://trmm.gsfc.nasa .gov/trmm_rain/Events/TRMMSenRev2007_pub.pdf.]

Wallace, J. M., 1975: Diurnal variations in precipitation and thunderstorm frequency over the conterminous United States. *Mon. Wea. Rev.*, **103**, 406–419.

Wang, S.-Y., T.-C. Chen, and J. Correia, 2009: Climatology of summer midtropospheric perturbations in the U.S. Northern Plains. Part I: Influence on northwest flow severe weather outbreaks. *Climate Dyn*., **36,** 793-810.

Wang, S. Y., T. C. Chen, and S. E. Taylor, 2009: Evaluations of NAM Forecasts on Midtropospheric Perturbation-Induced Convective Storms over the U.S. Northern Plains. *Wea. Forecasting.*, **24,** 1309–1333.

Zhang, D. L., 1992: The formation of a cooling-induced mesovortex in the trailing stratiform region of a midlatitude squall line. *Mon. Wea. Rev*., **120**, 2763–2785.

3.10 Tables

Table 1. Case times and dates, maximum 200 hPa height and location, maximum 925 hPa wind and location, and maximum 850 hPa wind and location. Yellow indicates being beyond the standard deviation.

CASE Day and Time		Max φ 200 hPa		Max Location		Max *V* 925 hPa	Max Location		Max *V* 850 hPa	Max Location	
21z 08/01/04 to 18z 08/02/04		12543.00		101.99	30.16	20.72	96.06	39.38	15.07	98.03	39.09
21z 06/20/05 to 18z 06/21/05		12523.30		64.28	27.23	16.22	86.59	42.84	18.65	94.19	48.56
03z 06/29/05 to 18z 06/29/05		12544.80		106.47	27.53	20.88	96.25	40.31	23.27	99.63	38.91
06z 07/31/05 to 00z 08/01/05		12574.20		113.15	30.29	25.82	95.31	41.81	22.16	95.41	41.72
21z 08/17/05 to 18z 08/18/05		12562.20		100.47	32.30	21.70	96.06	37.03	19.44	98.31	39.56
03z 08/05/06 to 21z 08/05/06		12564.60		100.75	30.21	21.32	95.97	43.03	23.99	101.31	46.22
00z 08/09/06 to 18z 08/09/06		12561.70		96.76	33.91	19.14	96.81	36.00	18.20	101.50	36.94
15z 06/14/08 to 06z 06/15/08		12497.00		106.59	27.94	15.13	85.00	45.94	18.23	95.88	44.63
00z 07/10/08 to 00z 07/11/08		12532.40		108.04	30.83	13.83	96.44	40.97	19.51	99.53	39.38
06z 07/12/09 to 21z 07/12/09		12567.80		99.31	31.47	18.34	93.44	36.56	20.05	83.22	49.88
18z 07/10/10 to 18z 07/11/10		12583.40		103.06	29.69	18.40	95.78	41.91	20.18	99.91	37.50
15z 08/04/11 to 06z 08/05/11		12589.90		90.63	33.47	12.97	86.22	49.03	12.01	89.78	48.84
03z 08/16/11 to 21z 08/16/11		12567.90		107.85	31.63	19.67	96.06	39.56	27.92	104.03	46.41
12z 08/18/11 to 06z 08/19/11		12563.50		104.61	32.52	14.46	90.81	49.13	14.78	90.91	48.94
03z 08/22/11 to 18z 08/22/11		12569.50		98.28	31.56	18.15	99.06	48.28	17.42	91.38	36.38
	AVERAGE	**12556.35**		**100.15**	**30.72**	**18.45**	**93.73**	**42.12**	**19.39**	**96.20**	**42.86**
	STD DEV	**24.34**		**11.33**	**2.03**	**3.48**	**4.41**	**4.34**	**3.96**	**5.51**	**4.94**

3.11 Figures

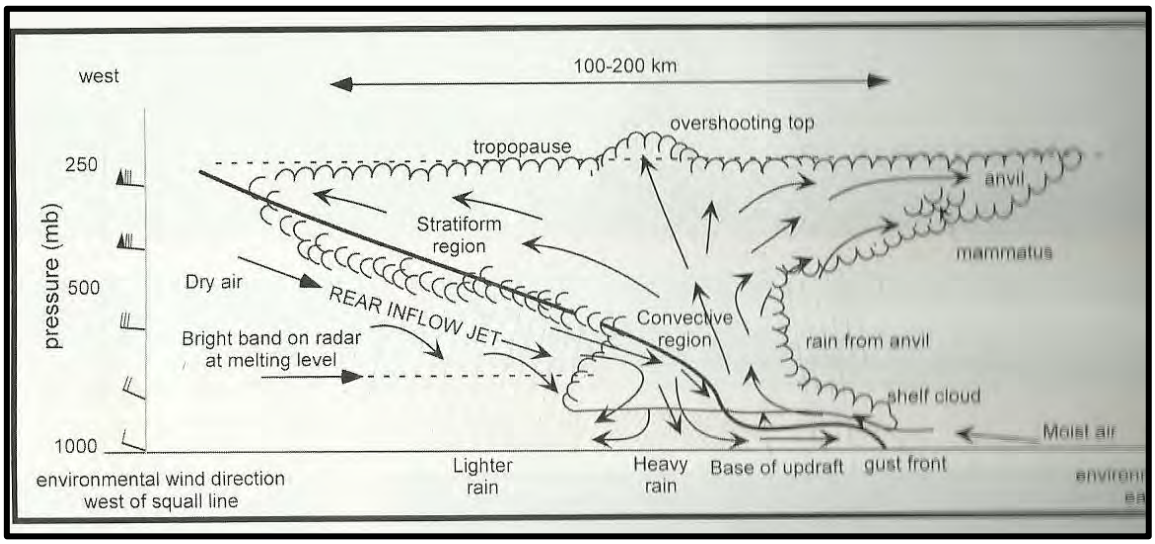

Figure 1. Typical squall line cross-section from Raubert et al. (2002).

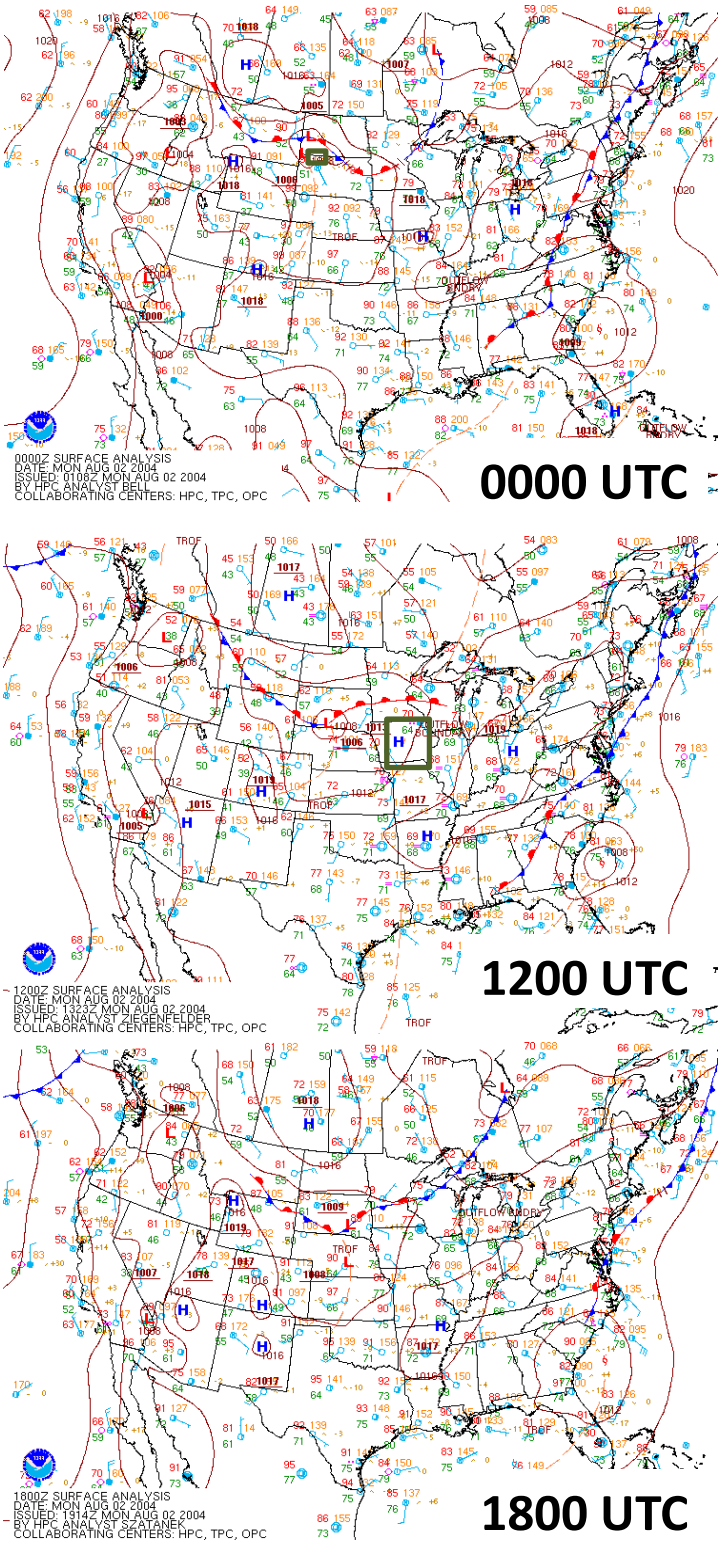

Figure 2. Surface analysis maps from the WPC for three different times for 02 August 2004. The black box highlights the area of rainfall.

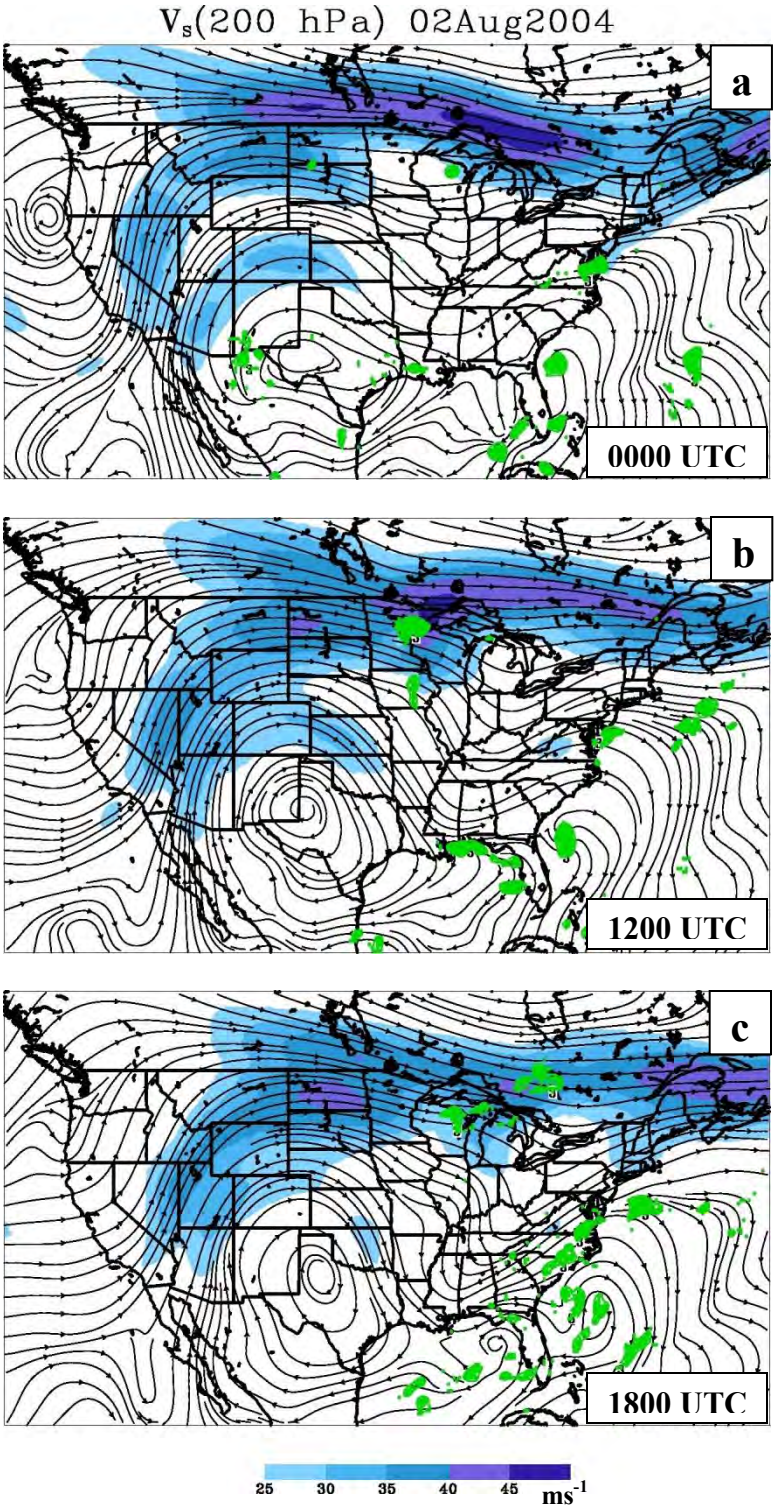

Figure 3. Streamlines at 200 hPa for 0000, 1200, and 1800 UTC 02 August 2004. The rainfall (mm) is contoured in green. The shaded variable is the magnitude of the wind.

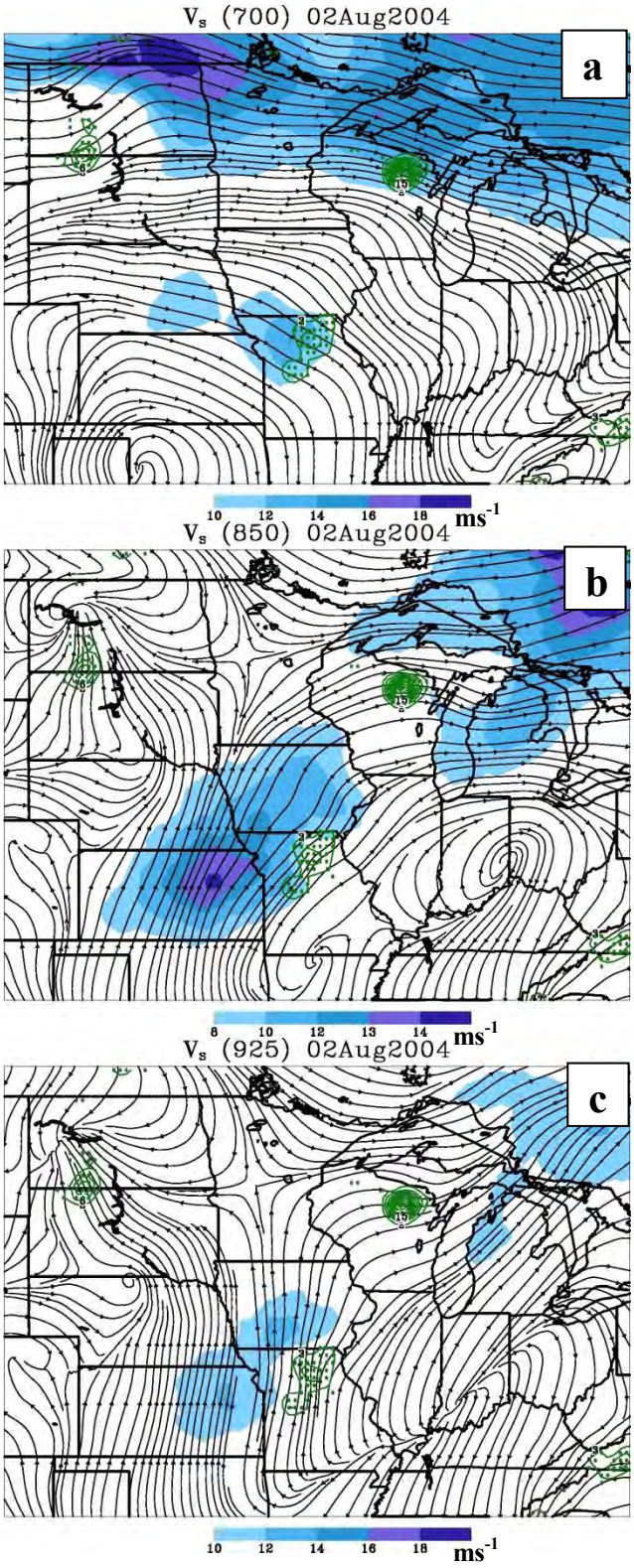

Figure 4. Streamlines at 925, 850, and 700 hPa at 0000 UTC. The rainfall (mm) is contoured in green and the shading is the magnitude of the wind.

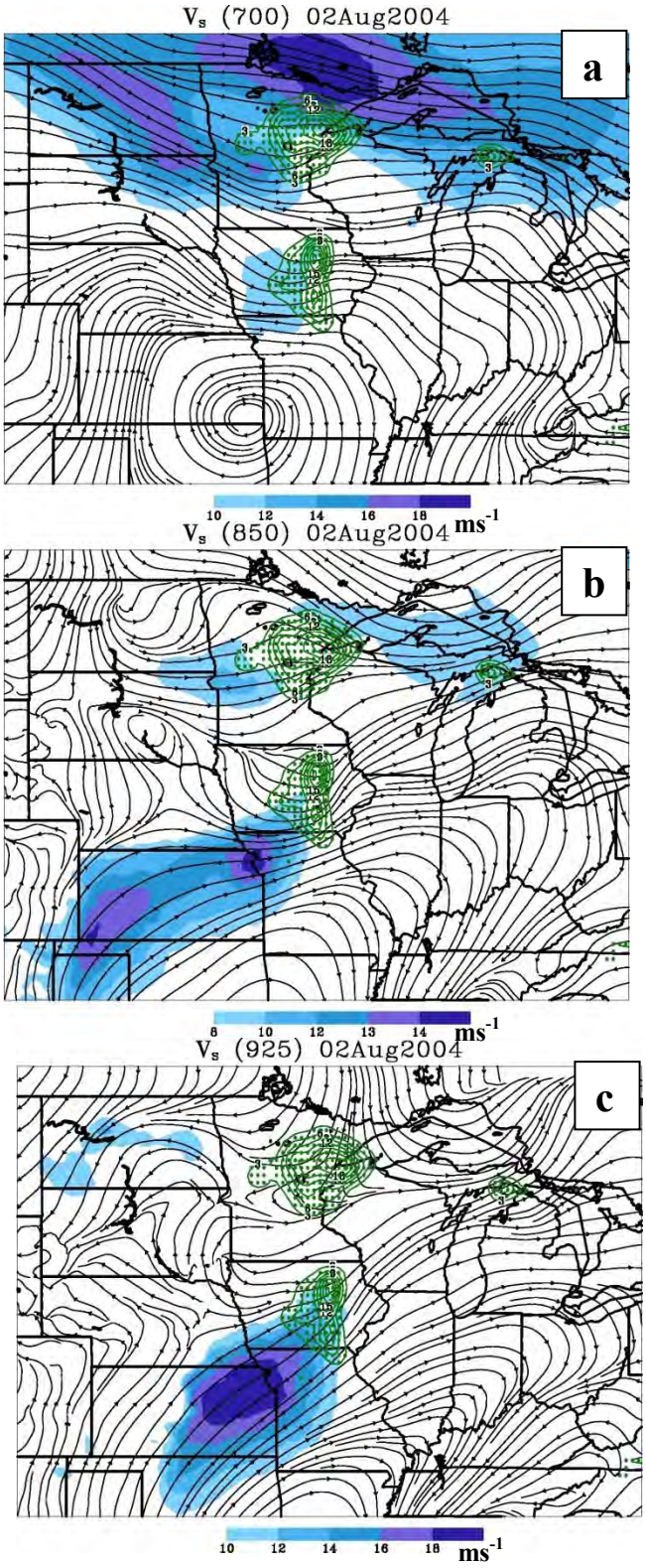

Figure 5. Same as in figure 4, but for 1200 UTC.

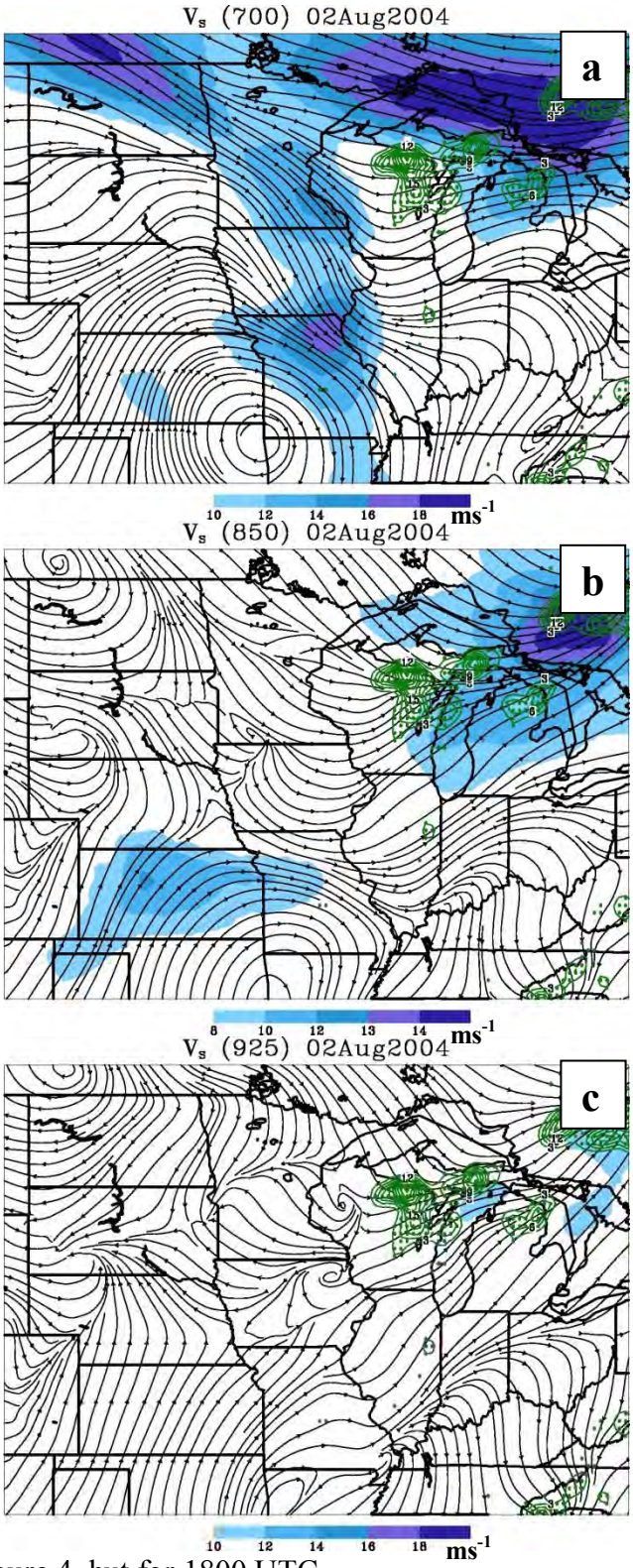

Figure 6. Same as in figure 4, but for 1800 UTC.

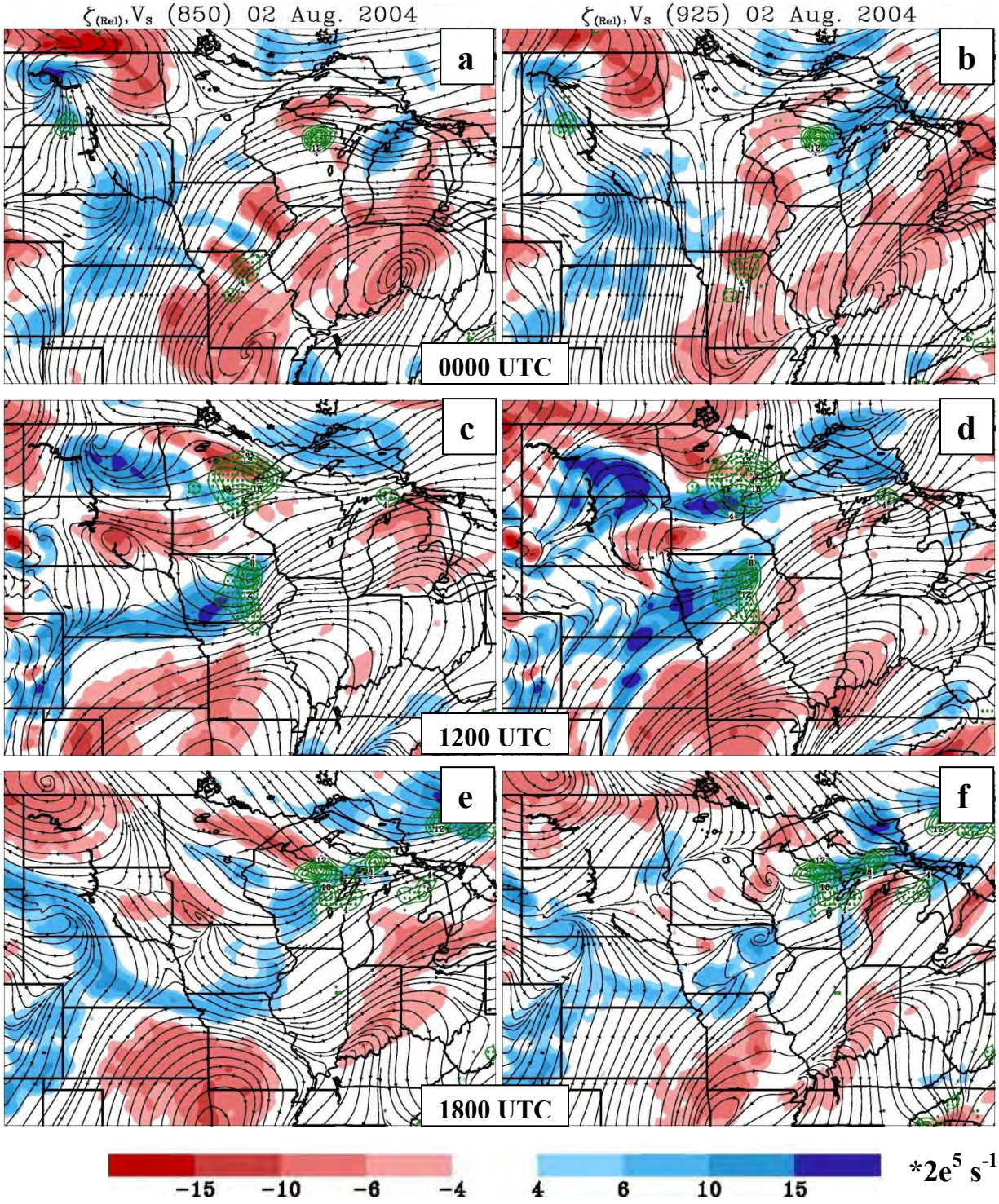

Figure 7. The relative vorticity field and streamlines at 925 and 850 for all three stages. The rainfall (mm) is contoured in green.

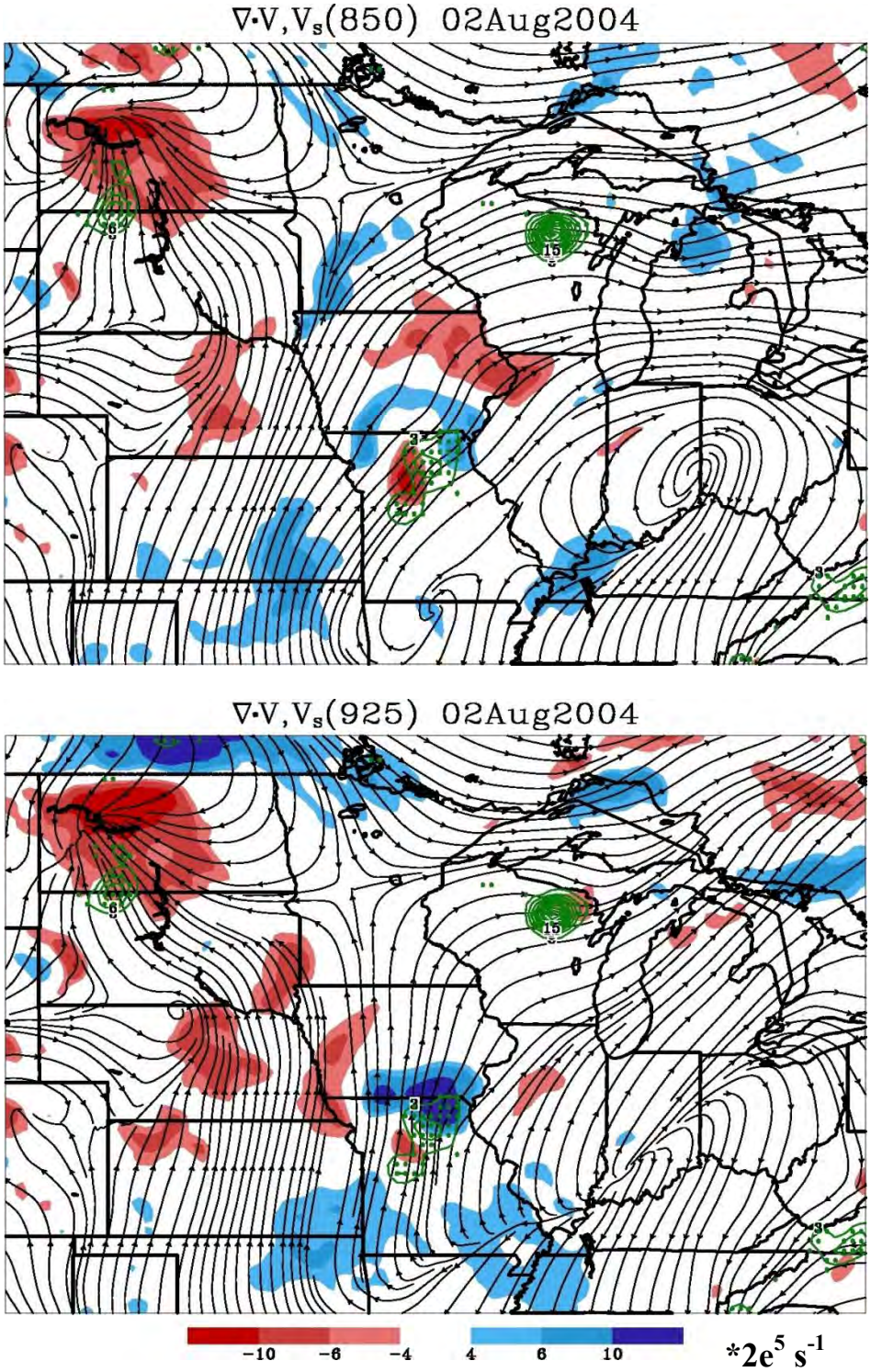

Figure 8. The divergence field and streamlines at 925 and 850 hPa for the initial time step 0000 UTC. The rainfall (mm) is contoured in green.

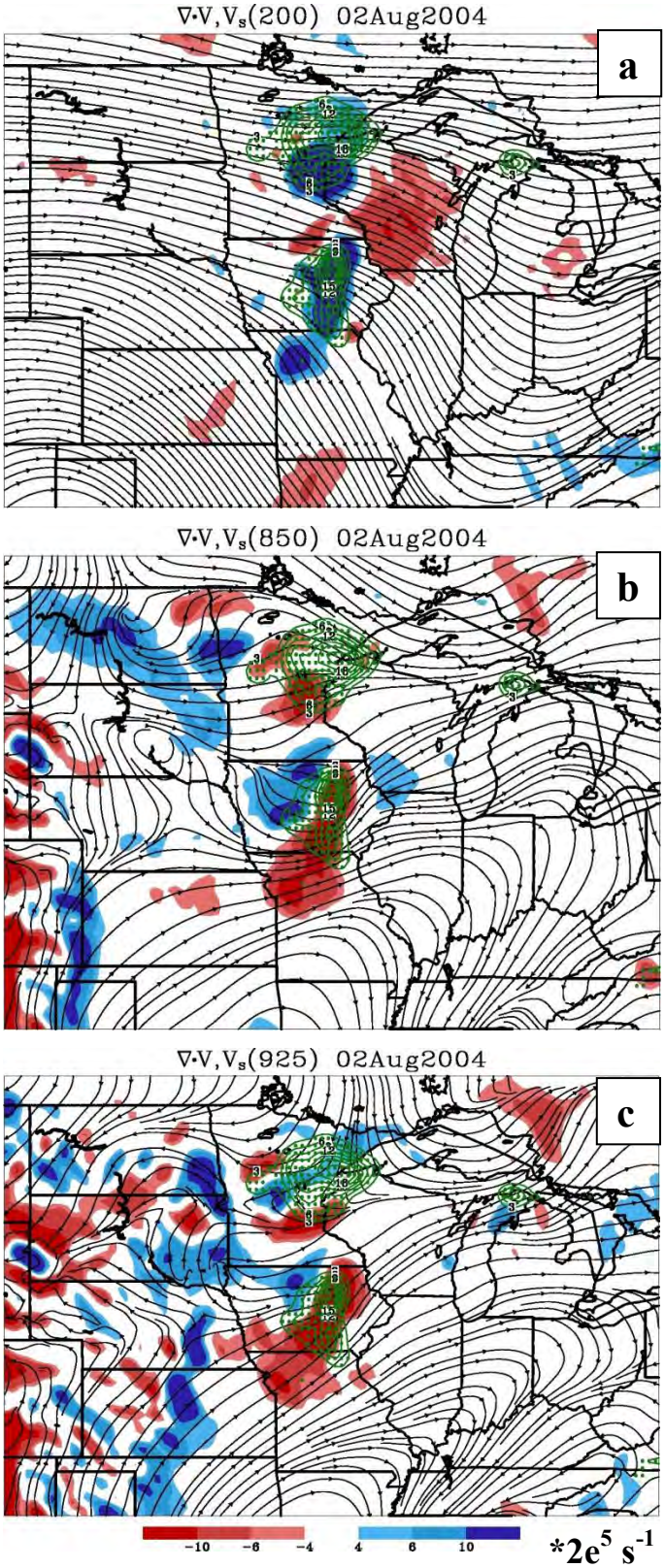

Figure 9. The divergence field and streamlines at 925, 850, and 200 hPa at 1200 UTC. The rainfall is contoured in green.

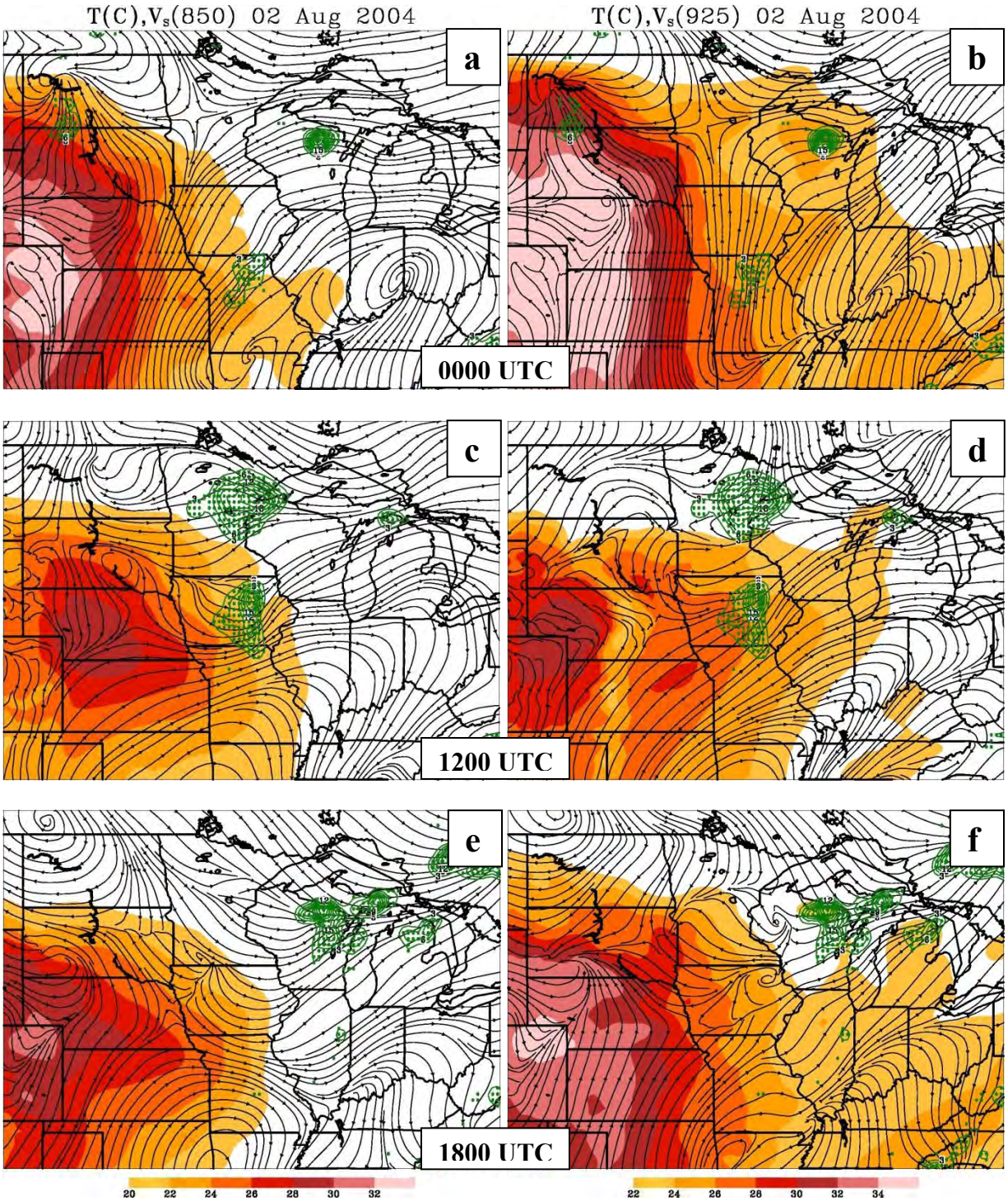

Figure 10. The temperature (C) and streamlines at 925 and 850 for all three stages. The rainfall (mm) is contoured in green.

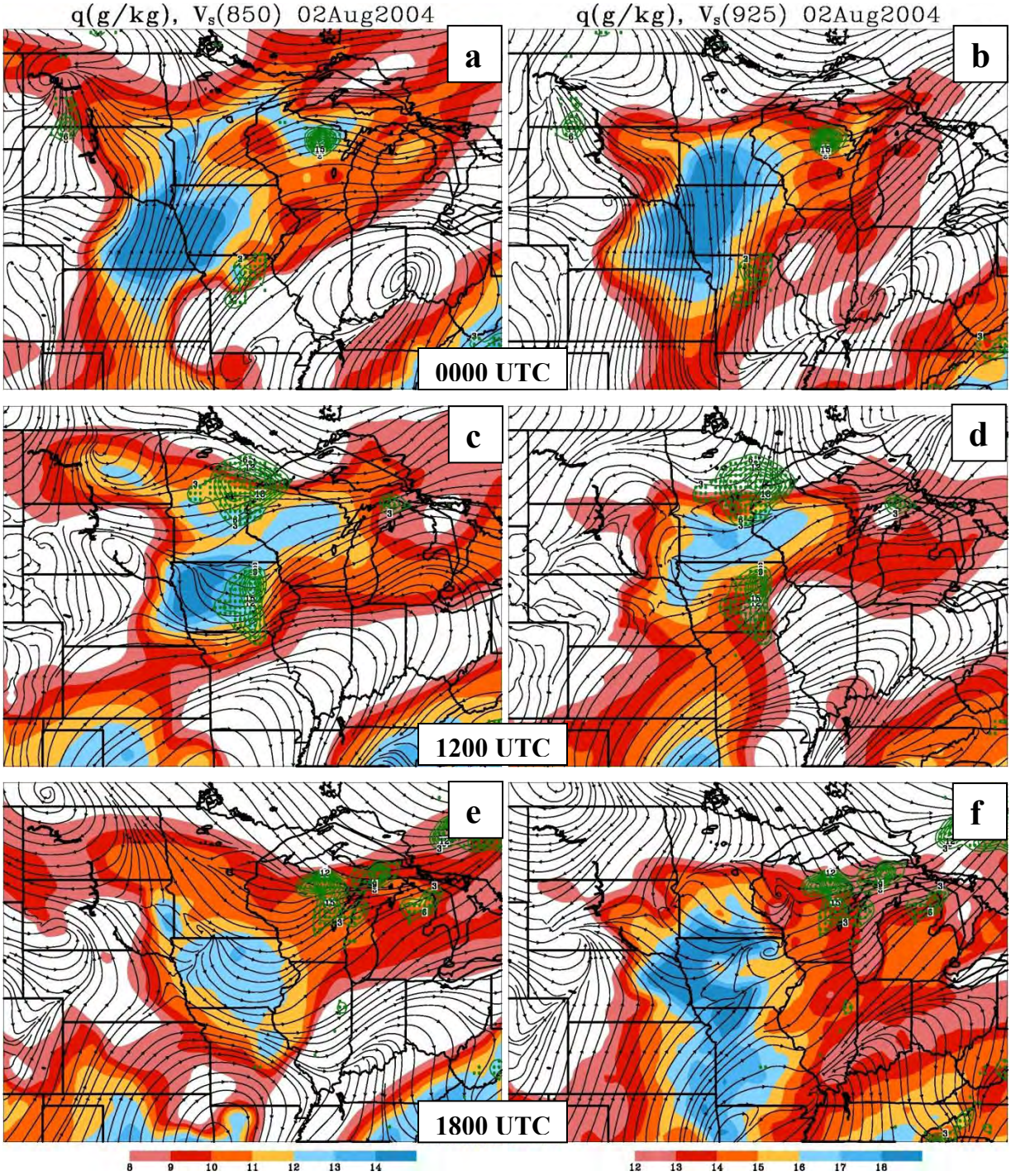

Figure 11. Specific humidity (g/kg) and streamlines at 925 and 850 hPa for all three stages. Rainfall (mm) is contoured in green.

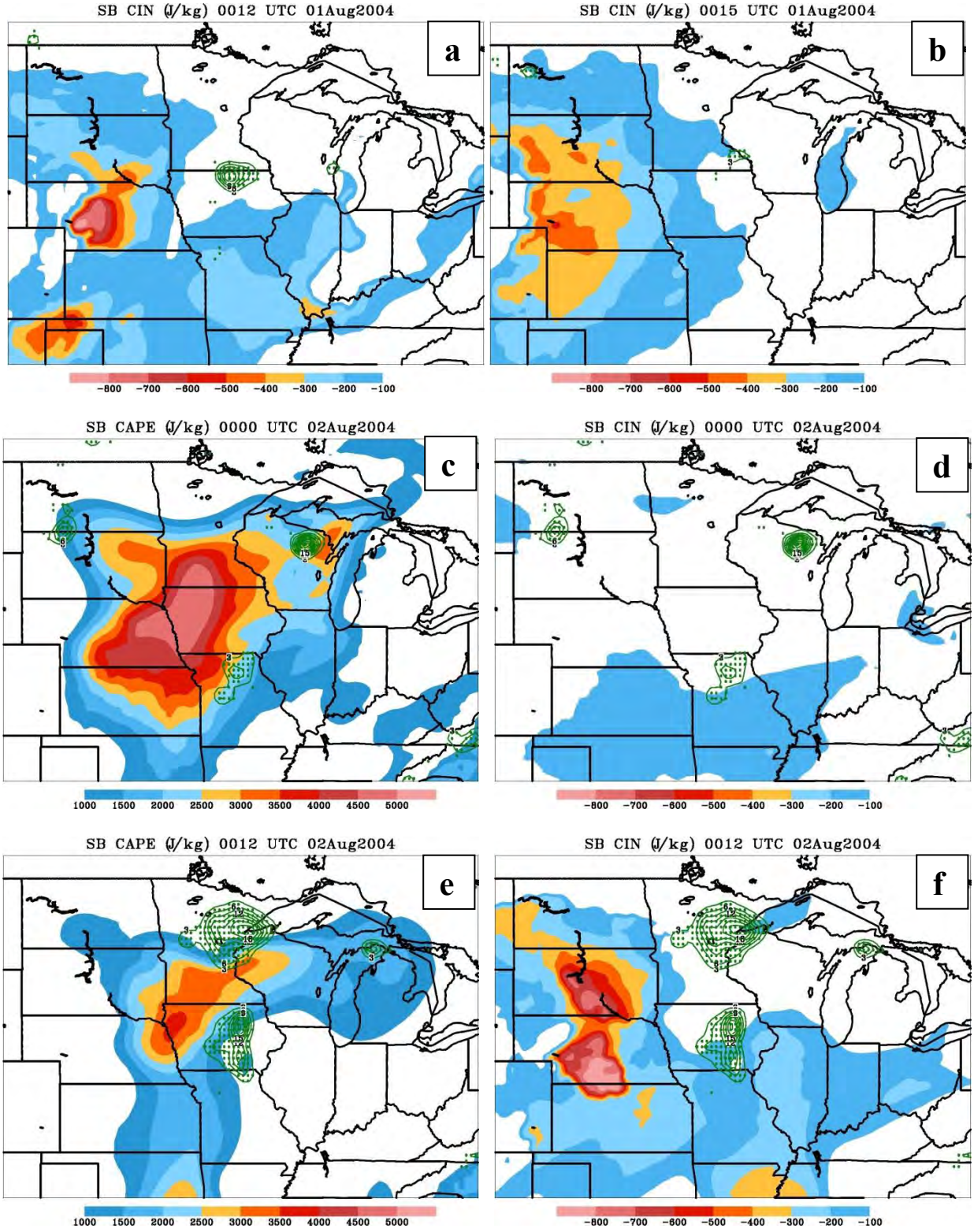

Figure 12. Surface based CAPE and CIN for 0000 and 1200 UTC 02 August 2004 along with just CIN for 1200 and 1500 UTC 01 August 2004. The rainfall is contoured in green.

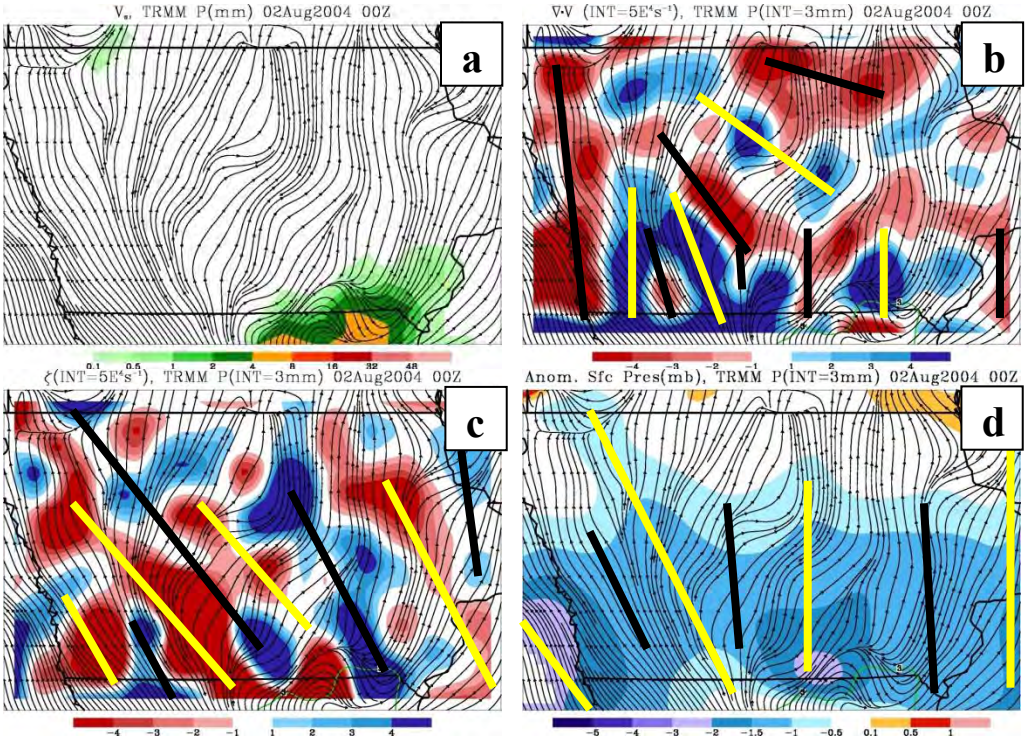

Figure 13. The mesonet plots inlcuding the streamlines, rainfall, divergence, vorticity, and surface pressure fields for 0000 UTC. The solid lines indicate the waves seen in the respective fields.

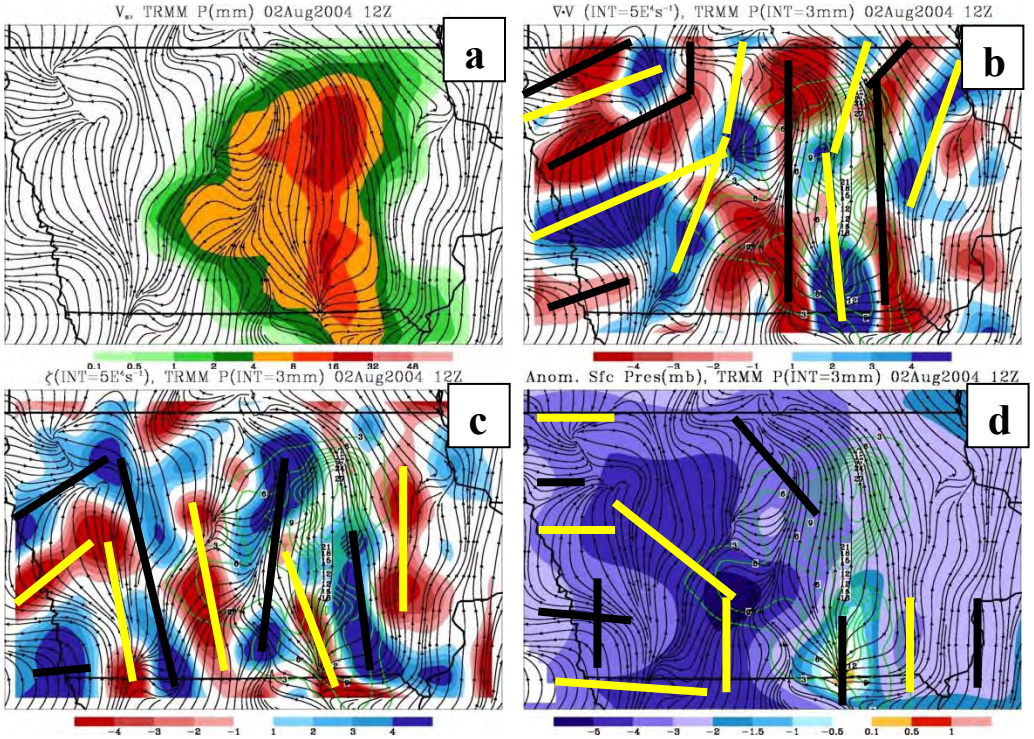

Figure 14. Same as in figure 13, but for 1200 UTC when the rainfall is its most intense.

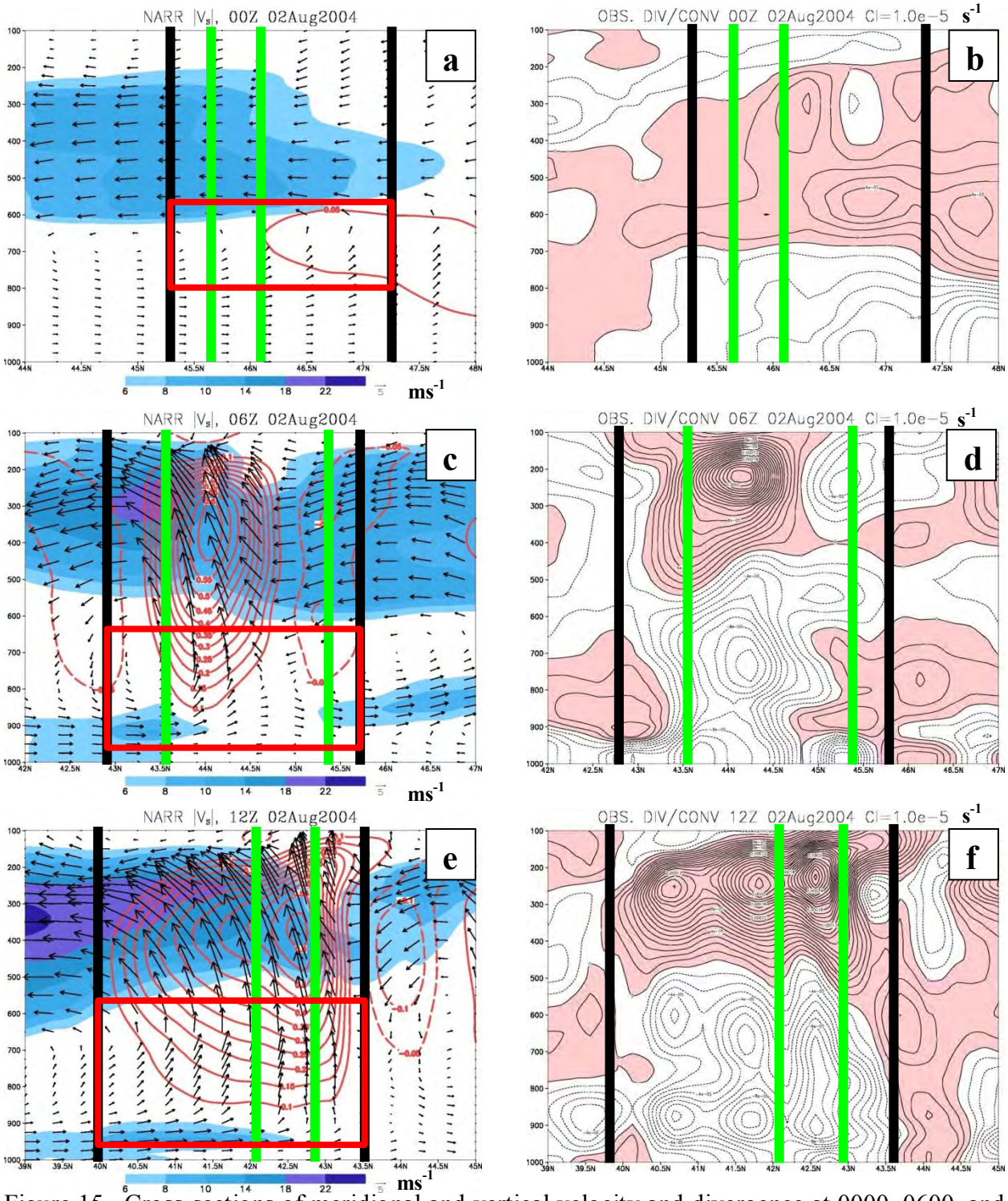

Figure 15. Cross-sections of meridional and vertical velocity and divergence at 0000, 0600, and 1200 UTC. The black lines indicate the location of the rainfall and the green lines indicate the heaviest rainfall. The red box indicates where the greatest shear is occurring. The shaded value in the wind vector plot is the magnitude of the winds while the red contour is the vertical velocity.

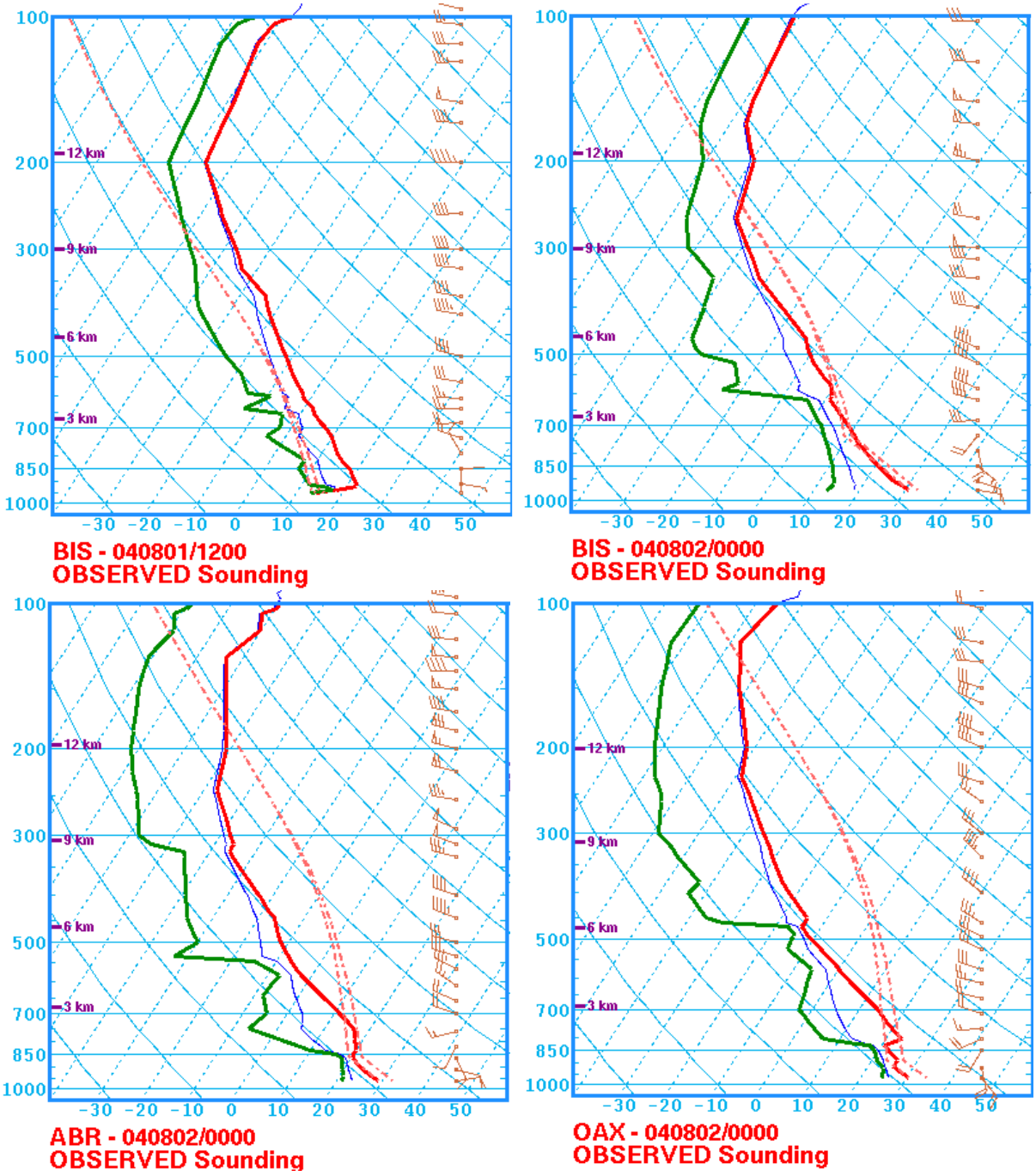

Figure 16. The top two soundings are taken from Bismarck, ND (BIS) at 1200 on 01 Augusts and 0000 UTC on 02 August. Soundings taken at 0000 UTC on 02 August for Aberdeen, South Dakota (ABR) and Omaha, Nebraska (OAX).

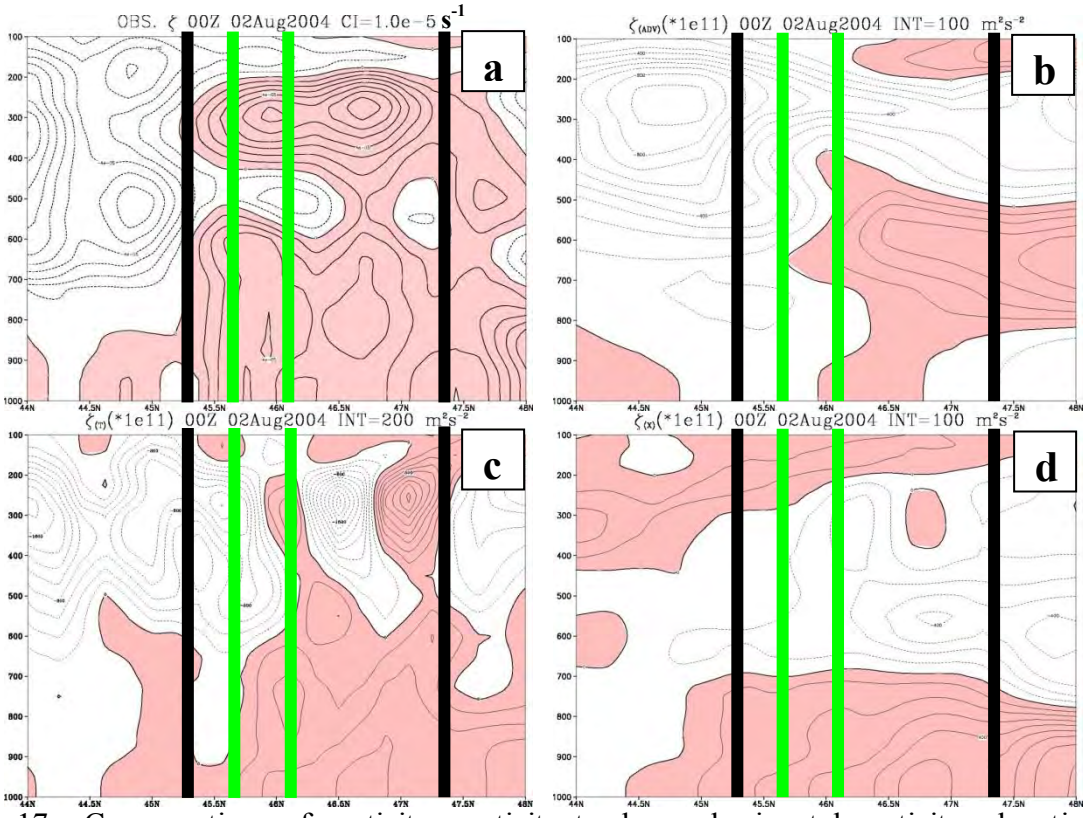

Figure 17. Cross-sections of vorticity, vorticity tendency, horizontal vorticity advection, and vortex stretching at 0000 UTC. The black and green lines are similar to figure 15.

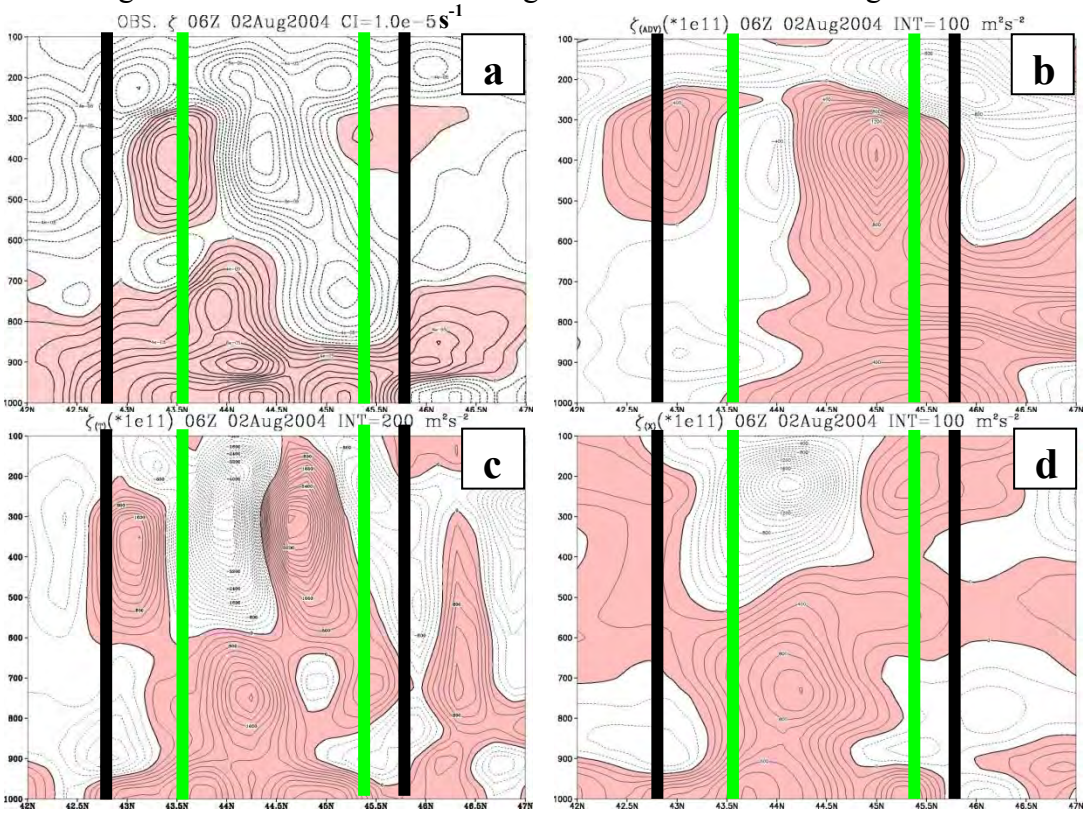

Figure 18. Similar to figure 17, but at 0600 UTC.

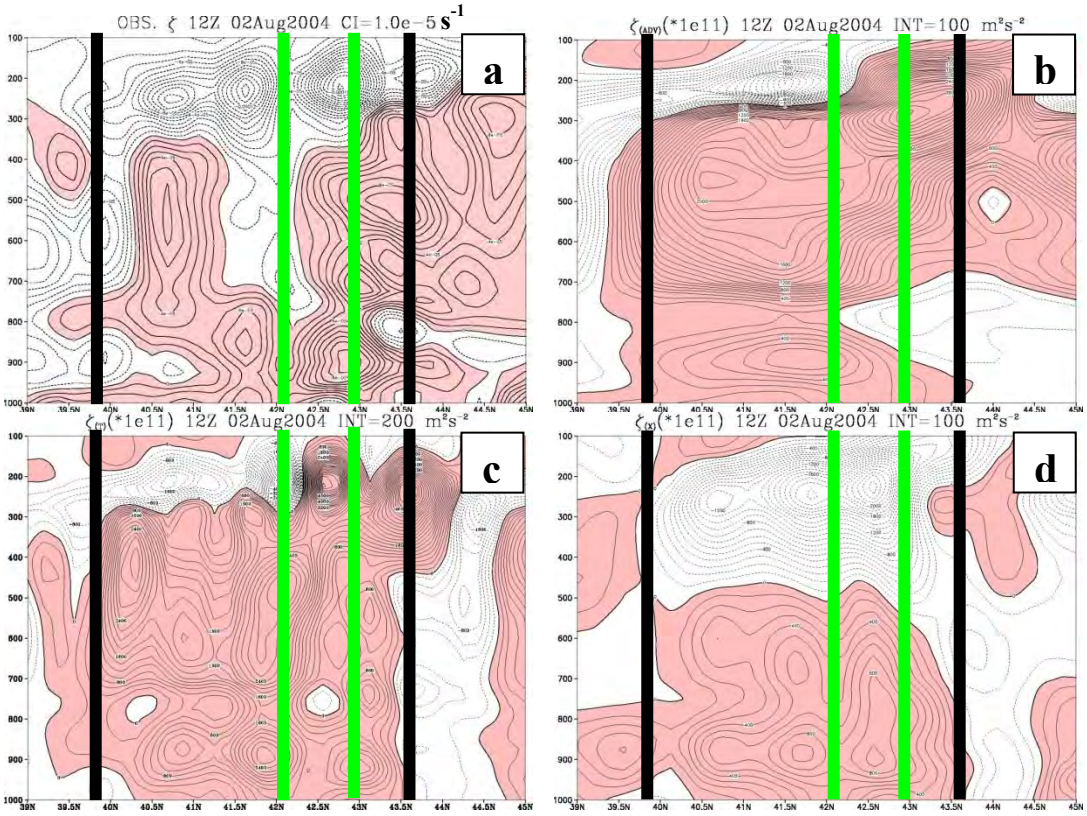

Figure 19. Similar to figure 17, but at 1200 UTC.

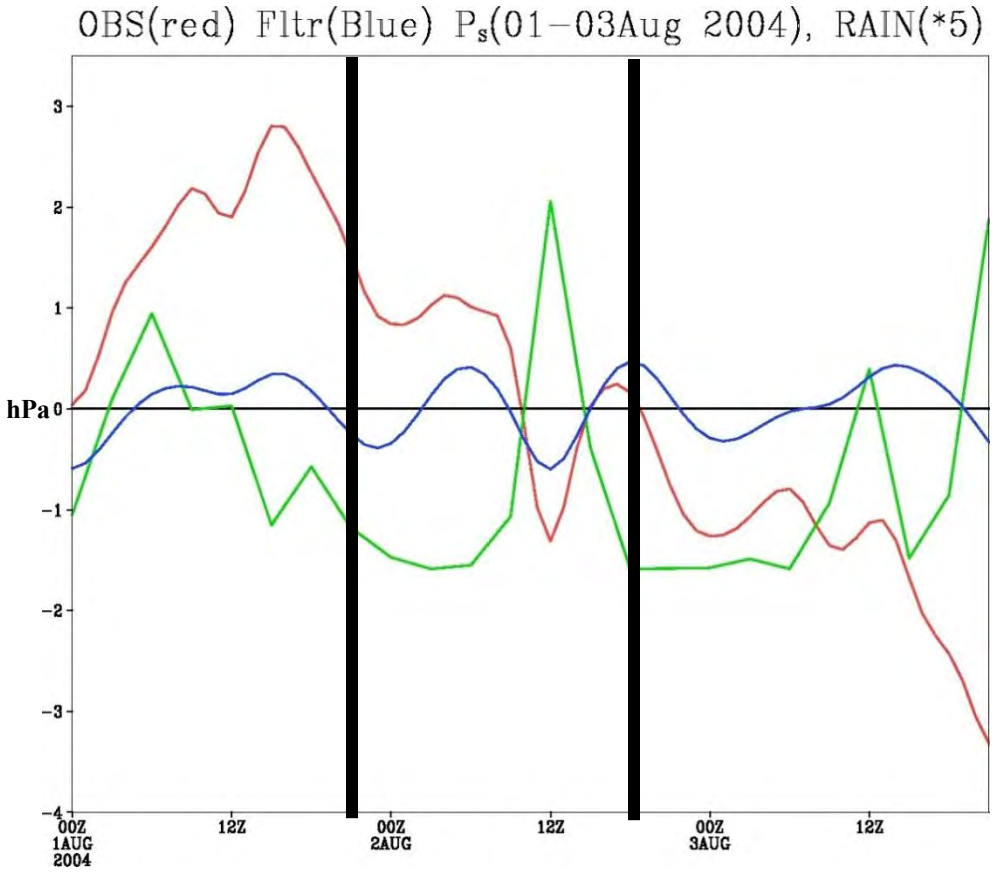

Figure 20. Surface pressure over a three-day period including 02 August 2004. Rainfall is contoured in green, the observed surface pressure in red, and the filtered surface pressure is in blue.

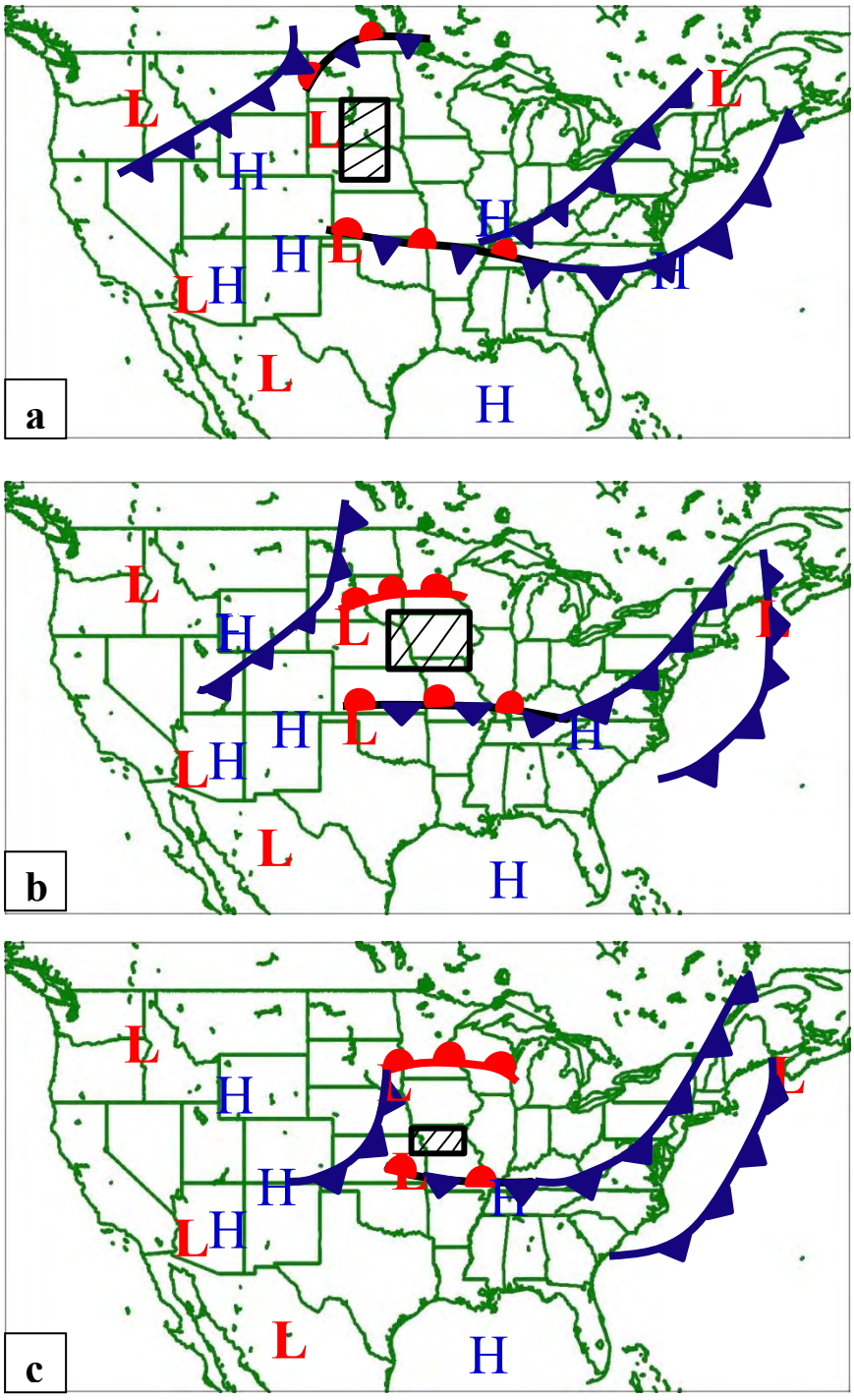

Figure 21. The composite surface analysis charts at the three stages of the convection. The black box highlights the composite rainfall.

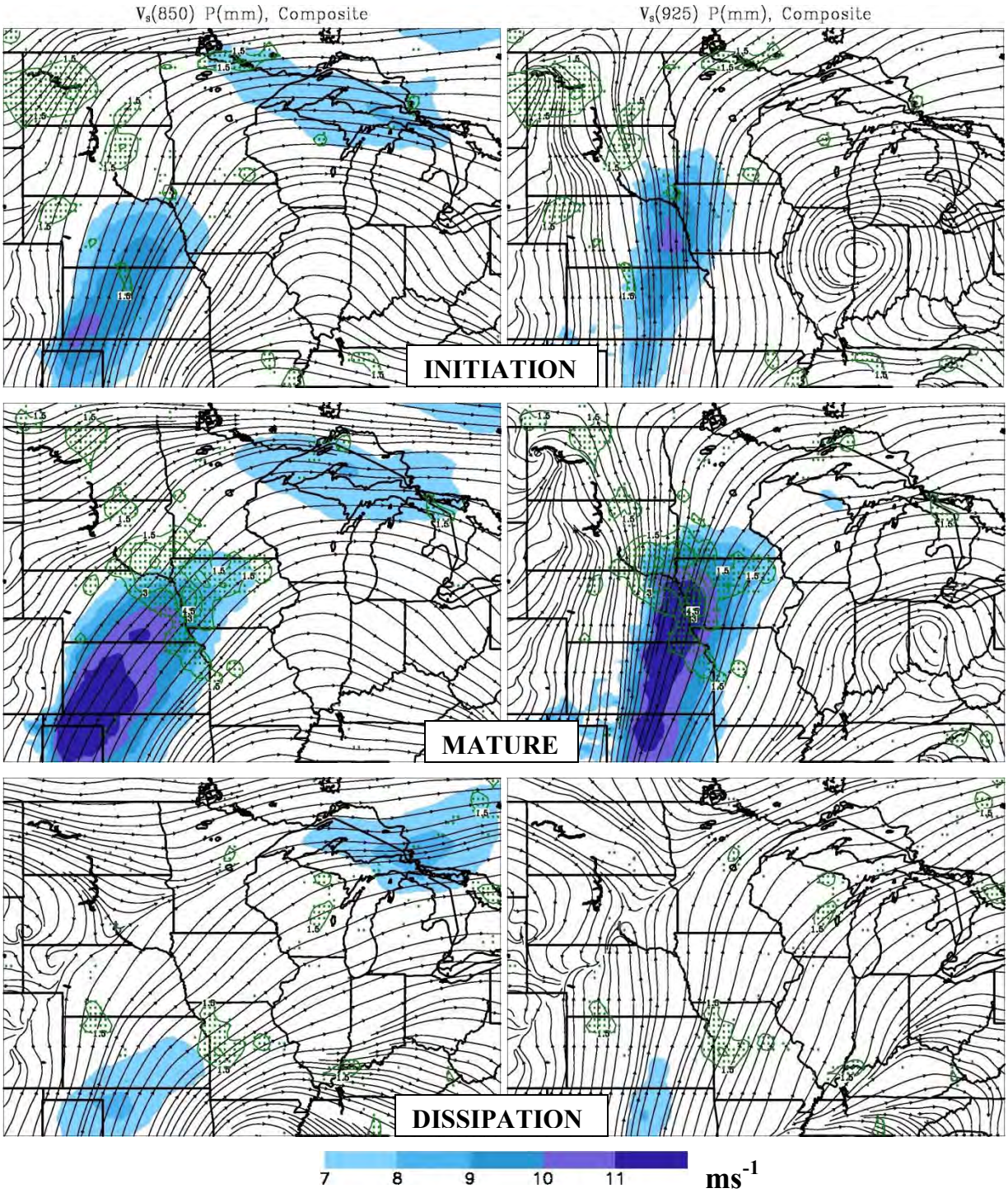

Figure 22. Streamlines at all three stages for the composite. The magnitude of the wind is shaded and the rainfall (mm) is contoured in green.

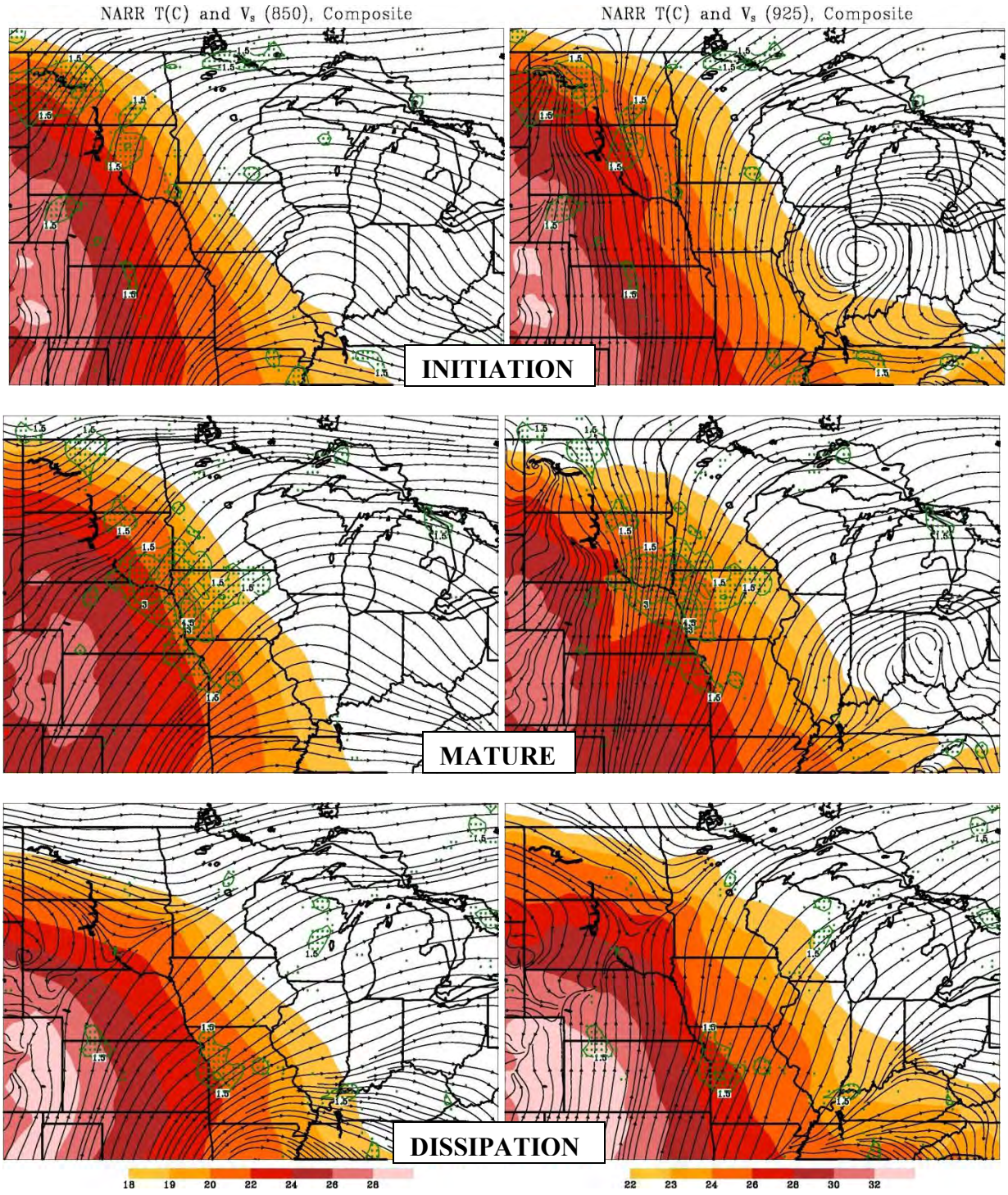

Figure 23. Temperature (C) and streamlines at three different stages for the composite. Rainfall (mm) is contoured in green.

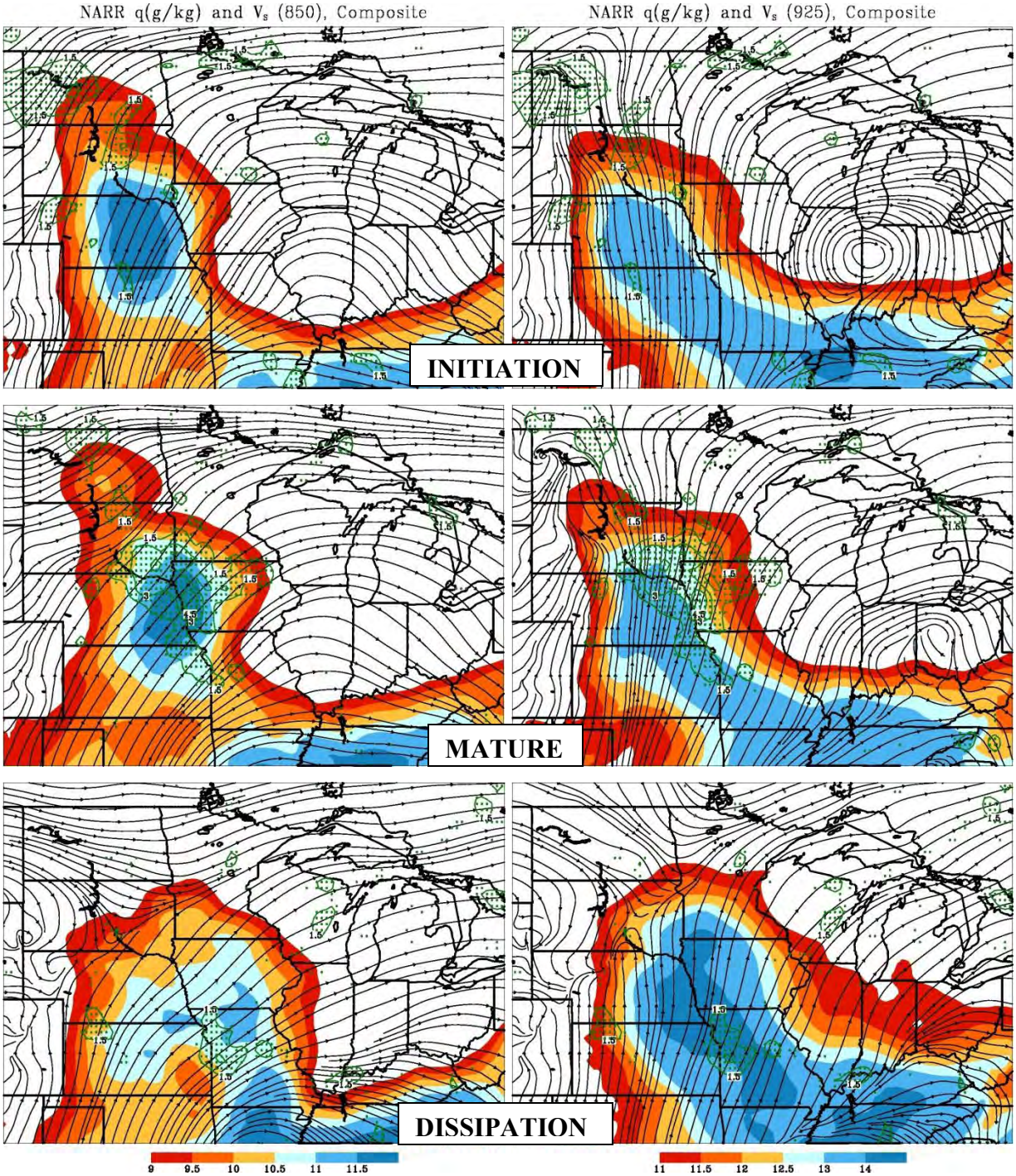

Figure 24. Specific humidity (g/kg) and streamlines at three stages of the composite. The rainfall (mm) is contoured in green.

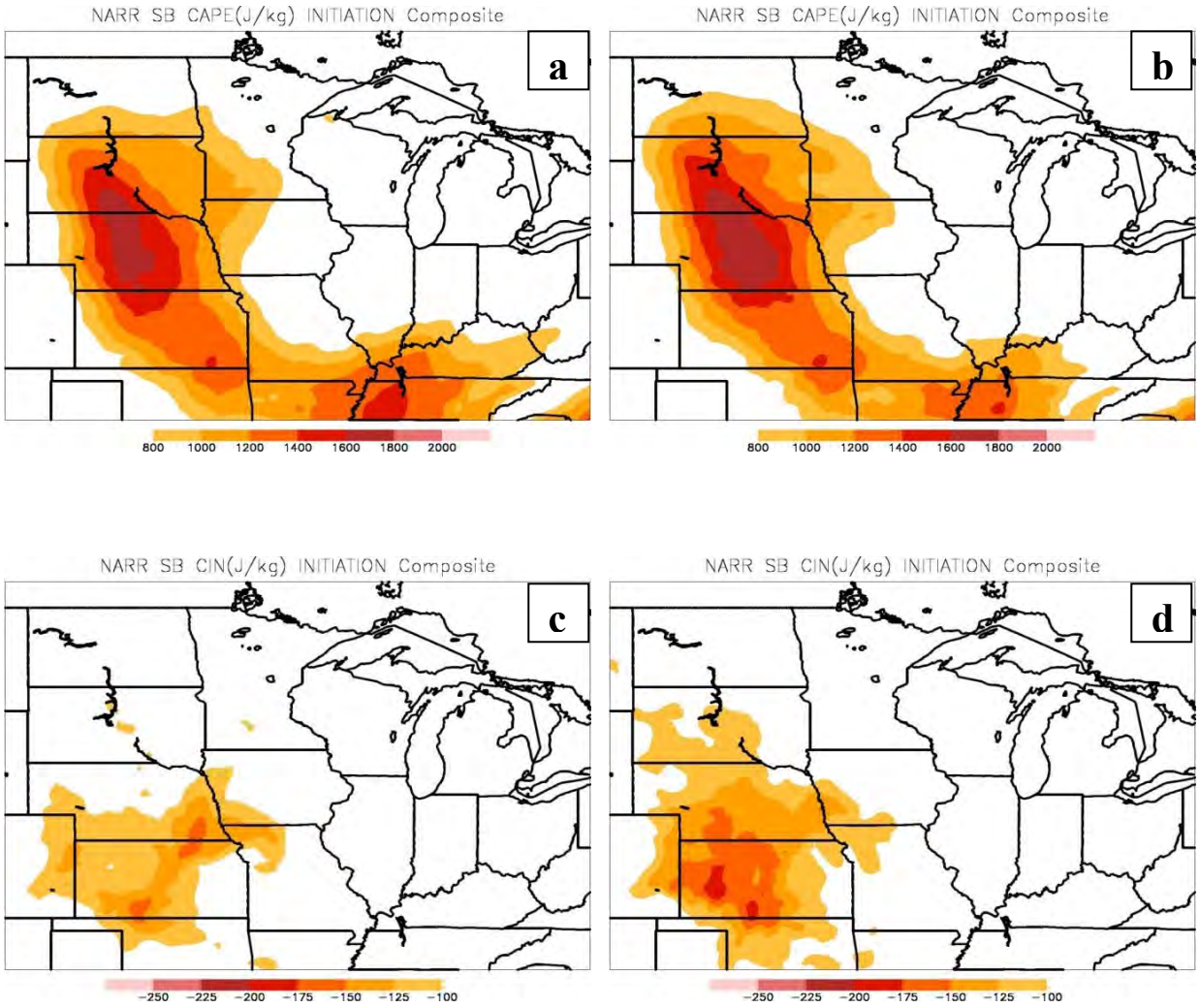

Figure 25. Surface-based CAPE and CIN at the initiation stage timesteps.

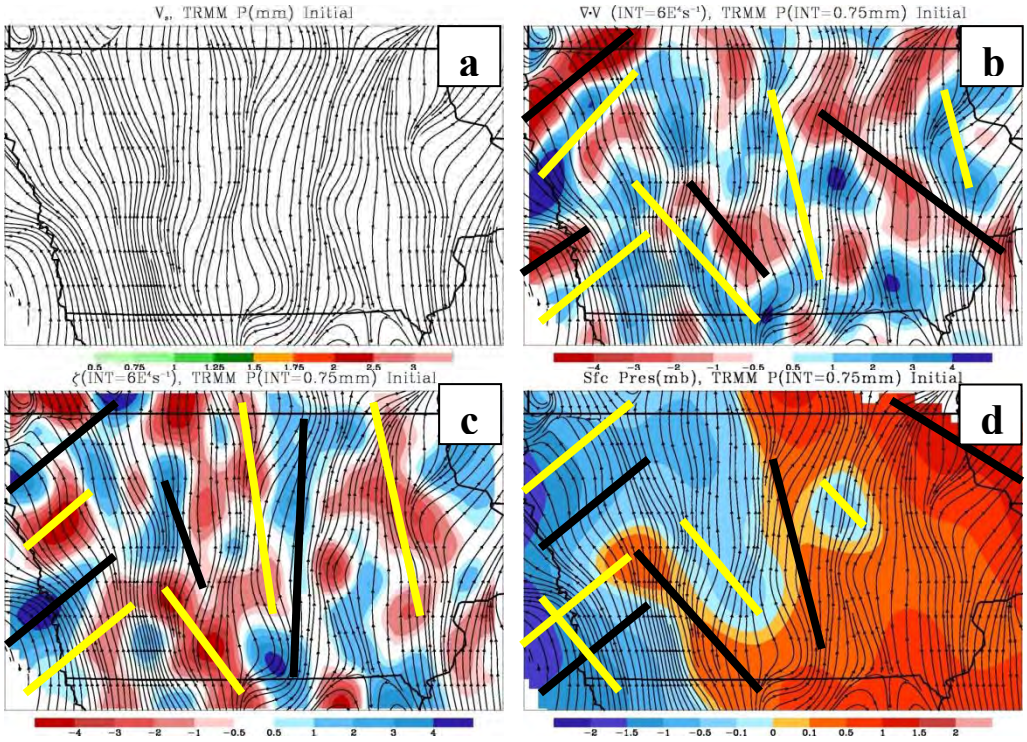

Figure 26. Mesoanalysis plots at the initial stage as in figures 13 and 14.

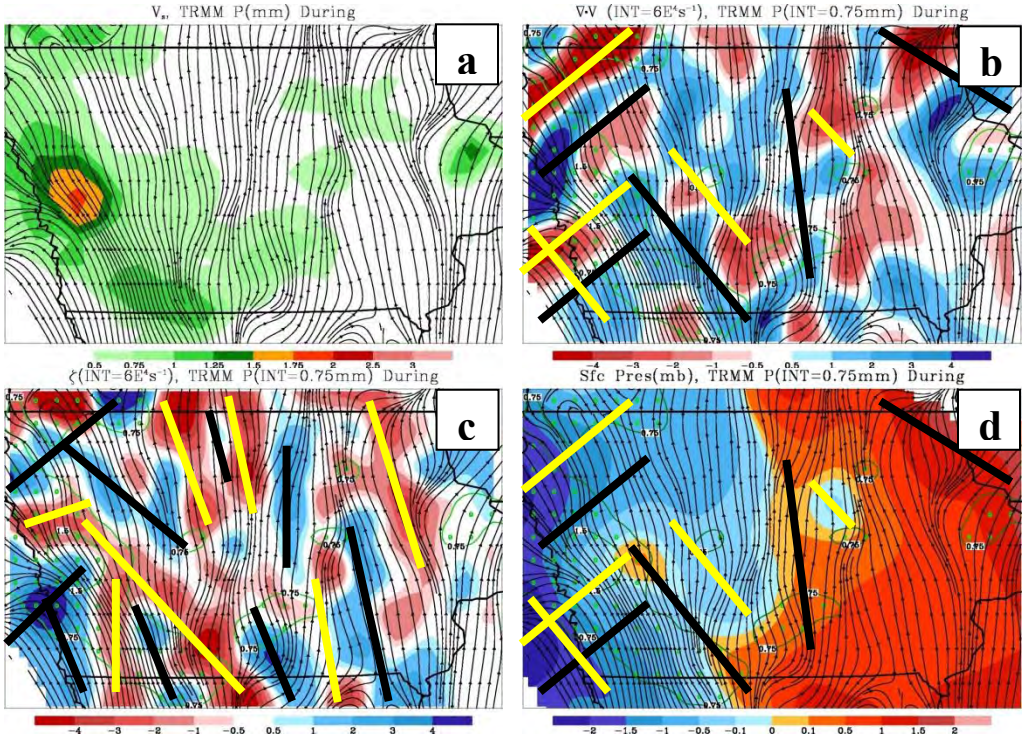

Figure 27. Mesoanalysis plots at the mature stage similar to figure 26.

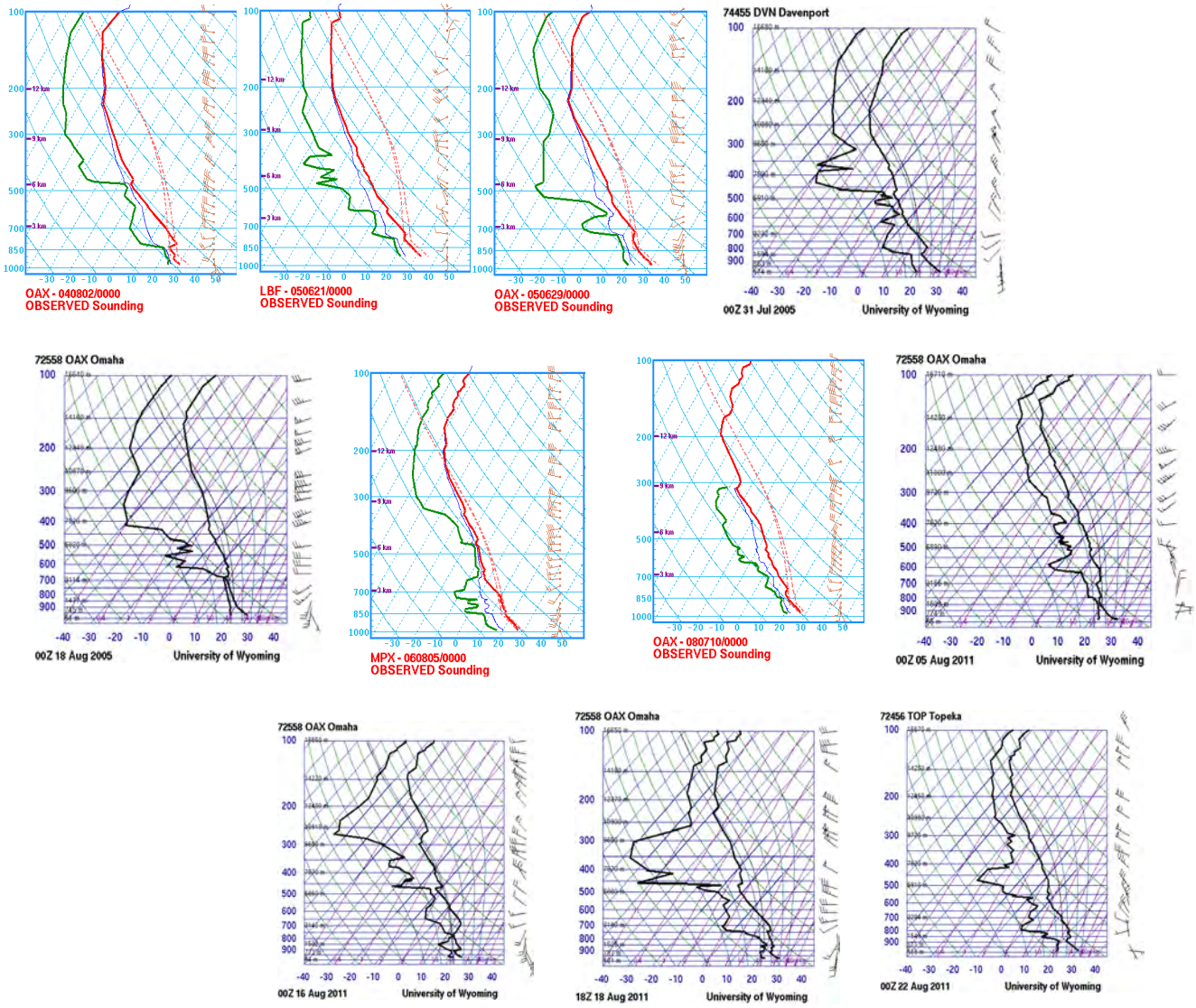

Figure 28. An array of the soundings taken at locations around the Central Plains near the time of initiation.

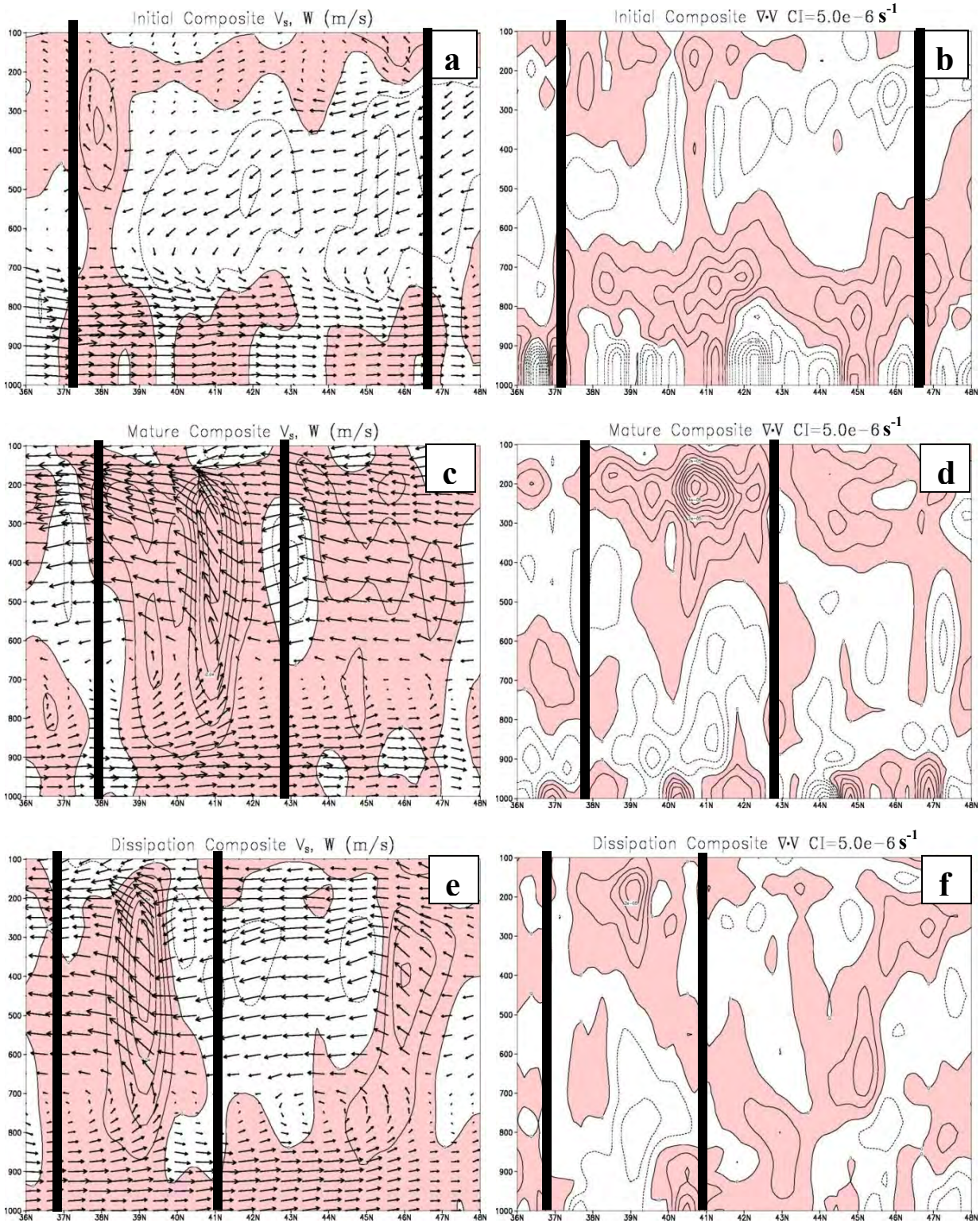

Figure 29. Cross-sections for all three stages for meridional and vertical veloctity and divergence. The black lines indicate where the composite rainfall is occuring

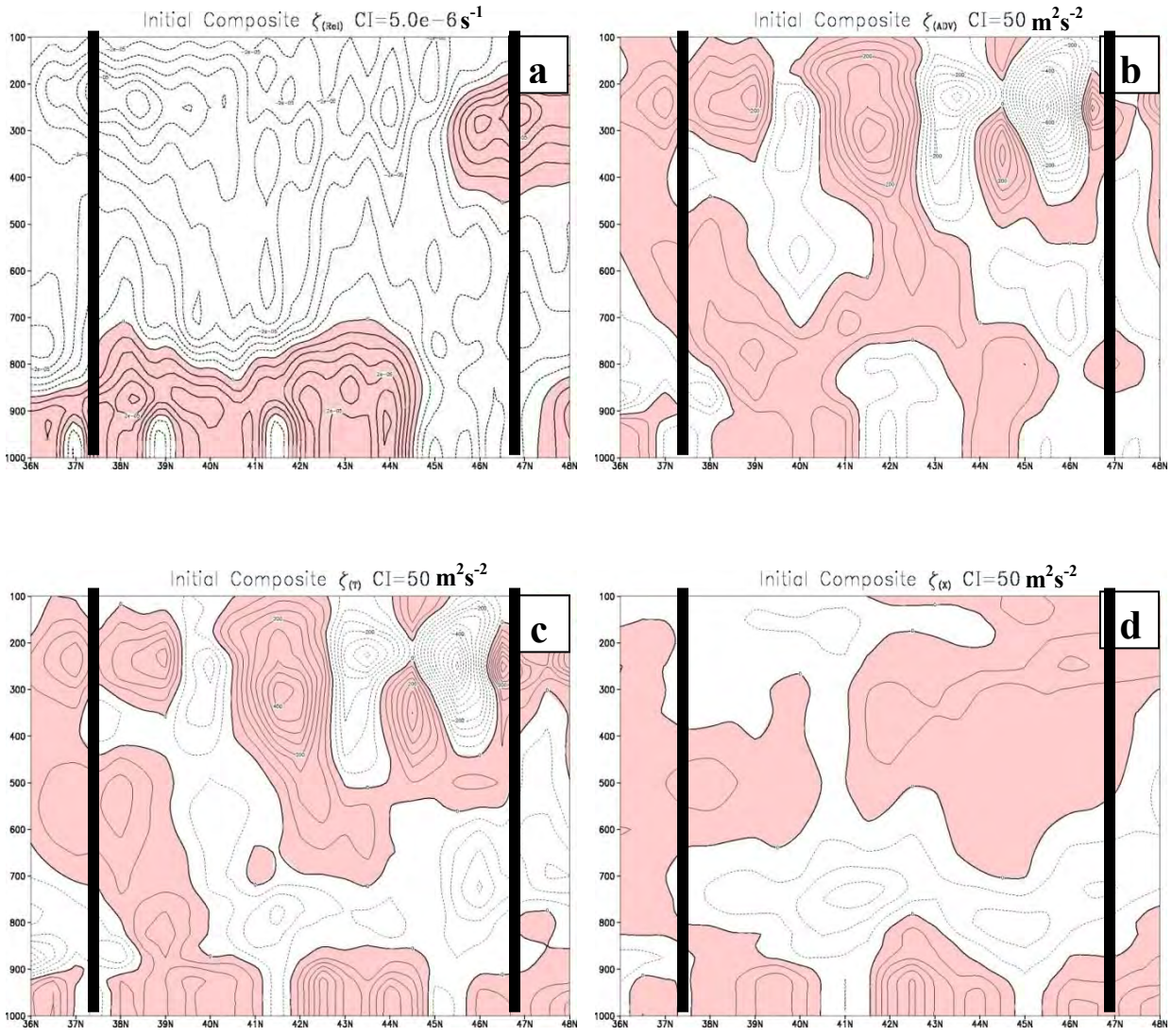

Figure 30. Cross-sections of relative vorticity, vorticity tendency, horizontal vorticity advection, and vortex strecthing at the initiation stage near the rainfall.

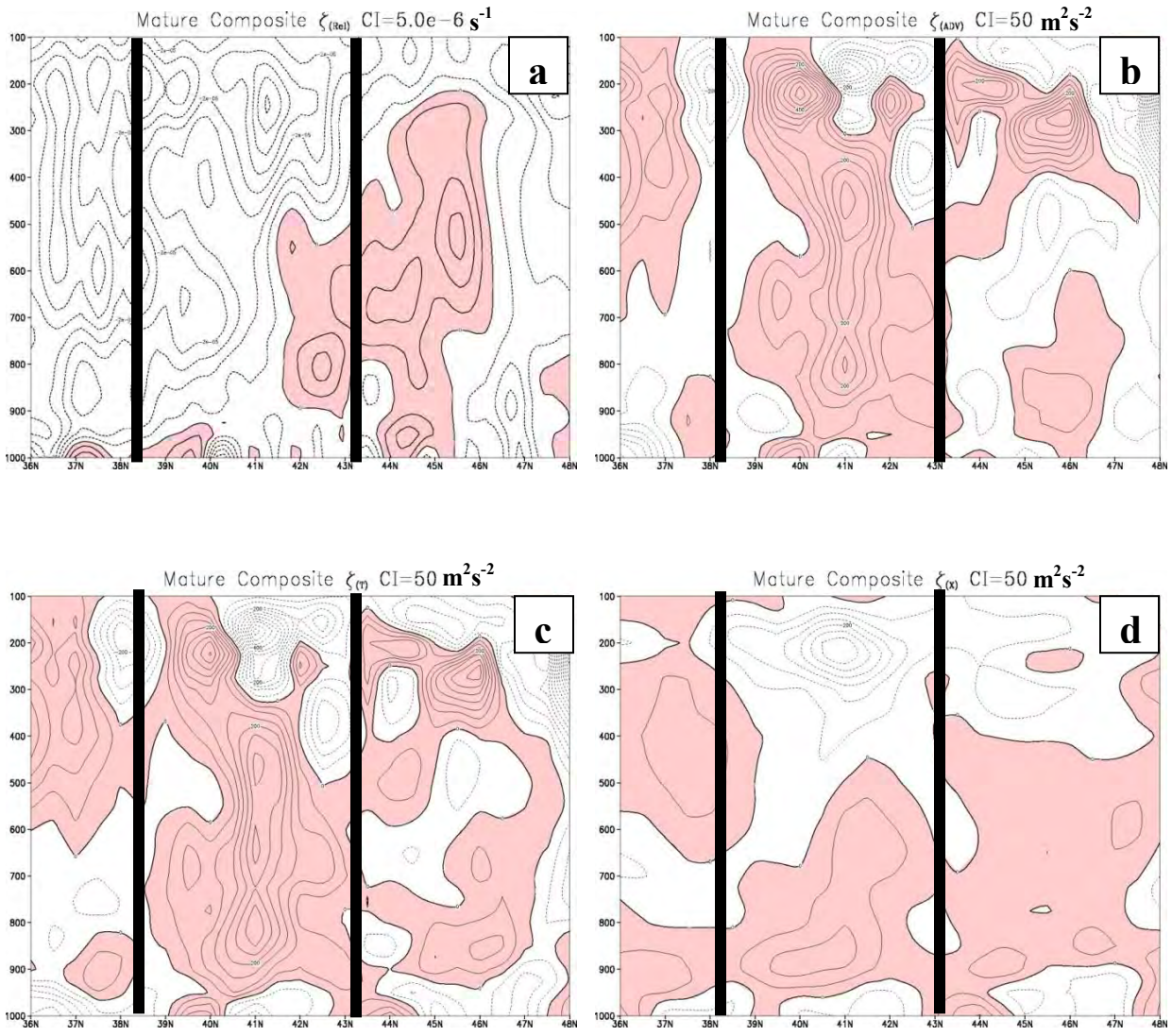

Figure 31. Same as in figure 30, except for the mature stage.

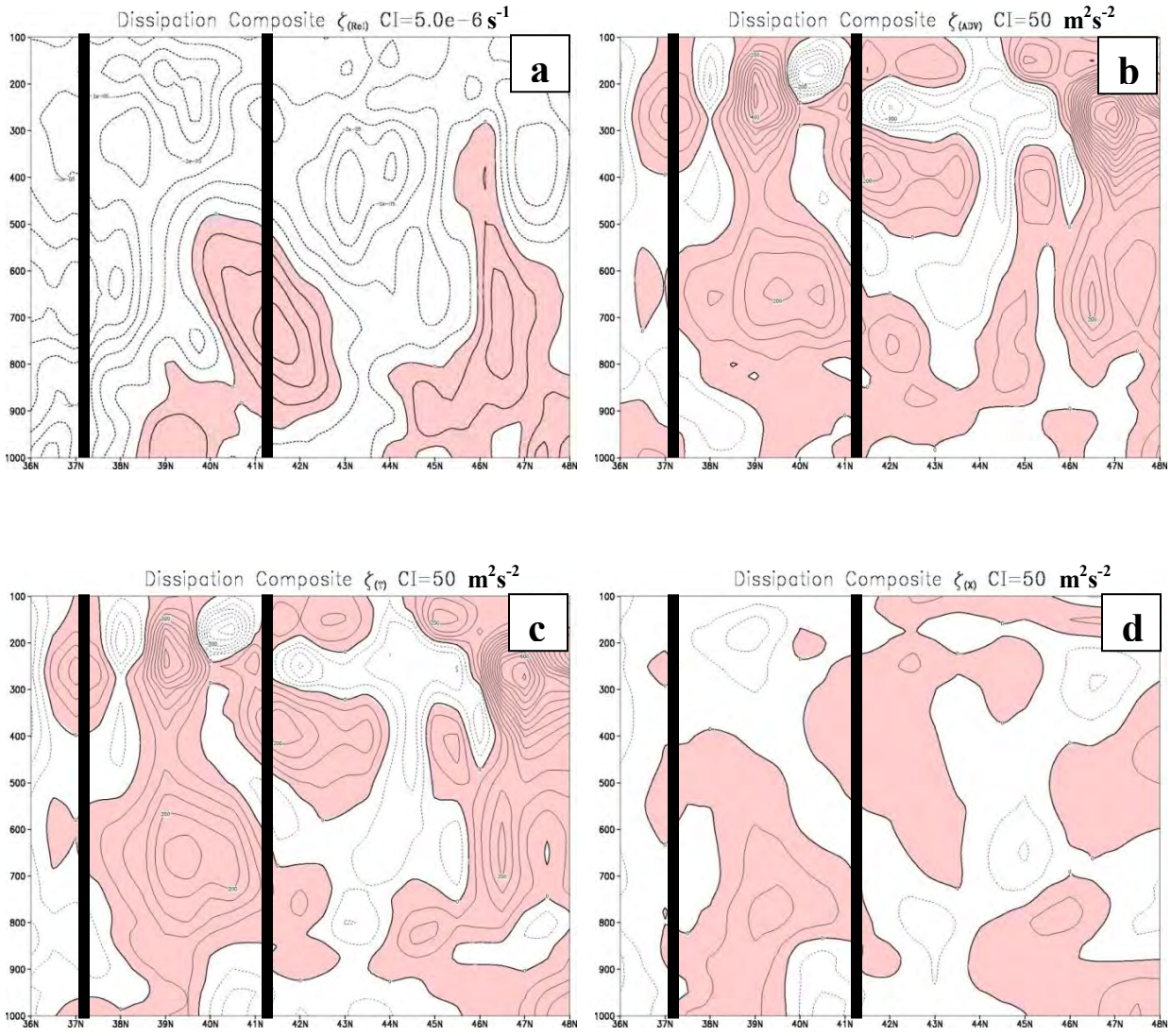

Figure 32. Same as in figure 30, but the dissipation stage.

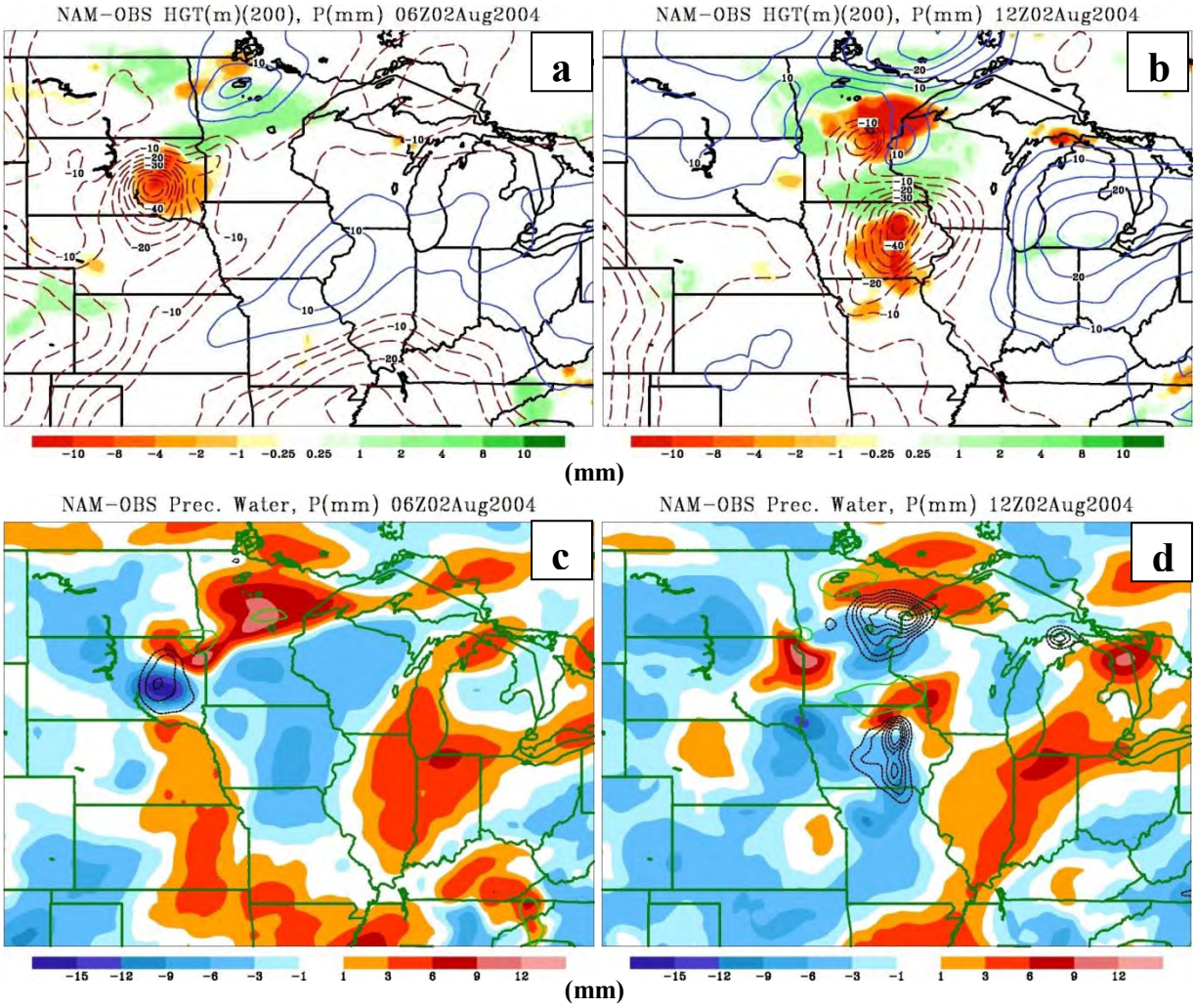

Figure 33. The geopotential height (a and b) difference between the forecast and observed at 0600 and 1200 UTC for 02 August 2004. The rainfall difference in shaded. The precipitable water error (c and d, shaded) is also shown. The rainfall difference is contoured; green for over-predicted, black for under-predicted.

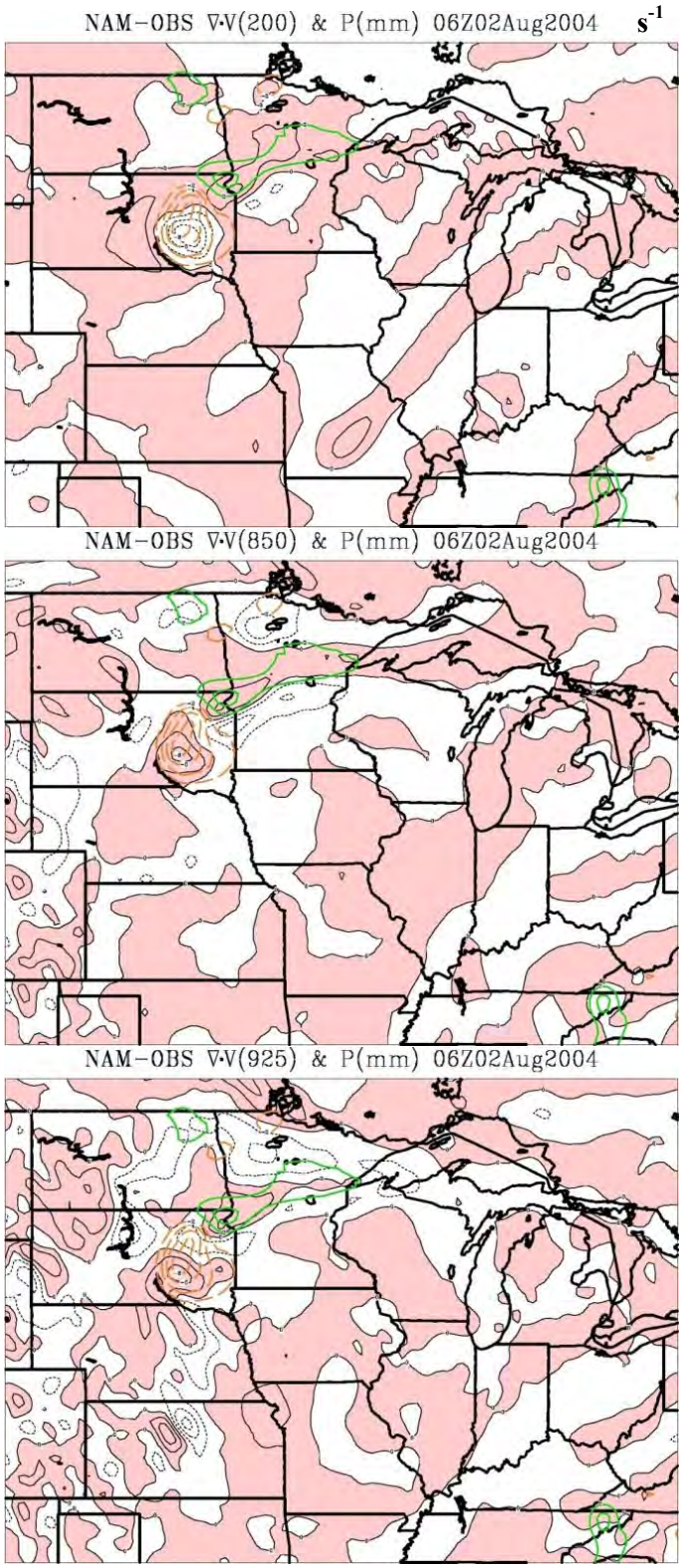

Figure 34. The divergence error at 0600 UTC for 925, 850, and 200 hPa for 02 August 2004 along with the rainfall error. The white/pink shows a negative/positive error. The over-forecasted rainfall is contoured in green and the under-forecasted rainfall is in orange.

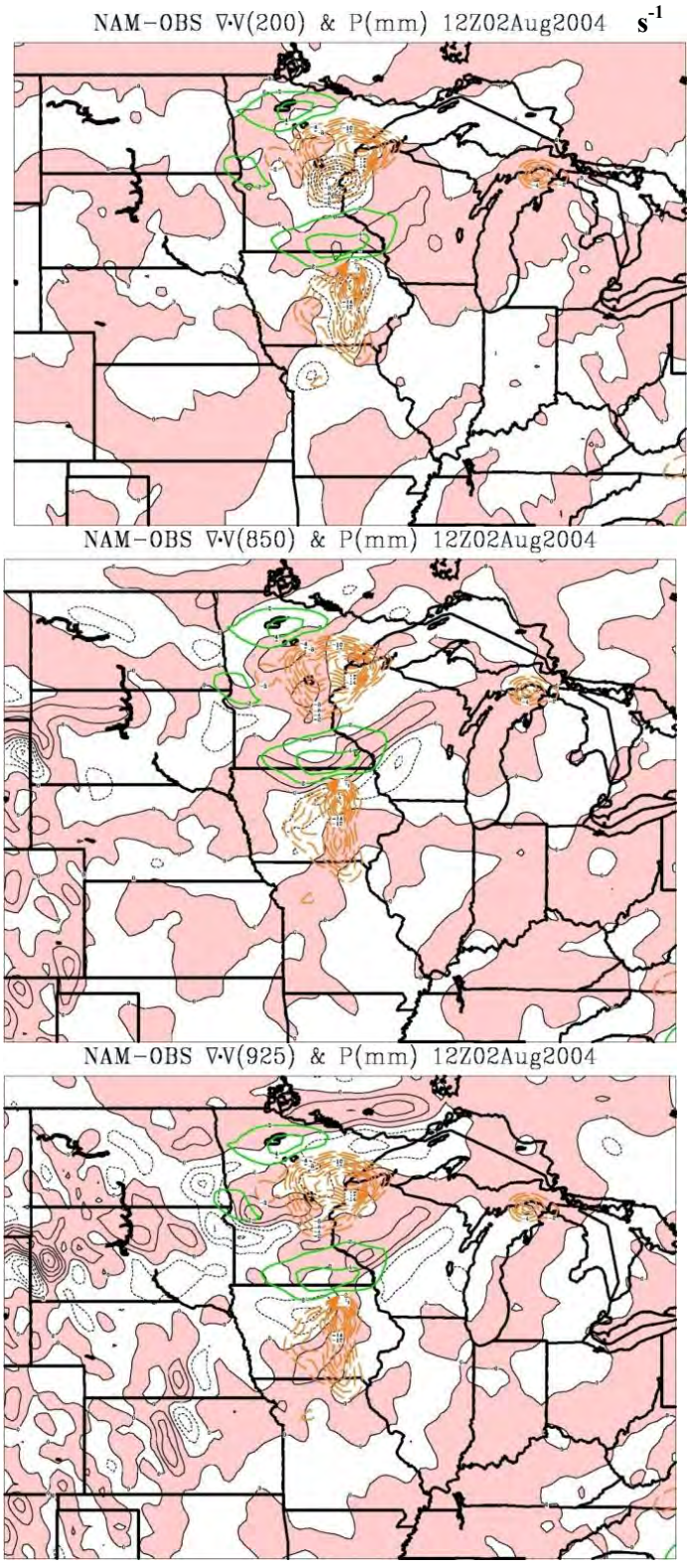

Figure 35. Same as in figure 34, except for 1200 UTC.

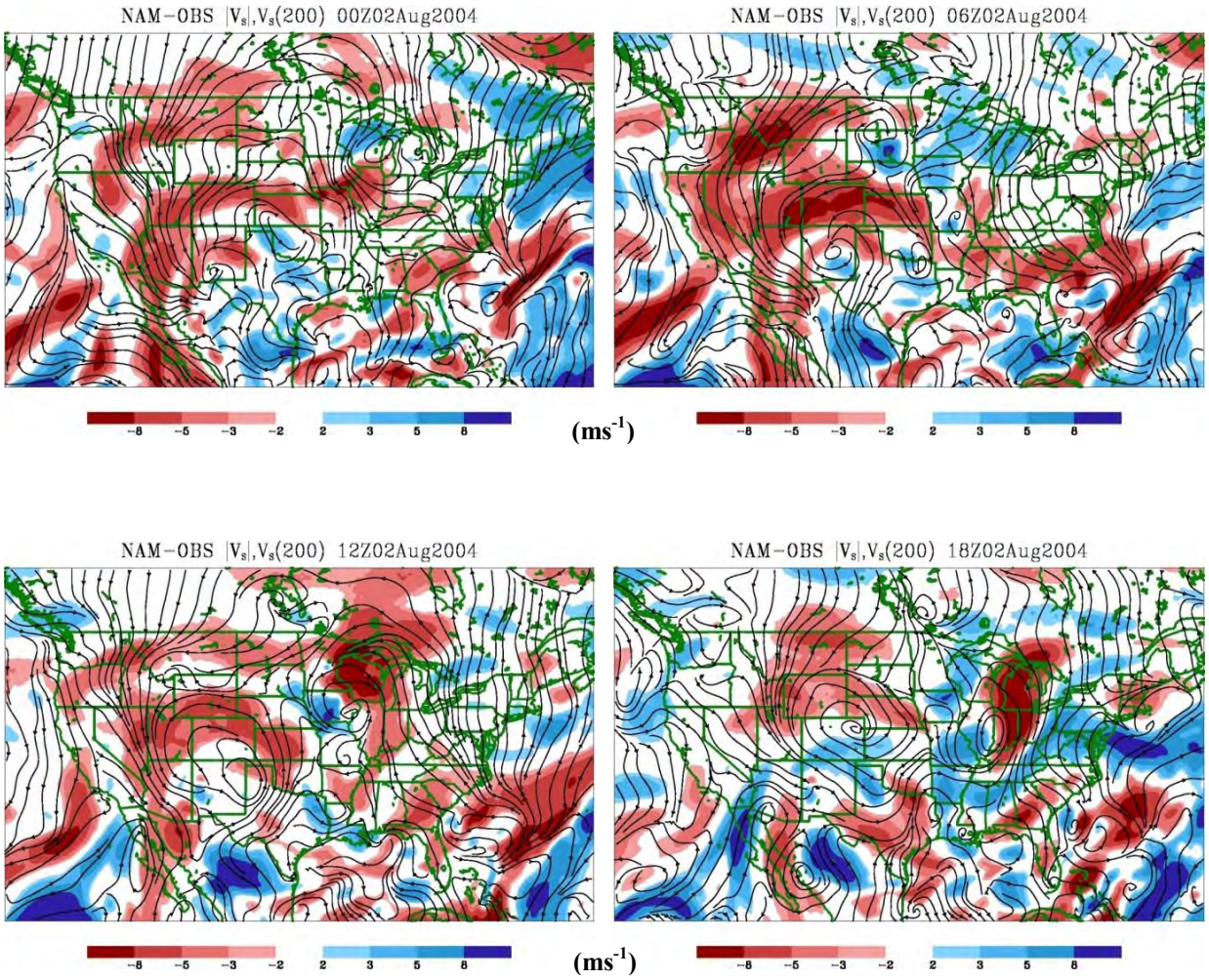

Figure 36. Forecasted error in the streamlines and magnitude for 200 hPa for 0000, 0600, 1200, and and 1800 UTC.

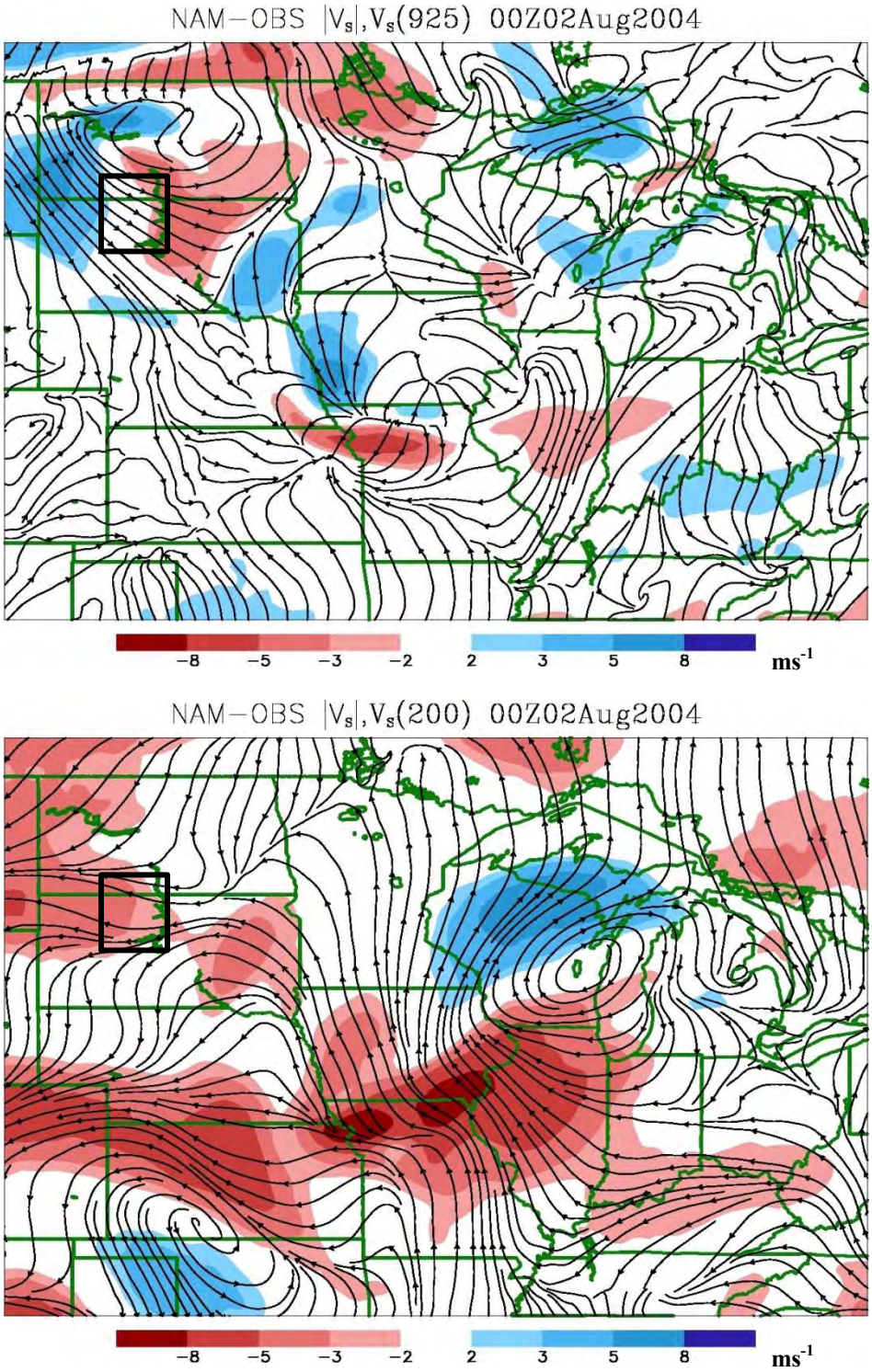

Figure 37. The error in the streamlines and magnitude for 0000 UTC 02 August 2004 at 925 and 200 hPa. The black box highlights the rainfall.

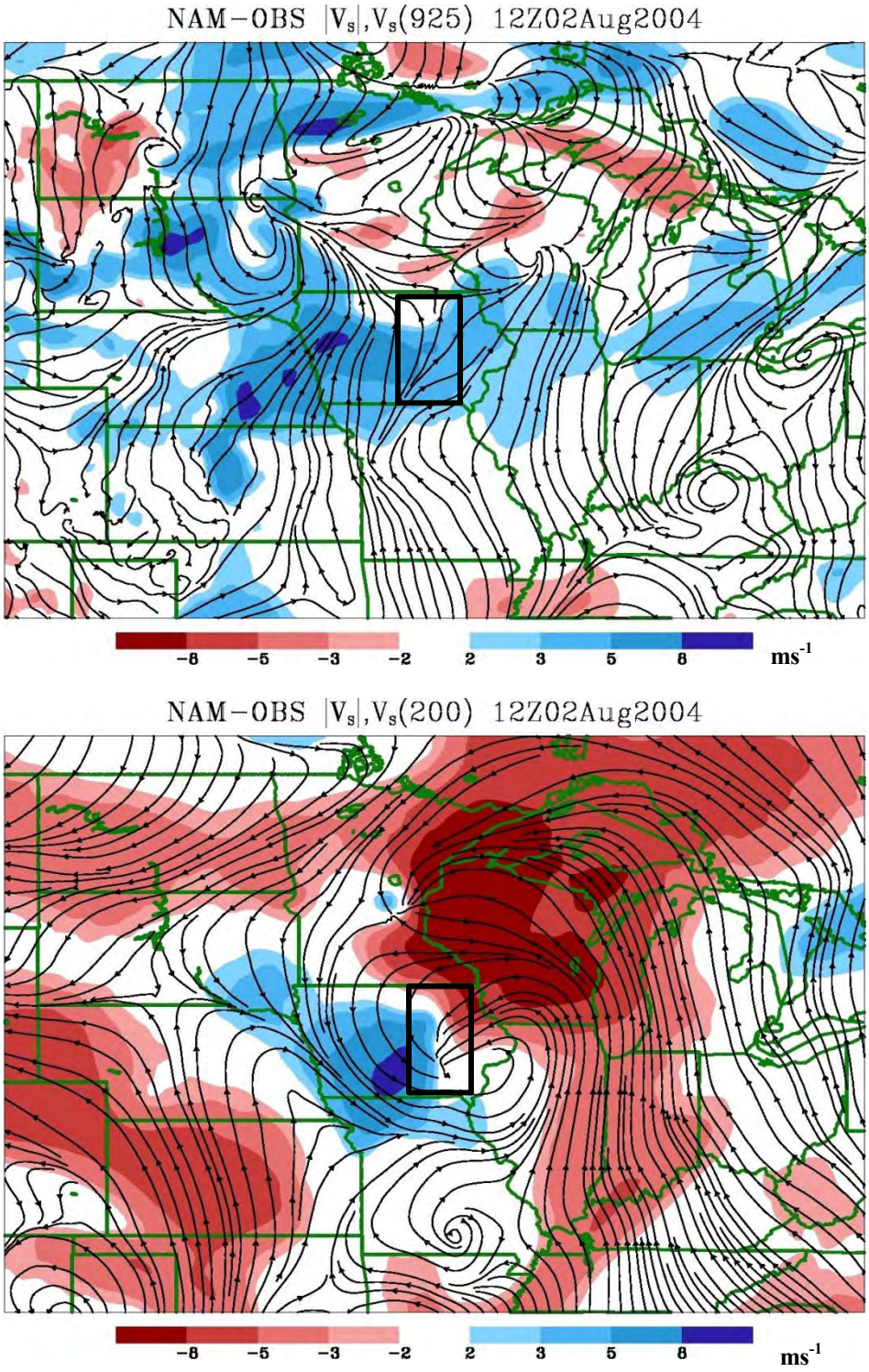

Figure 38. Same as in figure 37, but for 1200 UTC.

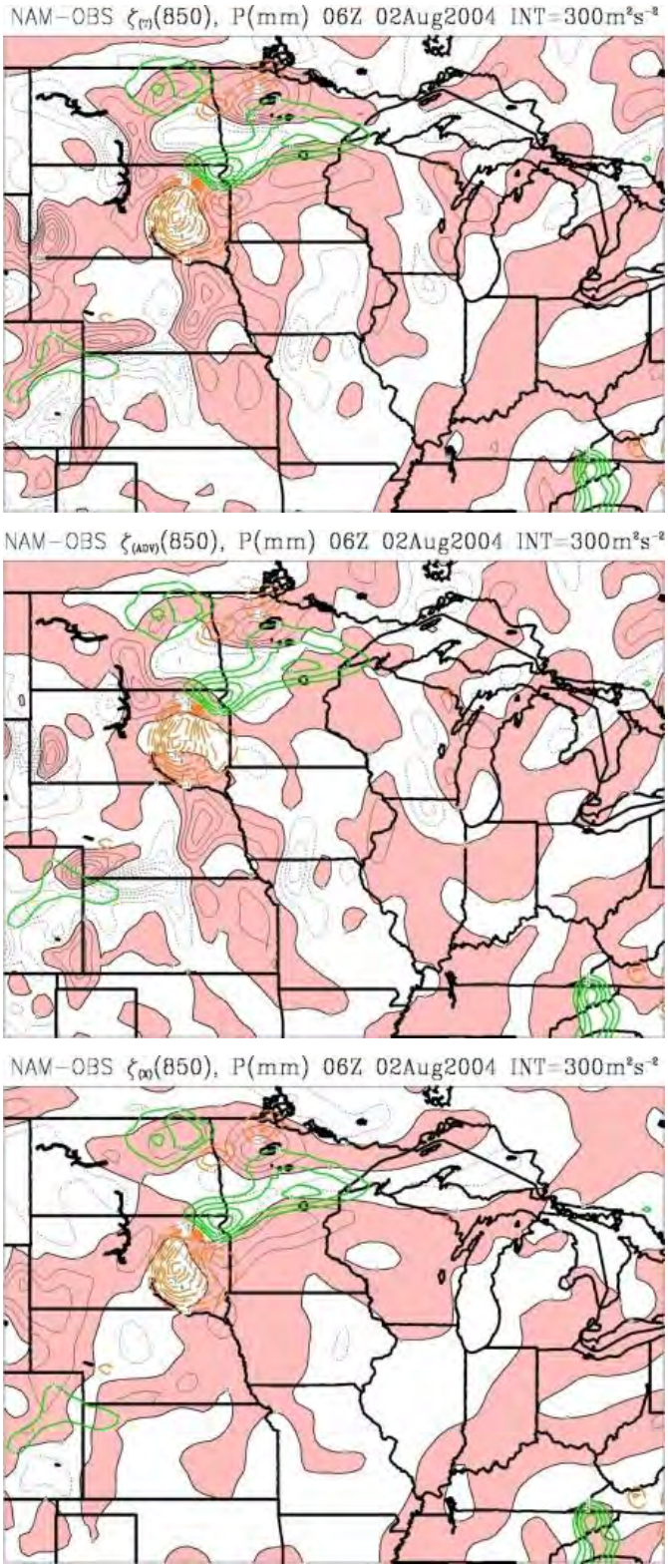

Figure 39. Forecasted error in the vorticity budget terms for 0600 UTC at 850 hPa. The rainfall error is contoured in green and orange similar to figure 34. The white shows a negative error and the pink shows a positive error in the vorticity budget terms.

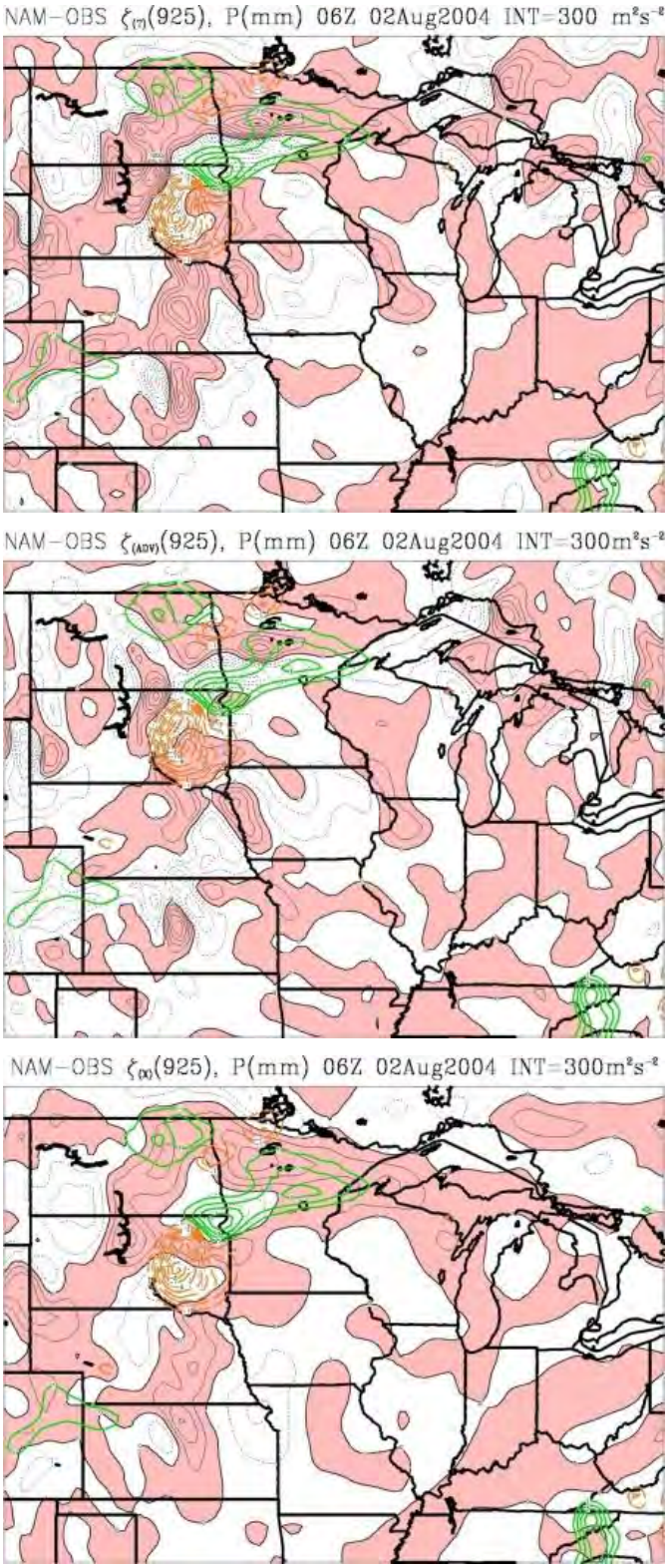

Figure 40. Similar to fig. 39, but for 925 hPa.

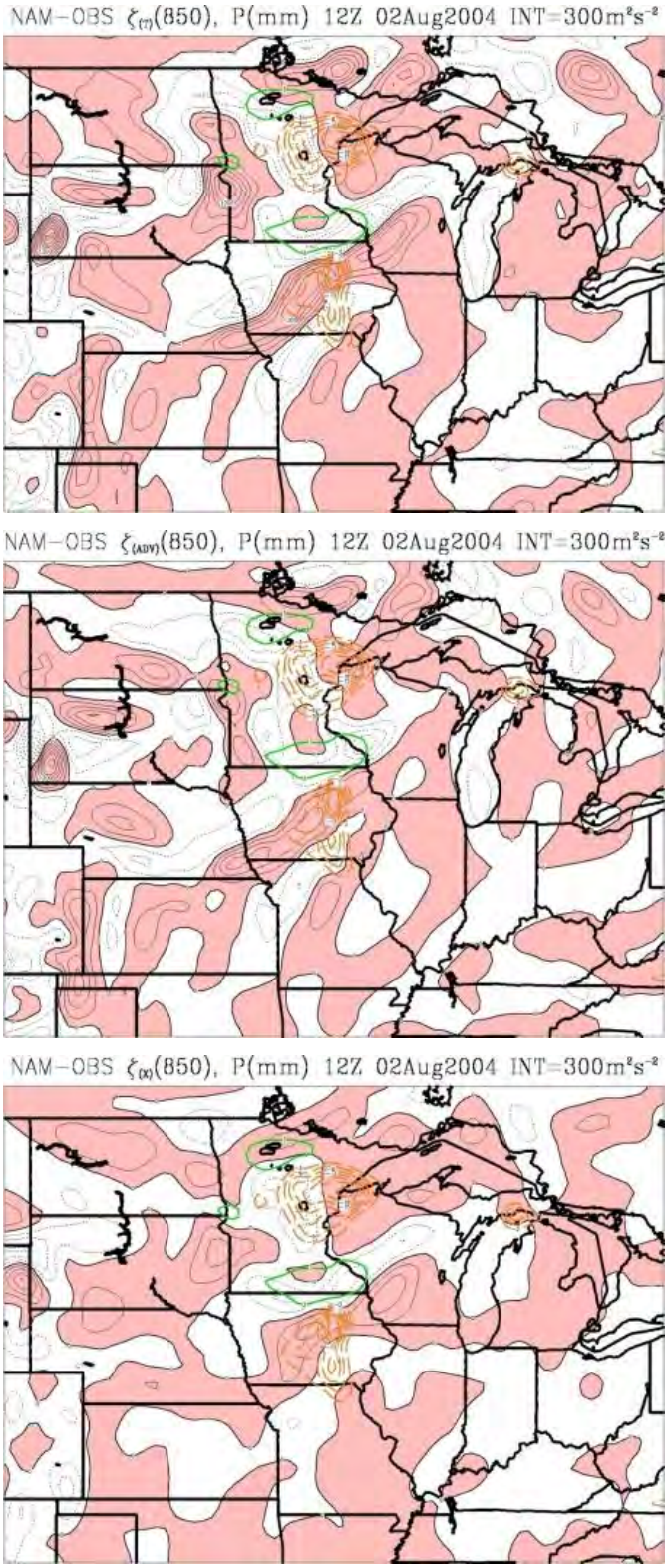

Figure 41. Same as in figure 39, but for 1200 UTC.

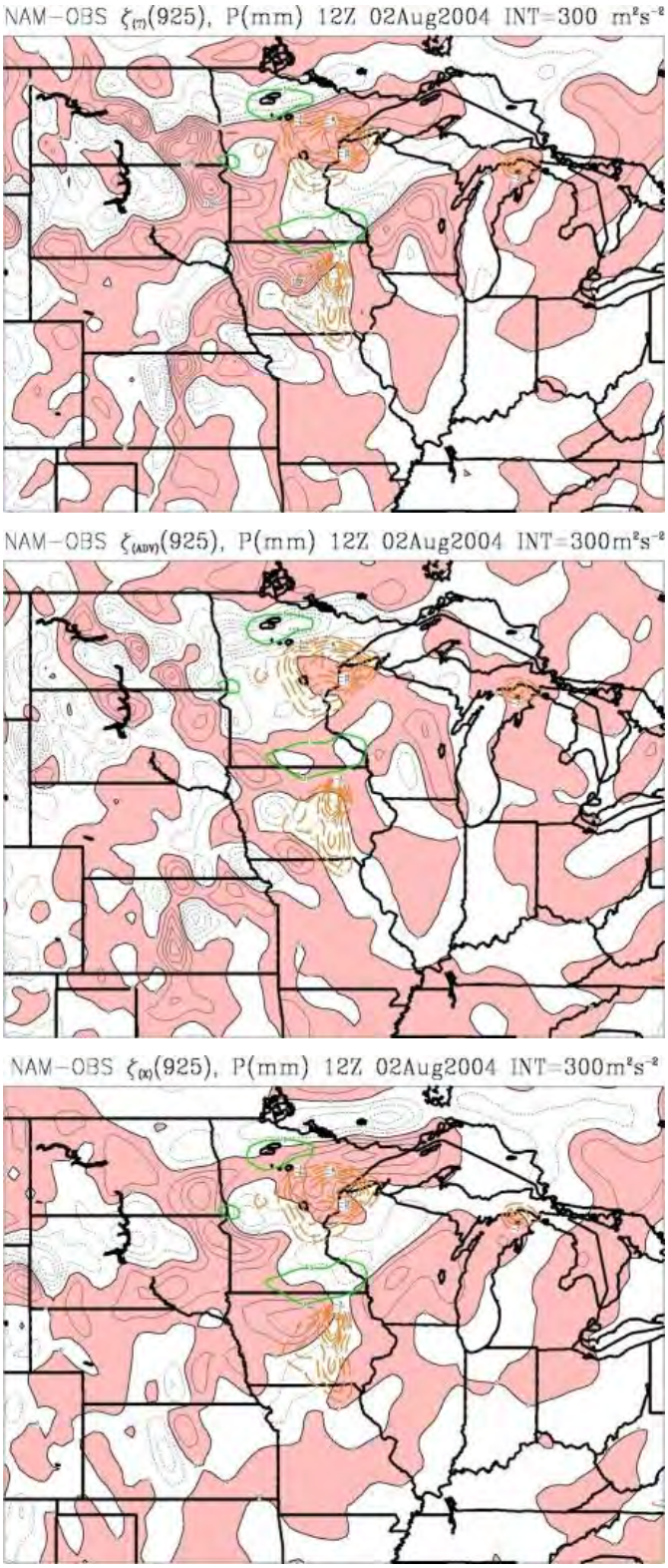

Figure 42. Same as in figure 40, but for 1200 UTC.

CHAPTER 4. ADDITIONAL RESULTS

4.1 Large-Scale Semidiurnal Surface Pressure Environment

In addition to the line graph shown in fig. 20, the large-scale surface pressure environment is shown in fig. 43 for 02 August 2004. The westward propagation of the semidiurnal component is obvious in this figure. At 1200 UTC, the semidiurnal component of surface pressure is negative as it is in fig. 20. This is further confirmation that the semidiurnal surface pressure wave does perturb the large-scale environment as well as the mesoscale environment in Iowa. Fig. 44 shows the time series of the diurnal component of surface pressure. At 1200 UTC, the surface pressure is positive, opposite to the semidiurnal component further indicating that the change in surface pressure is small. As proved earlier, the environment is very unstable with CAPE values exceeding 4500 J/kg, so any type of perturbation in this unstable environment can initiate or strenghten convection.

4.2 Further Composite Analysis

The wind field at 200 hPa (fig. 45) shows the dominant monsoon anticyclone over the southwest U.S. The jet stream at 200 hPa is located in the Northern Plains region and the rainfall initiates in the region directly underneath the core of the jet. The northwesterly flow at 200 hPa extends down to 700 hPa for all three stages. The rainfall remains situated underneath the jet core for all three stages as the jet moves slightly east. The monsoon anticyclone remains stationary throughout the life cycle of the composite rainfall.

The vorticity field at 850 and 925 hPa for all stages is shown in fig. 46. A ribbon of positive vorticity exists to the west of the jet core at 925 hPa at initiation (figs. 46b). In the mature stage, the ribbon of positive vorticity has moved east at 925 hPa (figs. 46d). A cyclonic vorticity perturbation develops at 850 hPa at the mature stage (fig. 46c) in the area of heavy rainfall. Once the rainfall has diminished, the strong cyclonic vorticity at 850 and 925 hPa (figs. 46e and f) has also dissipated from the mature stage. Clearly, as was also mentioned in the case study, the cyclonic perturbations at the lower levels are very important in maintaining the rainfall in Iowa without the presence of a front.

At initiation (figs. 47a and b), strong convergence exists near the area of low pressure and in the areas of initiation in north central Nebraska. The convergence in these areas in not associated with any type of major front. In the mature stage, strong convergence at 925 and 850 hPa (figs. 47c and d) located in northwest Iowa indicates the location of the heavy rainfall. The convergence at both levels is the result of the jet at each level as the strongest convergence occurs at the northern terminus. At the dissipation stage (figs. 47e and f), convergence still exists over the dissipating rainfall, but is not nearly as strong as it was. The diminishing jets at both 850 and 925 hPa clearly have an effect on the convergence, which diminishes, signaling the dissipating rainfall.

4.3 Additional Forecast Evaluations

Figure 48 shows three additional cases evaluating the NAM 12 hour forecast for the geopotential height, precipitable water, and precipitation. These cases show very similar results to the case study discussed earlier. The rainfall is under-forecasted for all three cases because the divergent circulation is not forecasted correctly. The observed heights are much higher than the forecasted heights revealing that the convergence in the lower levels and the divergence in the upper levels are not forecasted accurately. The model cannot handle the shallow convection at initiation and therefore will not be able to forecast the location or intensity of the rainfall as it propagates eastward.

The forecast is also unable to produce the observed precipitable water in each case as well. The moisture content is under-forecasted for the three cases shown here similar to the case study. Clearly, the model will not forecast the amount of rainfall correctly if it does not have the observed amount of precipitable water to precipitate out. The combination of the incorrect moisture content and the incorrect divergent circulation suppress (enhance) the rainfall when the observed rainfall is stronger (weaker).

4.4 Figures

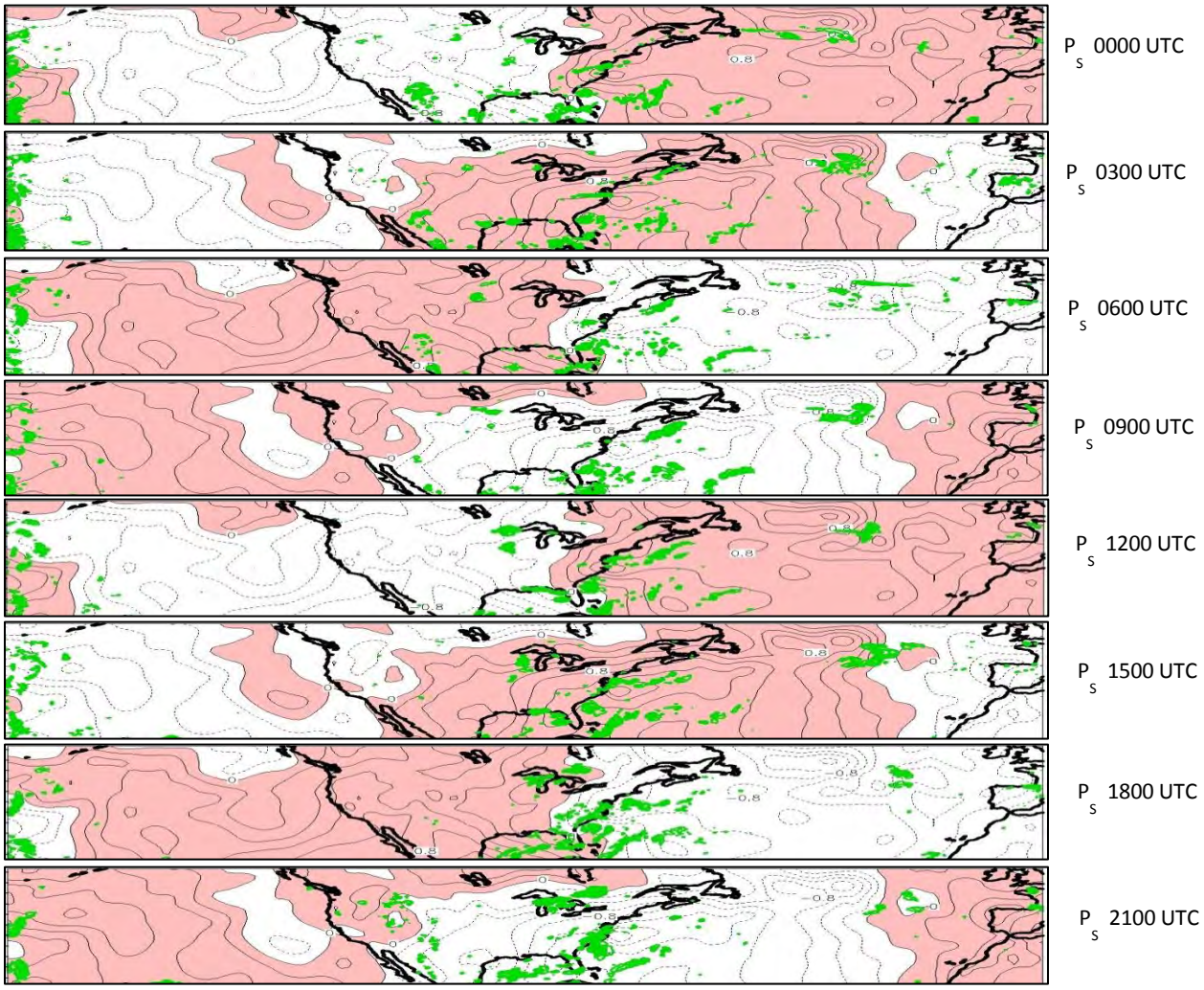

Figure 43. Time-series of the semidiurnal component of surface pressure (hPa) for 02 August 2004. The rainfall (mm) is contoured in green.

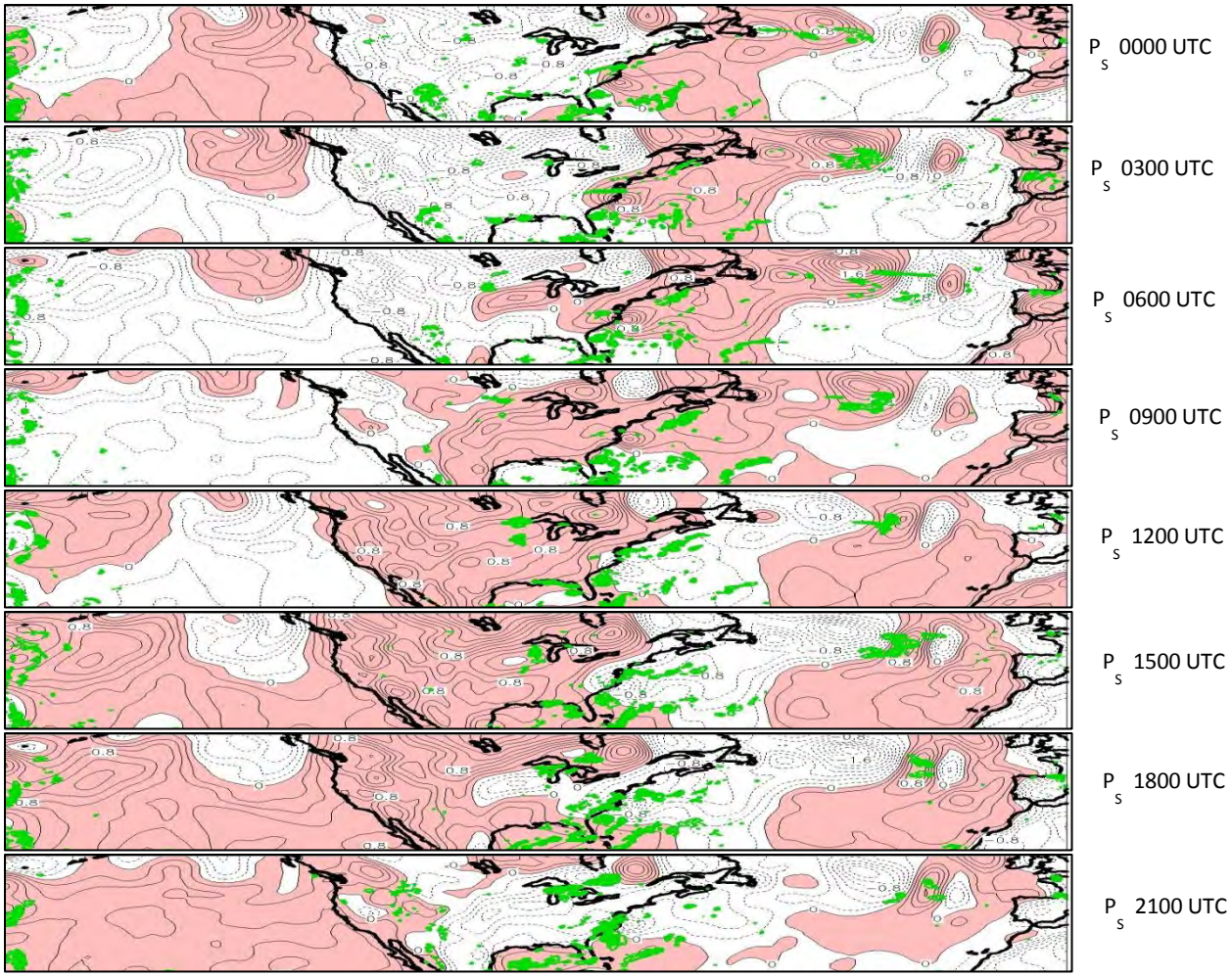

Figure 44. Time-series of the diurnal component of surface pressure (hPa) for 02 August 2004. The rainfall (mm) is contoured in green.

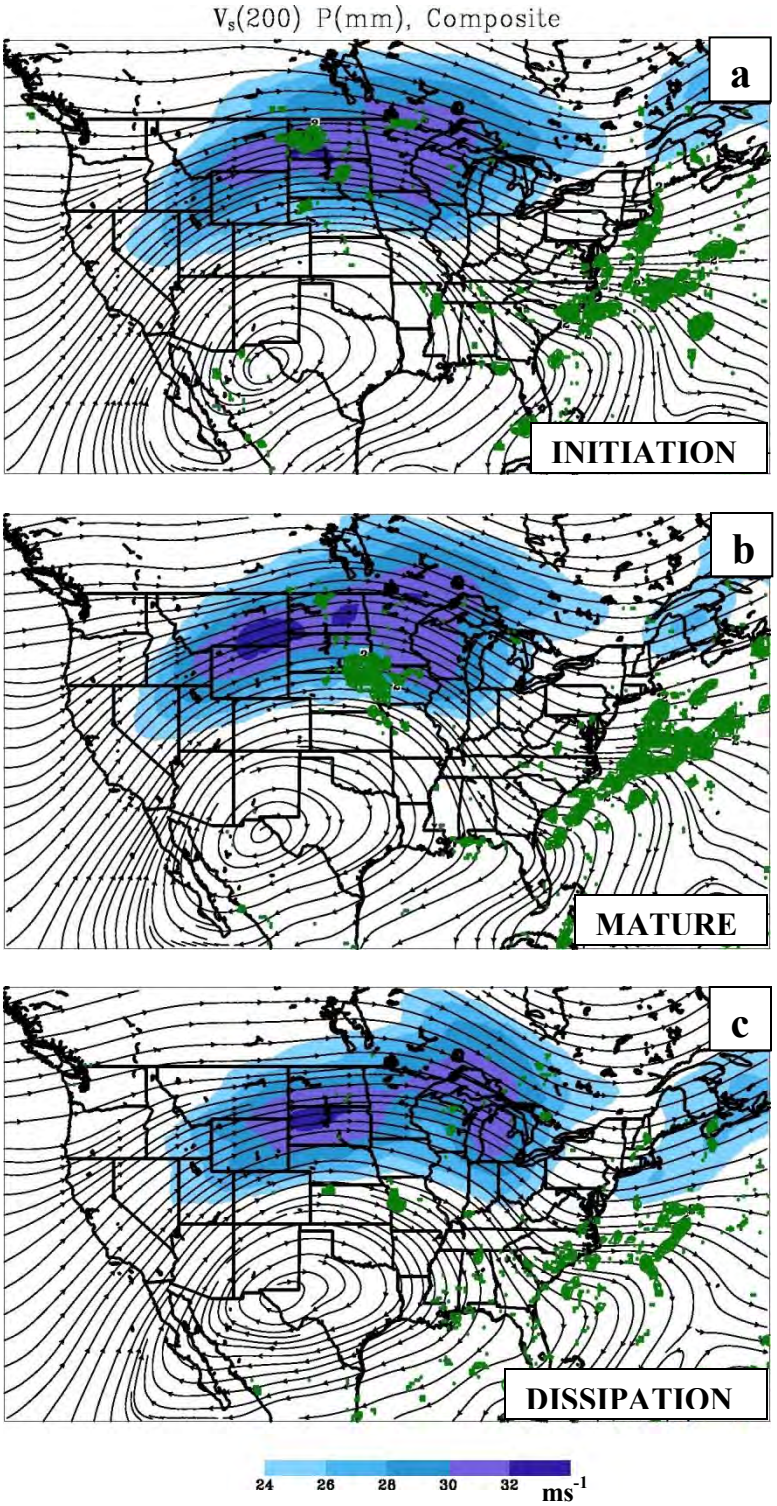

Figure 45. Streamlines at 200 hPa for all three stages of the composite. The rainfall (mm) is contoured in green. The shaded variable is the magnitude of the wind.

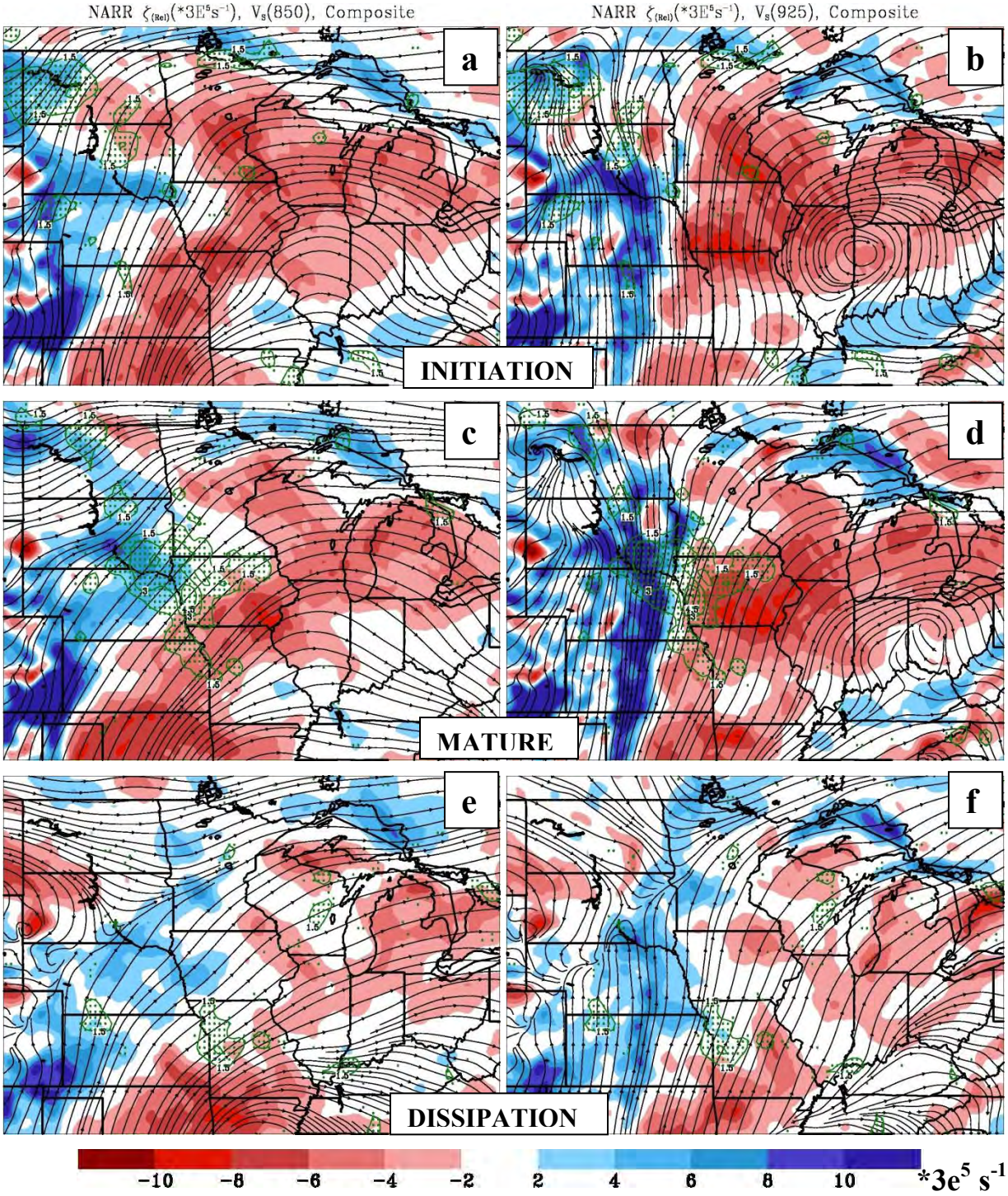

Figure 46. The relative vorticity field and streamlines at 925 and 850 for all three stages. The rainfall (mm) is contoured in green.

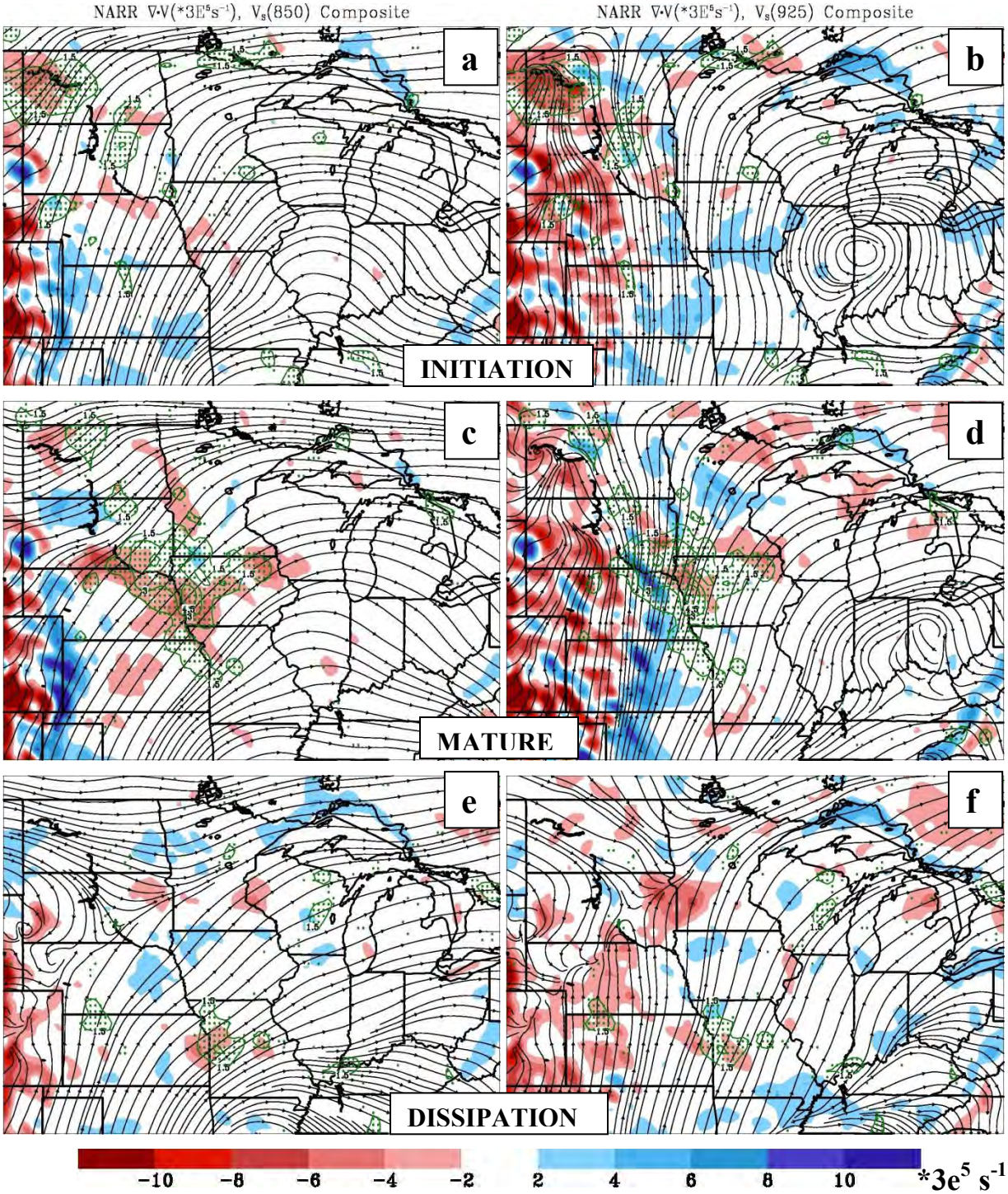

Figure 47. The divergence field and streamlines at 925 and 850 for all three stages. The rainfall (mm) is contoured in green.

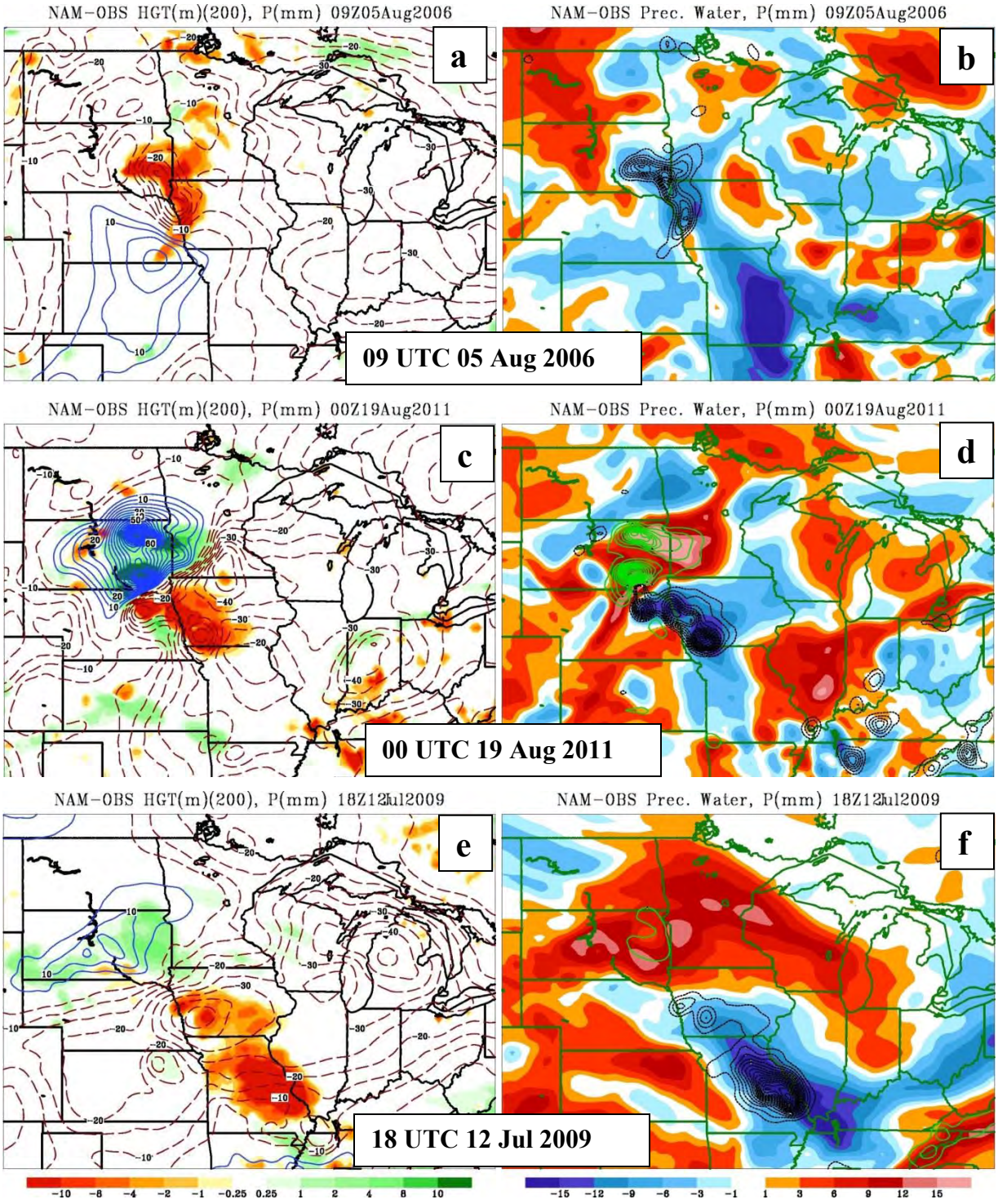

Figure 47. Geopotential height, precipitable water, and precipitation errors for three different cases. The rainfall error is shaded on the left side and contoured on the right (black-negative, green-positive). The geopotential height error is contoured on the left and the precipitable water error is shaded on the right.

CHAPTER 5. GENERAL CONCLUSIONS

Convection initiating away from major frontal boundaries becomes very important to the Central Plains especially in the late summer where the North American Monsoon dominates the mid- to upper level circulation. The monsoon anticyclone prevents large-scale waves from developing, which are responsible for the late-spring early summer deep troughs. In this weak dynamic regime, the low-level conditions become very important, especially because of the inversion layer seen in many soundings for these convective events. Low-level warm and moist air advection aided by the LLJ helps to initiate convection away from major fronts and helps to create a conditionally unstable environment. Large values of surface based CAPE and strong shear create an environment that any type of small-scale perturbation can initiate convection.

The monsoon anticyclone in the Central Plains suppresses the convection at initiation and confines it to the lower troposphere. Vertical cross-sections of the vorticity budget show that intense vortex stretching at the lower levels coupled with the LLJ and some type of perturbation either at the surface or in the lower troposphere are able to produce rainfall without the presence of a major front. Semidiurnal pressure fluctuations and mesoscale waves can disturb the atmosphere enough to perturb the flow and either strengthen or initiate convection. Fourier analysis of the surface pressure in the large-scale environment also showed a favorable environment for perturbing the atmosphere.

The shallow convection is not reproduced well in the forecast, showing incorrect placement and amounts of rainfall. The 200 hPa geopotential height error most often shows lower than observed heights because the rainfall is most often under-predicted. Smaller (larger) values of precipitable water in the forecast are associated with under-forecasted (over-forecasted) rainfall amounts. The divergent circulation in the forecast seems to be the reason for inaccurate forecasts showing anticyclonic bias where the observed rain is falling seen in both the wind error and the vorticity budget error.

From what has been shown in this paper, it is evident that the forecast needs to be improved. The late summer brings many problems because many convective rainfall events are not associated with extratropical cyclones. Some of these events are not even associated with fronts and the model cannot reproduce the observed results. Accounting for the error in the

divergent circulation would be something that would be used to improve the Weather Research and Forecasting (WRF) model. A better understanding of the mechanism for initiating the rainfall in these types of events needs to be added into the model somehow, which is beyond the scope of this study. The Global Precipitation Measurement (GPM) satellite can also be used when it is launched to better study the mid-latitude precipitation events of all kinds including these types of events occurring away from major frontal boundaries.

ACKNOWLEDGMENTS

I would like to thank my advisor, Dr. Tsing-Chang (Mike) Chen for his guidance and assistance throughout the process of this research task and writing this thesis. I would also like to thank Jenq-Dar (Paul) Tsay for his assistance with helping me to learn FORTRAN and GrADS. I appreciate the support given to me by my family, friends, and fellow graduate students. I also am very thankful for the feedback given to me by my committee members Dr. Xiaoqing Wu and Dr. Gene Takle. I would also like to thank Dr. Jordan Alpert at NCEP for his assistance in gaining access to some NAM forecast data. Partial funding was given to support this work by the Cheney Research Fund.

REFERENCES

Bernardet, L. R., L. B. Nance, H.-Y. Chuang, A. Loughe, M. Demirtas, S. Koch, and R. Gall, 2005: The Developmental Testbed Center Winter Forecasting Experiment (DWFE). Preprints, *21st Conf. on Weather Analysis and Forecasting/17th Conf. on Numerical Weather Prediction*, Washington, DC, Amer. Meteor. Soc., 7.1. [Available online at http://ams.confex. com/ams/pdfpapers/94730.pdf.]

Bonner, W. D., 1968: Climatology of the low level jet. *Mon Weather Rev*, **96**, 833–850.

Browning, K. A., 1977: The structure and mechanisms of hailstorms. *Meteor. Monogr.*, **38**, 1-46.

Black, T. L., 1994: The new NMC mesoscale Eta model: description and forecast examples. *Wea. Forecasting*, **9**, 265–278.

Chen, T. C., 2003: Maintenance of summer monsoon circulations: a planetary-scale perspective. *J. Climate*, **16**, 2022–2037.

_____ , and J. A. Kpaeyeh, 1993: The synoptic-scale environment associated with the low-level jet of the great plains. *Mon. Wea. Rev.*, **121**, 416–420.

Clark, A. J., W. A. Gallus Jr., and T. C. Chen, 2007: Comparison of the diurnal precipitation cycle in convective-resolving and non-convection-resolving mesoscale models. *Mon. Wea. Rev*., **135**, 3456–3473.

Heideman, K. F., J. M. Fritsch, 1988: Forcing mechanisms and other characteristics of significant summertime precipitation. *Wea. Forecasting*, **3**, 115–130.

Higgins W. R., Y. Yao, X.L. Wang, 1997: Influence of the North American Monsoon System on the United States summer precipitation regime. *J. Clim*., **10**, 2600–2622.

Holton, J. R., 2004: *An Introduction to Dynamic Meteorology*. 4th ed. Academic Press, 535 pp.

Jankov, I., and W. A. Gallus, 2004: MCS rainfall forecast accuracy as a function of large-scale forcing. *Wea. Forecasting*, **19**, 428–439.

Johns, R. H., 1984: A synoptic climatology of northwest-flow severe weather outbreaks. Part II: Meteorological parameters and synoptic patterns. *Mon. Wea. Rev.*, **112**, 449–464.

Kummerow, C., and Coauthors, 2000: The status of the Tropical Rainfall Measuring Mission (TRMM) after two years in orbit. *J. Appl. Meteor.,* **39,** 1965–1982.

Maddox, R. A., C. A. Doswell, 1982: An examination of jet stream configurations, 500 mb vorticity advection and low-level thermal advection patterns during extended periods of intense convection. *Mon. Wea. Rev.*, **110**, 184–197.

Marwitz, J. D., 1972: The structure and motion of severe hailstorms. Part II: Multi-cell storms. *J. Appl. Meteor.*, **11**, 180–188.

Mesinger, F., and Coauthors, 2006: North American Regional Reanalysis. *Bull. Amer. Meteor. Soc*., **87**, 343–360.

Newton, C. W., 1950: Structure and mechanism of the pre-frontal squall line. *J. Meteor.*, **7,** 210-222.

Rauber, R. M., J. E. Walsh, and D. J. Charlevoix, 2002: *Severe and Hazardous Weather.* Kendall/Hunt, 616 pp.

Stensrud, D. J. and J. M. Fritsch, 1994: Mesoscale convective systems in weakly forced large-scale environments. Part II: Generation of a mesoscale initial condition. *Mon. Wea. Rev*., **122**, 2068–2083.

Stull, R. B., 1988: *An Introduction to Boundary Layer Meteorology*. Kluwer, 666 pp.

Trier, S. B., C. A. Davis, D. A. Ahijevych, M. L. Weisman, and G. H. Bryan, 2006: Mechanisms supporting long-lived episodes of propagating nocturnal convection within a 7-Day WRF model simulation. *J. Atmos. Sci.*, **63**, 2437–2461.

TRMM Senior Review Proposal, 2007. [Available online at http://trmm.gsfc.nasa .gov/trmm_rain/Events/TRMMSenRev2007_pub.pdf.]

Wallace, J. M., 1975: Diurnal variations in precipitation and thunderstorm frequency over the conterminous United States. *Mon. Wea. Rev.*, **103**, 406–419.

Wang, S.-Y., T.-C. Chen, and J. Correia, 2009: Climatology of summer midtropospheric perturbations in the U.S. Northern Plains. Part I: Influence on northwest flow severe weather outbreaks. *Climate Dyn*., **36,** 793-810.

Wang, S. Y., T. C. Chen, and S. E. Taylor, 2009: Evaluations of NAM Forecasts on Midtropospheric Perturbation-Induced Convective Storms over the U.S. Northern Plains. *Wea. Forecasting.*, **24,** 1309–1333.

Zhang, D. L., 1992: The formation of a cooling-induced mesovortex in the trailing stratiform region of a midlatitude squall line. *Mon. Wea. Rev*., **120**, 2763–2785.